HYDRAULICS OF MOUNTAIN RIVERS

Prepared for

COLORADO STATE UNIVERSITY
EXPERIMENT STATION

Prepared by

J.C. Bathurst
R.M. Li
D.B. Simons

Civil Engineering Department
Engineering Research Center
Colorado State University
Fort Collins, Colorado

May 1979

CER78-79JCB-RML-DBS55

ABSTRACT

The hydraulics of mountain rivers, and the processes of flow resistance in particular, are examined using the results of a flume study.

Mountain rivers have slopes of about 0.4 to 10 percent and depths of the same order of magnitude as the roughness element size. Flow resistance depends on the form drag of the elements and the distortions of the flow about the elements. The drag of individual elements is determined by processes of fluid mechanics related to Reynolds number and Froude number, the latter affecting the appearance of local hydraulic jumps and the generation of drag from distortions of the free surface. The combined drag of the elements is determined by processes connected with roughness and channel geometries. Roughness geometry is described by the effective roughness concentration which accounts for roughness effects dependent on depth and bed material characteristics. Channel geometry affects the relative roughness area, a parameter which determines the degree of funnelling of the flow between elements.

In the flume study, measurements were made with five fixed roughness beds, each composed of a different gravel, at three slopes. A few measurements were also made with loose beds. Using the results, a flow resistance equation for fixed beds with large-scale roughness and free surface drag is developed. Comparison with the loose bed results and with independent river data shows that the equation does not apply where there are Reynolds number effects, standing waves and sediment transport. Within its limitations, though, it can be applied using a simple iterative technique.

A literature review shows that sediment transport depends on the geomorphic properties of the watershed as well as on hydraulic factors.

ACKNOWLEDGMENTS

This report is based on a series of flume experiments which could not have been carried out without the help of many people. Two sets of the materials used for the roughness beds had to be collected by hand from a gravel pit and the experiments with the loose roughness beds required considerable help with measurements and shovelling. The authors would therefore like to thank the following who provided great assistance with the work: Dr. Timothy Ward, Michael Ballantine, Kenneth Eggert, William Fullerton, David Hartley, Jau-Yau Lu, Curtis Orvis, Michael Stay and Carla Worley.

The authors would also like to thank Ewald Patzer, Machine Shop Foreman, and his team who arranged technical help and laboratory details in a most helpful and efficient manner, even anticipating some of the requirements. Without them it would not have been possible to install the roughness beds, obtain supplies of sediment and operate the flume. Special thanks are due, too, to Arlene Nelson, Head of Technical Typing, and those members of the typing pool who ensured that this report was typed and to Tamra McFall and Annette Ward who supervised production of the report.

The visiting author, James Bathurst, would like to take this opportunity to thank the Commonwealth Fund of New York for providing him with a Harkness Fellowship to study in the United States of America. This fellowship supported him during his 21 month stay at Colorado State University and enabled him to travel widely and visit many of the institutions concerned with river mechanics in the United States. He is also most grateful to Professors Daryl Simons and Ruh-Ming Li who provided him with the opportunities and the facilities, including the unique steep-stream flume, with which to join in work on the hydraulics of mountain rivers. The kind support and interest shown by them and their colleagues in the Department of Civil Engineering and the Engineering Research Center contributed greatly to an enjoyable visit to Colorado State University and is much appreciated. Finally James Bathurst would like to thank Dr. Don Doehring (Department of Natural Resources, Colorado State University) and Professor J. Dungan Smith and Dr. Arthur Nowell (Department of Oceanography, University of Washington), for helpful discussions on mountain rivers and relevant processes of fluid mechanics, and Professor Dale Bray (Department of Civil Engineering, University of New Brunswick) and Drs. Colin Thorne and Richard Hey (School of Environmental Sciences, University of East Anglia, England), for their field measurements of bed material size distribution.

TABLE OF CONTENTS

TABLE OF CONTENTS--Continued

LIST OF PHOTOGRAPHS IN THE MAIN TEXT

LIST OF FIGURES IN THE MAIN TEXT

LIST OF FIGURES IN THE MAIN TEXT--Continued

LIST OF FIGURES IN THE MAIN TEXT--Continued

LIST OF TABLES IN THE MAIN TEXT

HYDRAULICS OF MOUNTAIN RIVERS

J. C. Bathurst
R. M. Li
D. B. Simons

Department of Civil Engineering
Engineering Research Center
Colorado State University
Fort Collins, Colorado

May 1979

CER78-79JCB-RML-DBS55

SECTION 1 INTRODUCTION

Traditionally civil engineers have not had to contend with mountain rivers to any great extent. In recent decades, though, there has been an increasing human involvement with upland and mountain regions and activities such as agriculture, forestry, recreation, reservoir construction, river regulation and highway construction have encroached to a considerable degree on the upland environment. Examples of such development include the transAlaska oil pipeline, the Kielder scheme for interbasin transfers of water in England, irrigation channels in Nepal and ski resorts in Colorado. Mountain rivers have therefore increasingly felt the impact of human activities and have also themselves become the focus of engineering projects.

At present little is known about the properties of such rivers so their response to development can not easily be predicted. However, there is an abundance of examples which show that poor development practices can quickly and seriously damage the physical, chemical and biological environments of these rivers through erosion, siltation, increased flood magnitudes, pollution, destruction of fish spawning grounds and so on. Consequently there is an urgent need to develop a knowledge of mountain rivers and to produce methods of management which will allow both the prediction and minimization of the impact of human activities.

The first step towards this goal requires that the fundamental processes of river flow and channel adjustments be understood. This study, based on flume experiments, is intended to shed some light in that area, its principal subject being the processes of fluid mechanics which determine the resistance to flow in a channel. Quantification of the flow resistance is essential in any problem, such as flow routing or prediction of flood levels, which requires knowledge of flow depth and velocity.

A mountain river is just one of the forms assumed by rivers which can be generally classified as gravel-bed, cobble-bed or boulder-bed rivers. In this report such rivers will be called just cobble-bed rivers for ease of reference. The report therefore first considers the various types of cobble-bed rivers and the different approaches to describing their flow resistance and identifies the characteristic features of mountain rivers. Previous studies of mountain rivers are reviewed and then the theoretical approach of this study is developed. The flume experiments are described and a flow resistance equation is derived from the results. Finally a brief study of sediment transport in mountain rivers is presented.

Throughout the report the processes of flow are carefully considered. Consequently the derived equations, while inevitably semi-empirical in form, contain only terms which have definite physical meaning.

SECTION 2 FLOW RESISTANCE OF COBBLE-BED RIVERS

The purpose of a flow resistance equation is to relate the velocity of flow to all the factors which might affect that velocity. Mathematically this can be achieved by defining a resistance coefficient which accounts for all the relevant resistive factors. Three coefficients are widely used, these being the Manning, Chézy and Darcy-Weisbach coefficients (American Society of Civil Engineers, 1963). The Darcy-Weisbach coefficient, f, is the only one which is dimensionless and it is therefore used in this report. For a channel cross section it is defined by the equation:

$$\left(\frac{8}{f}\right)^{0.5} = \frac{\bar{U}}{\bar{u}_*} \qquad (1)$$

where $\bar{U}$ = mean velocity of flow at the section and $\bar{u}_*$ = mean shear velocity at the section. Shear velocity at a point is defined as:

$$u_* = \left(\frac{\tau_o}{\rho}\right)^{0.5} \qquad (2)$$

where τ_o = boundary shear stress at a point and ρ = density of the fluid. In steady, uniform flow, mean shear velocity is given by:

$$\bar{u}_* = (gRS)^{0.5} \qquad (3)$$

where R = hydraulic radius; S = the energy gradient, which in this case equals the channel slope; and g = acceleration due to gravity (American Society of Civil Engineers, 1963; Henderson, 1966, p. 95).

The basic problem in flow resistance work is the evaluation of the resistance coefficient. Two approaches can be used but neither is yet completely satisfactory.

The first is an empirical approach in which values are assigned using experience. Aids to this process include tables of values which have been found to be typical of given channels (e.g., Henderson, 1966, p. 99) and a set of photographs of various channels which enables coefficients to be evaluated by a technique of visual comparison (Barnes, 1967). The empirical approach is simple to follow but the potential errors are large. The method is subjective and the chosen coefficient is assumed to apply at all discharges, despite the large changes in flow resistance which occur as discharge varies.

In the second approach the coefficient is calculated by some equation based, to a greater or lesser extent, on a theoretical description of the relevant processes of flow. The potential for accuracy is greater but the method is inevitably more complex and at present only simple flows can be described in this fashion.

This report adopts the second approach. Consequently the characteristics of cobble-bed rivers and the various processes of flow resistance in cobble-bed rivers need to be identified. It is assumed that the boundary of a gravel-bed or cobble-bed river is composed of noncohesive material greater than about 10 mm (0.0328 ft) in diameter and that there are no significant outcrops of bedrock or patches of vegetation. This restricts the following theory to flows within the channel banks. It is also assumed that the only significant bedform is the pool/riffle sequence. Although ripples have been observed in gravel-bed rivers at high discharges (Galay, 1967) they are not common.

Given these restrictions, the velocity of flow is affected by the resistance of the boundary material, by energy losses caused by distortions of the free surface and by changes in flow pattern related to channel cross-sectional shape, longitudinal profile and pattern or planform. The relative influence of these factors, and the processes by which they exert their influence, change with the type of flow and type of channel. Consequently the resistance coefficient has to be calculated by a different flow resistance equation in each different case. Generally, in natural rivers, the area of application of a given equation seems to be defined by the channel slope and the boundary relative roughness (the ratio of the bed material height to the flow depth) or its reciprocal, the relative submergence. Additional limitations may be imposed by such factors as bed material movement and air entrainment.

2.1 SMALL-SCALE ROUGHNESS

Most research has concentrated on flows with small-scale roughness, where depth is at least an order of magnitude larger than the height of the bed material (Plate 1a). In such cases the roughness elements on the boundary act collectively as one surface, exerting a frictional shear on the flow. The shear is translated into a velocity profile, the shape of which is determined by the roughness geometry, channel geometry and any free surface distortions. Using boundary layer theory the profile can be described mathematically and thence related to the resistance coefficient. The general form of the equation for a channel cross section is:

$$\left(\frac{8}{f}\right)^{0.5} = A \log\left(\frac{R}{k}\right) + B \tag{4}$$

where k = vertical roughness height and R/k = relative submergence (American Society of Civil Engineers, 1963). A and B are constants

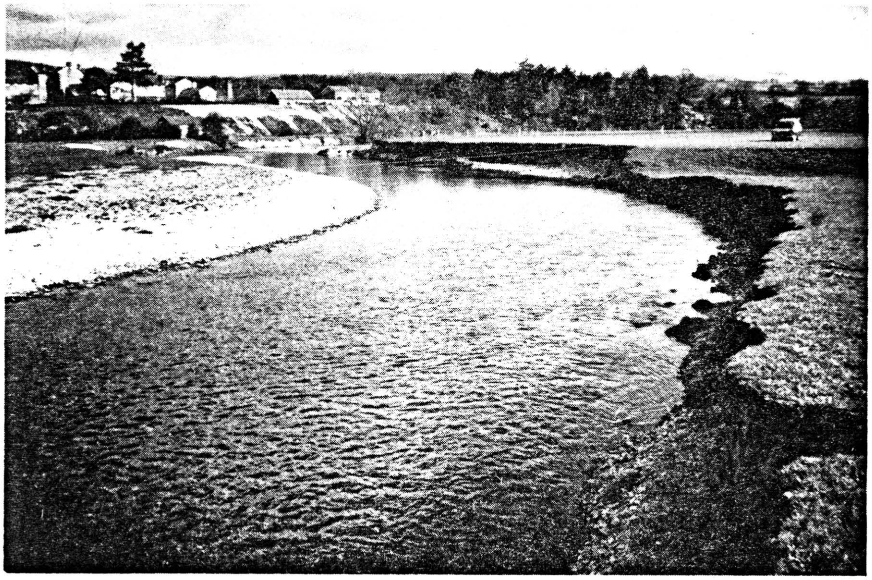

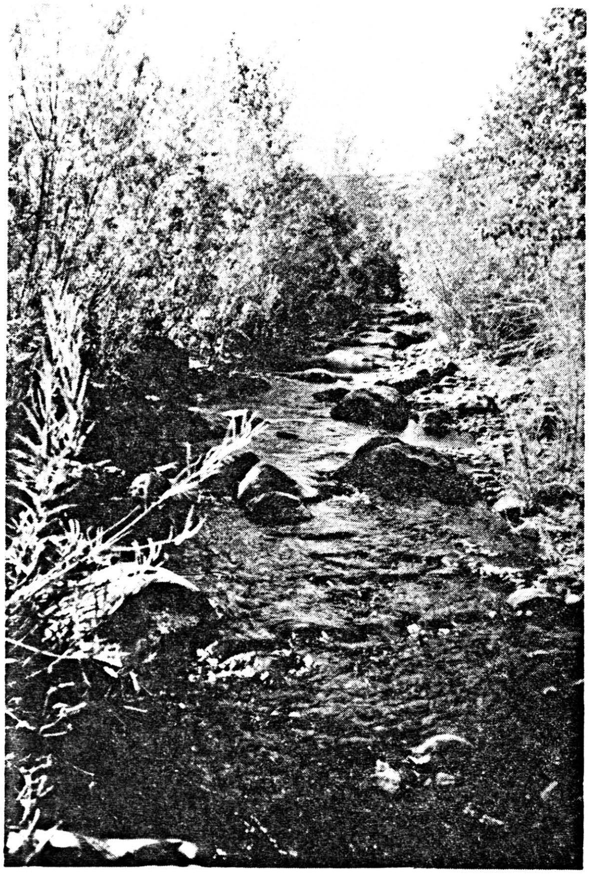

Plate 1. (a) Small-scale roughness and flow in the tranquil regime: River Severn at Caersws, Wales, looking downstream.
(b) Large-scale roughness and flow in the tranquil regime: Reynolds Creek near Reynolds, Idaho, looking upstream.

which have precise theoretical meanings but which in practical hydraulics projects are often empirically derived for the channel under consideration.

Past disciples of this approach have been less than perfect in their consideration of the assumptions underlying boundary layer theory, with the result that no general equation of the form of Equation (4) has been produced (Bathurst, 1977). However, an equation of this form can usually be empirically derived for a given river section.

2.2 LARGE-SCALE ROUGHNESS

In the case of large-scale roughness, where the depth is of the same order of magnitude as the bed material height (Plate 2), the approach based on boundary layer theory can not be used. The velocity profile is completely disrupted and the roughness elements act individually, producing a total resistance based mainly on the sum of their form drags. Wall effects dominate the flow, so roughness geometry and distortions of the free surface around elements have most effect on the flow resistance, while channel geometry is important indirectly and only to the extent that it affects the flow around elements. The semi-logarithmic equation for small-scale roughness does not then apply (Hartung and Scheuerlein, 1967; Scheuerlein, 1973; Ashida and Bayazit, 1973). Preliminary work by Judd and Peterson (1969) and Bathurst (1978) suggests that a more realistic equation is a power law relating the friction factor mainly to functions of roughness geometry.

2.3 INTERMEDIATE-SCALE ROUGHNESS

There is unlikely to be a well-defined boundary between the regions of large-scale and small-scale roughness. Presumably there is a transitional region of intermediate-scale roughness in which flow resistance

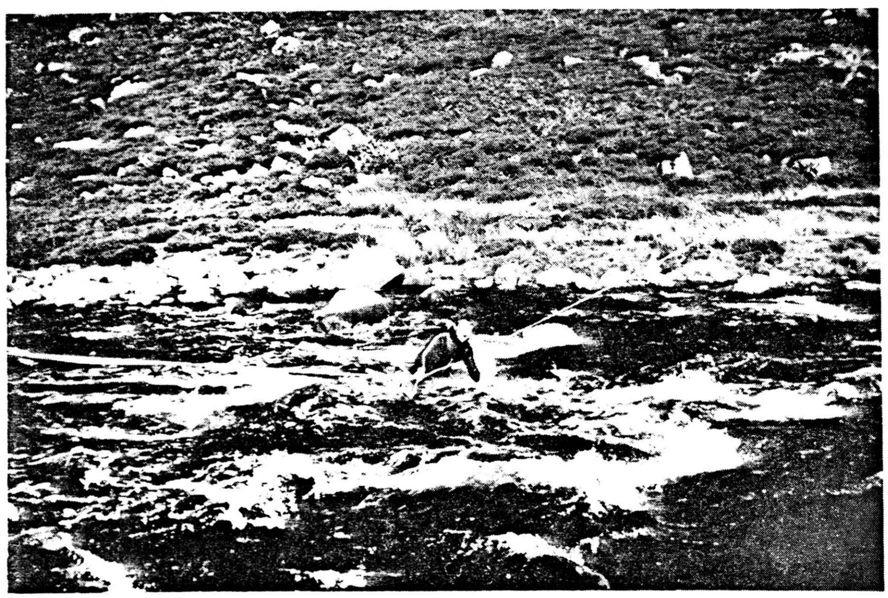

Plate 2. Large-scale roughness and flow in the tumbling regime: River Tees at Whiddybank Farm, England.
(a) Looking upstream.
(b) Looking across the channel.

is determined to a greater or lesser extent by the processes of the two extremes (Plate 3). In this region the resistance equation might be either semilogarithmic in form (Aguirre Pe, 1975) or a power law (Judd and Peterson, 1969).

2.4 LIMITS TO THE ROUGHNESS SCALE

Because relative roughness can change by an order of magnitude as discharge varies, it is possible for a channel section to display more than one scale of roughness. Some of the river sites studied by Judd and Peterson (1969) and Virmani (1973) fall into this category, so the data collected at those sites can be used to delineate approximately the limiting relative roughness of the roughness scales. Accordingly plots of the resistance function, $(8/f)^{0.5}$, against the logarithm of relative submergence are presented in Figure 1. The roughness height is represented by S_{50}, the size of the short axis of the bed material which is bigger than or equal to fifty percent of the short axes by count. Although roughness height is more commonly represented in the literature by the median axis, the short axis is chosen here since, as is mentioned in Section 7.1.6, it is the closer approximation to roughness height. Values of short axis used in Figure 1 were calculated from the values of median axis given in the references according to precepts outlined in Section 11.

Distinct breaks of slope are evident in the plots. At relative submergences greater than 10 to 15 the plots are straight lines. This region should correspond to the region of small-scale roughness in which Equation (4) should apply. At lower relative submergences a different set of straight line plots occurs, presumably corresponding to the region of intermediate-scale roughness. According to the plotted data

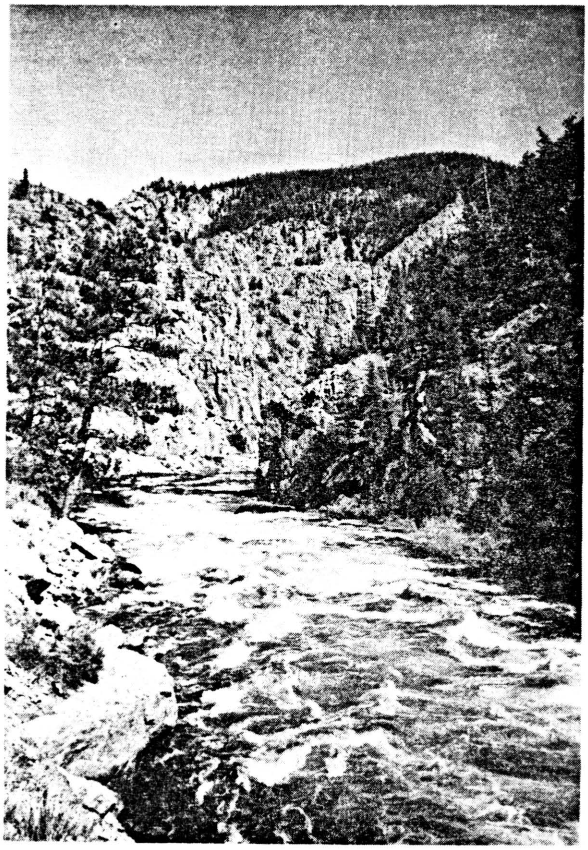

Plate 3. (a) Intermediate-scale roughness and flow in the rapid regime with standing waves: Cache La Poudre River near Poudre Park, Colorado, looking downstream.
(b) Intermediate-scale roughness and flow in the rapid regime: Cache La Poudre River near Rustic, Colorado, looking upstream.

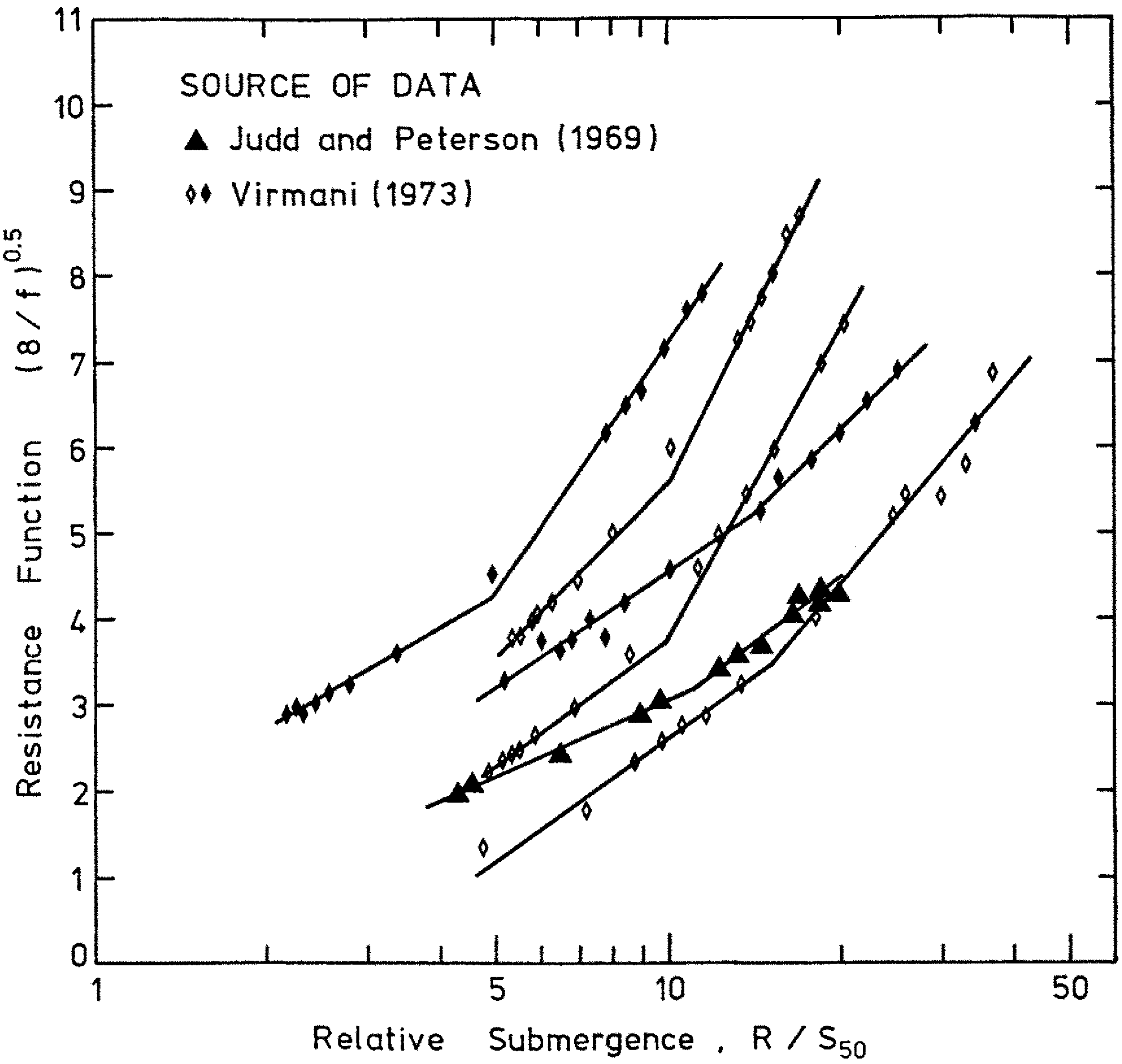

Figure 1. Variation of the resistance function with relative submergence at selected river sites.

the resistance coefficient increases more slowly, as relative submergence decreases, in the region of intermediate-scale roughness than in the region of small-scale roughness.

There are insufficient field data to delineate the boundary between the regions of large-scale and intermediate-scale roughness. However, Bayazit's (1976) laboratory study indicates that it probably occurs at a relative submergence of about three or four. At lower relative submergences the resistance to flow increases more rapidly as relative submergence decreases.

It will be shown later that the lower limit to the region of small-scale roughness is probably determined by the depth at which the proportion of a channel cross section occupied by roughness elements becomes negligible and that the upper limit to the region of large-scale roughness is probably determined by the depth at which the effect of the elements in distorting the free surface becomes negligible.

The relative submergence marking the upper limit to the region of small-scale roughness remains undefined. It may be surmised, though, that in natural channels the limiting relative submergence is likely to be of the order of 100. Considering the range of depths in rivers, larger relative submergences would depend either on the bed material being too small to be classified as gravel or cobble or on the depth being boosted by a high discharge. In both cases the boundary roughness characteristics would be significantly affected by bed forms and it would not then be possible to classify the type of flow and the resistance equation solely in terms of the scale of the boundary material.

One set of Virmani's data in Figure 1 shows the apparent boundary between the regions of small-scale and intermediate-scale roughness to occur at a low relative submergence of about 5. It is possible that the site in question lies in a pool in which depth, and the water surface slope, are determined by the backwater effect and not by the boundary resistance. The resistance coefficient would then have a different relationship with relative roughness from that which it would have in uniform flow. Only where depth is determined by the boundary resistance and the flow is not ponded do the above limits apply.

2.5 CHANNEL SLOPE

In natural channels there appears to be a link between channel slope and the roughness scale. Generally, in channels with gentle slopes the roughness scale tends to be small, while in channels with steep slopes it tends to be intermediate or large. An investigation by Golubtsov (1969) suggests that the division occurs at slopes of 0.1 to 0.4 percent.

There is probably an upper limit to the range of slopes at which large-scale roughness exists in natural channels. At slopes below that limit, the flow can be considered to move in a generally uniform fashion over a channel bed composed of a uniformly distributed layer of material. At higher slopes the flow is characterized by a series of short pools and falls (Plate 4) and the processes of flow resistance are different from those for large-scale roughness. The limiting slope has not been delineated but casual observations by one of the authors (J. C. B.) suggest a value in the region of 10 to 20 percent.

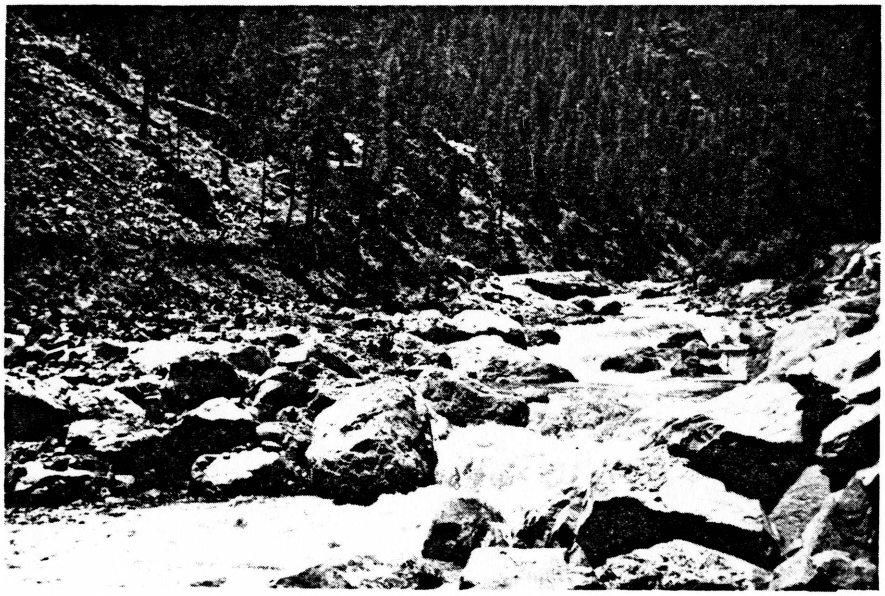

Plate 4. Flow in the pool/fall regime: Big Thompson River near Drake, Colorado, looking upstream.

The classification based on slope is rather vague since, whatever the slope, a change of depth can produce a change in the roughness scale. However, channel slope has a definite effect on the processes of flow. Thus a flow in a channel with a gentle slope is likely to present a more tranquil appearance than would a flow of the same relative submergence in a steep channel, where air entrainment and free surface waves and instabilities are likely to be important. The classification of flows according to roughness scale may therefore have to be subdivided according to channel slope.

2.6 BED MATERIAL CHARACTERISTICS

Different flow resistance equations may be required at different times at the same section because of changes in the bed material characteristics. At relatively low discharges in a river where bed armouring occurs, the finer sediment on the bed surface is removed until a protective layer composed of the larger material remains, overlying finer material. Typically the channel can then be classified as cobble-bed. At higher discharges the larger material is also moved and the finer material exposed. The channel may then be classified as sand-bed. Consequently different flow resistance equations are needed at high and low discharges.

A similar effect can be observed where the land adjacent to a river has a sparse vegetal cover. During most flows the river might be classified, for example, as cobble-bed with large-scale roughness. During a major storm, though, erosion of the surrounding land or collapse of the channel banks could result in the release of enormous amounts of fine sediment to the channel. The cobbles or boulders would then be covered with this sediment and the channel would act as a sand-bed channel until the effects of the storm diminished (Simons, Al-Shaikh Ali and Li, 1979).

In addition to the differences in bed material characteristics caused by changes in the representative material, differences can be caused by bed material movement. Owing to the different processes by which momentum is extracted from the flow, a channel with a moving bed is likely to have a different resistance from an otherwise identical channel with a fixed bed.

In conclusion, roughness scale provides the simplest means of identifying the various types of channel flow and their characteristic processes of resistance but more detailed classifications depend on channel slope and bed material characteristics. A summary is given in Table 1.

TABLE 1.--Categories of Roughness for Inbank Flows in Natural Cobble-Bed Rivers

Type of roughness (1)	Approximate range of relative submergences in uniform flow (2)	Characteristic range of natural channel slopes (3)	Main sources of flow resistance (4)	Sites of occurrence (5)
Pool/Fall	$\leq$ 4?	$\gtrsim$ 0.1	Unknown	Very steep channels
Large-scale	$\leq$ 4	0.004-0.1	Form drag, free surface distortions	Steep channels, riffles
Intermediate-scale	4-15	0.004-0.1	Form drag, boundary shear, free surface distortions, sediment movement	Steep channels, riffles
Small-scale	15-100?	$\leq$ 0.004	Boundary shear, channel geometry, sediment movement	Pools

SECTION 3 FEATURES OF MOUNTAIN RIVERS

Mountain rivers are characterized chiefly by steep slopes and large-scale or intermediate-scale roughness. Owing to the disruption caused by the roughness elements, the flow is locally nonuniform with zones of separation, acceleration and deceleration. However, in a macroscopic sense the flow can be considered uniform on average.

Because of the steep slopes, changes in discharge at a section can bring about large variations in velocity, Froude and Reynolds numbers and relative submergence. Consequently the flows of mountain rivers exhibit considerable variation.

A classification of flows according to Froude number has been constructed by Peterson and Mohanty (1960). Tranquil flow is characterized by subcritical conditions and a generally smooth free surface (Plate 1). It apparently occurs only at channel slopes of less than 3 percent. Tumbling flow, perhaps the most common type, is characterized by the fluid spilling over roughness elements or being funnelled in jets between elements (Herbich and Shulits, 1964). This is possible only if the roughness is large-scale (Plate 2). The flow is accelerated to supercritical past an element and then decelerates to subcritical in a hydraulic jump just downstream of the element (Plates 8 and 9, pages 40 and 41). Consequently distortions of the free surface are evident. Rapid flow is characterized by supercritical conditions everywhere and the flow tends to skim over the elements. The roughness is therefore likely to be intermediate-scale (Plate 3).

A study of tumbling flow by Morris (1968) indicates that stable and unstable regimes can occur. Unstable tumbling flow develops at discharges higher than those for stable tumbling flow and lower than those for rapid flow and is characterized by pulsating surges. The appearance of this flow regime also seems to depend on the areal roughness concentration.

Morris also shows that tumbling flow produces the maximum energy dissipation for a given discharge. Because of the repeated formation of hydraulic jumps the average Froude number for the flow must be near unity and at this value the specific energy (potential plus kinetic) of a given discharge is at a minimum (Henderson, 1966, p. 36). Consequently tumbling flow is constrained to accept a minimum specific energy and must dissipate any excess energy.

In channels which have steep slopes, high discharges tend to produce relatively high velocities at relatively low depths, so Froude numbers of greater than unity can be achieved. Consequently as discharge varies from low to high values, it is possible for all of the flow regimes identified by Peterson and Mohanty to be observed at one section. In comparison, Froude numbers in channels with small-scale roughness and gentle slopes seem to rarely exceed a value of 0.5 and flows remain in the tranquil regime (Leopold et al, 1960).

If the flow is very rough, entrainment of air can be significant (Hartung and Scheuerlein, 1967; Scheuerlein, 1973). This is most likely at rather steep slopes (the upper end of the natural range for large-scale roughness) and is not considered here.

Mountain rivers are not characterized by major bedforms. Well defined pool/riffle sequences are infrequent and the channel usually maintains the aspect of a continuous riffle (Miller, 1958). However, in channels with slopes of greater than 1 percent it is possible for a series of small transverse bars or steps to develop (Judd and Peterson, 1969). These are small weirs which form out of the bed material and may extend all or part of the way across the channel (Plate 5). Their longitudinal spacing seems to depend on the bed material size, the channel slope and the type of channel.

Channel banks are not always very obvious since, particularly at low discharges, the channel cross sections tend to be saucer-shaped (see, for example, the photographs of Miller, 1958; Barnes, 1967; Judd and Peterson, 1969; and Bathurst, 1978). This complements the observation that channels with coarse bed material have high ratios of width to depth by comparison with sand-bed channels (Schumm, 1977, p. 108).

Bed material is transported mainly as bed load and therefore moves either by rolling or saltation. During most flows rates of transport are smaller than in lowland rivers since even the bankfull discharge does not always seem to be sufficient to move much bed material (Miller, 1958) and movement of the whole bed is likely to occur only at very high discharges. Part of the reason for this is that the larger boulders may have arrived at their position in the channel not by fluvial action but by falling from a nearby cliff and are too large to be moved except by extreme floods (Plate 6). They probably act, therefore, to armour and stabilize the bed. When floods of sufficient magnitude do occur, very large quantities of bed material are moved and the channel can change its course considerably (Gole, Chitale and Galgali, 1973).

Plate 5. Steps on a channel bed: River Tees at Whiddybank Farm, England, looking upstream.

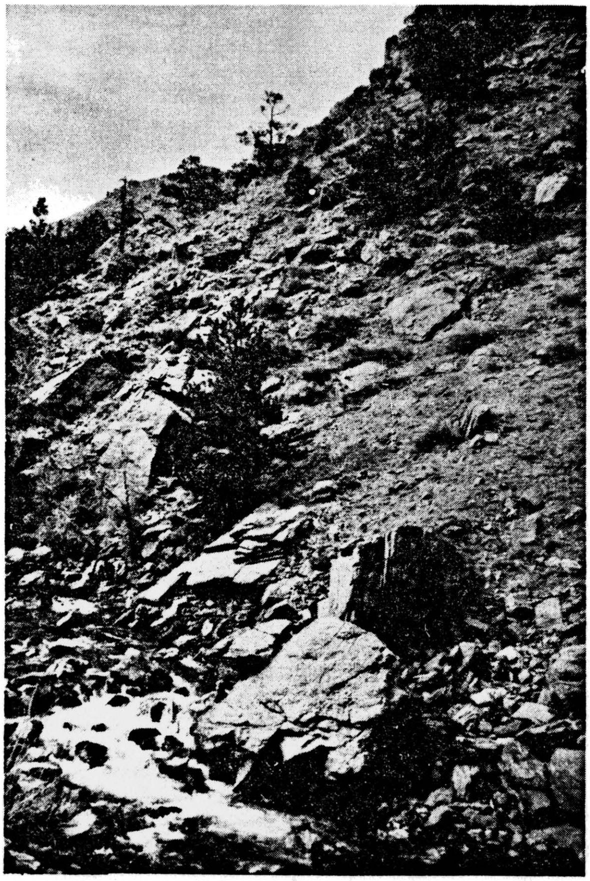

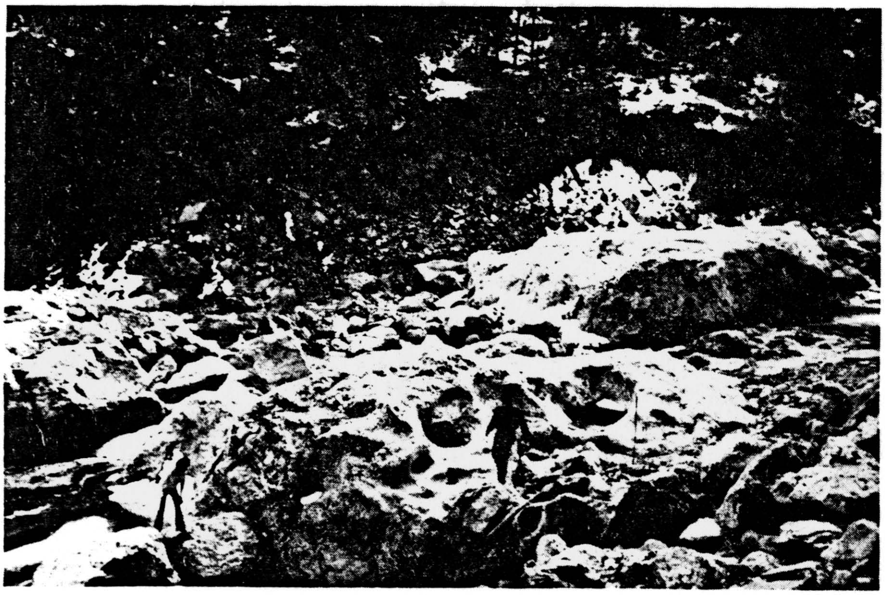

Plate 6. Bed material derived from cliffs above the channel.
(a) Cache La Poudre River near Poudre Park, Colorado.
(b) Big Thompson River near Drake, Colorado; potholes on the boulder in the foreground suggest that the boulder was not moved by the flood of 31 July, 1976 which was an all-time recorded maximum of 883.5 $m^3 s^{-1}$.

SECTION 4 PREVIOUS WORK

4.1 FLOW RESISTANCE

As mountain rivers are characterized by large-scale and intermediate-scale roughnesses, their flow resistance is determined largely by the boundary roughness and its interaction with the channel geometry and the free surface.

A laboratory study by Herbich and Shulits (1964) indicated that the flow resistance is related to the pattern and areal concentration of the roughness elements. The importance of roughness geometry has also been indicated by a widely ranging programme of research carried out at Utah State University, Logan, Utah, in the 1960s and summarized by Judd and Peterson (1969). Using field data, Judd and Peterson showed resistance to be a power function of channel cross-sectional shape (characterized by the ratio of width to depth), roughness concentration λ_1 (the ratio of frontal cross-sectional area of an element to the area of boundary per element) and relative roughness (with roughness height given by D_{50}):

$$\frac{\bar{U}}{(gRS)^{0.5}} = \left(\frac{8}{f}\right)^{0.5} = \text{fn}\ (\lambda) \left(\frac{d}{w}\right)^{7(\lambda_1 - 0.08)} \left(\frac{d}{D_{50}}\right)^{0.333} \qquad (5)$$

where D_n = the size of median axis bigger than or equal to n percent of the median axes by count; $\bar{U}$, d, S and w are respectively the mean velocity, depth, longitudinal water surface slope and surface width of the flow; g = the acceleration due to gravity; and fn() = a function. The equation covered a range of rivers but it suffers from the drawback that the function of roughness concentration is poorly defined.

The pattern of roughness concentration was further studied by Overton, Judd and Johnson (1972). In a laboratory study they found that the maximum flow resistance is provided by a random, rather than a regular, distribution of elements. The random patterns appear visually like the patterns assumed by the larger elements in a natural channel, which suggests that natural channels operate in such a way as to maximize their resistance.

Calhoun (1975) concentrated on the relationship between flow resistance and roughness size distribution, shape and wake effects. In his approach the smaller elements were considered as a small-scale background roughness exerting a boundary shear stress on the flow and the larger elements were considered as a large-scale roughness acting via their form drags. Statistical techniques were applied to calculate the flow resistance at several field sites. However, this method is probably valid only where there is a distinct difference in size between the large and small elements and the size distribution is effectively bimodal. In many cases this is not so and the distinction between large and small elements is then more difficult to ascertain objectively.

Simpson (1978) used field data to derive a regression equation for the Chézy resistance coefficient:

$$\log C = 1.70 - 0.58 \left(\frac{\phi}{R}\right) - 3.34\ S \tag{6}$$

where C = the Chézy resistance coefficient and ϕ is a measure of the roughness size determined by fabric analysis (Briggs, 1977, Chapter 5). Variant equations were also produced to account for the effects of rising and falling stages. The equations fit the data well but it should be noted that the correlation with channel slope has no direct physical meaning. Slope itself is not a resistive factor but it does influence those factors, such as the range of Froude numbers and roughness scales at a given site, which determine the processes of resistance.

Bathurst (1978) enlarged upon the approach of Judd and Peterson. In that approach roughness concentration, λ_1, is calculated by considering all the elements on the bed. Bathurst showed that roughness concentration and its resistive effects change with relative submergence and he therefore calculated concentration for only those boulders which protrude through the flow. Using field data from sites with similar roughness size distributions and roughness shapes and a restricted range of Froude numbers, he showed that:

$$\lambda_1 = 0.139 \log \left(1.91 \frac{D_{84}}{R}\right) \tag{7}$$

Consequently he was able to modify Equation (5) so that flow resistance was related to just relative submergence and channel shape. For his data:

$$\frac{\bar{U}}{(gRS)^{0.5}} = \left(\frac{8}{f}\right)^{0.5} = \left(\frac{R}{0.365\ D_{84}}\right)^{2.34} \left(\frac{w}{d}\right)^{7(\lambda_1\ -\ 0.08)} \tag{8}$$

The constants of the relative submergence term would be different at other sites but empirical calibration should enable Equation (8) to apply to individual sites with large-scale roughness. However, a more general equation should account for the effects of roughness shape and size distribution and of a wider range of Froude numbers. In addition the reasoning behind the modified Judd and Peterson channel shape parameter, $(w/d)^{7(\lambda_1 - 0.08)}$, needs to be clarified. Justification for use of this parameter was that it accounts for the variation of drag from boulder to boulder at a section. The parameter is certainly needed to resolve differences among the data but the method of its derivation and its physical meaning are unclear. For example, at Bathurst's sites, ratios of width to depth of up to a hundred were noted and at such magnitudes it would not be expected that the ratio would have any effect on the flow. Similarly it should be possible to apply the resistance theory to overland flow, for which the ratio has no meaning. It seems likely, therefore, that the parameter is not the fundamental term describing whatever process is at work but happens to be a good representation of that process for channel flows.

4.2 BED MATERIAL MOVEMENT

This report is concerned mainly with the flow resistance equation but, in order to provide a more complete picture of the hydraulics of mountain rivers, a short study of the processes of bed material movement is also included.

Most investigations of sediment transport have concentrated on sand-bed rivers. Not much is known about bed material movement in cobble-bed rivers and almost nothing is known about mountain rivers. Formulae describing bed material movement in sand-bed rivers do not seem to apply to mountain rivers.

The best known formula describing initiation of motion (in sand-bed rivers) is the Shields formula (e.g., Simons, and Sentürk, 1977, p. 409):

$$S_c = \frac{\tau_c}{(\gamma_s - \gamma)\, D_n} \tag{9}$$

where S_c = the critical Shields parameter; τ_c = the critical shear stress; γ_s = specific weight of the particle; γ = specific weight of the fluid; and D_n = bed material size. For fully developed rough flow over sand beds ($u_* D_n/\nu \gtrsim 70$ to 500, where ν is the kinematic viscosity of the fluid), the Shields parameter is independent of Reynolds number and is equal to about 0.06 (at least until $u_* D_n/\nu = 1000$). However, investigations by Ashida and Bayazit (1973) and Bayazit (1978) have shown that at low relative submergences, in steep channels with gravel beds, the Shields parameter varies with relative submergence. The lower the relative submergence, the higher is the critical Shields parameter. Apparently this is because the critical value of the instantaneous flow velocity needed for sediment movement is achieved at higher bed shear stresses by comparison with flows in gently sloping channels.

A study by Aguirre Pe (1975) also shows that, in steep channels with large-scale roughness, the critical Shields parameter can not be considered constant. An eventual solution to the problem of initiation of motion may therefore have to depend on a more theoretical approach accounting for the relevant processes of turbulence, lift and drag (Cheng and Clyde, 1972).

Bed material movement has received little attention. Laboratory work reported by Li et al., (1977) shows that in steep channels, with bed material composed of sand and gravel, sediment discharge varies as:

$$Q_s = \Delta\, Q \tag{10}$$

where Q_s = sediment discharge; Q = water discharge; and Δ = a constant which varies with channel slope. However, this work did not investigate the effects of bed armouring or restrictions in the supply of sediment, both of which appear to be important factors in mountain rivers.

Kellerhals (1967) and Milhous and Klingeman (1973) have shown that bed armouring regulates the supply and storage of bed material as discharge varies. Removal of the armouring layer at high discharges causes a shift in the relationship between sediment and water discharges and alters the flow resistance.

Nanson (1974) found that bed load in mountain rivers is not controlled solely by bed and hydraulic variables (as is usually assumed for traditional bed load formulae). The quantity of sediment available to be transported is also important and, as this quantity is often limited, the rivers are likely to be more than competent to transport the material supplied to them.

Because of the restrictions in sediment supply and because movement of the whole bed occurs only at high discharges (Miller, 1958), traditional bed load formulae overpredict the sediment discharge in mountain rivers by several orders of magnitude (Simpson, 1978; Haddock, 1978). To overcome this deficiency Simpson investigated various parameters which might affect the sediment supply and characteristics and, using field data, developed a regression equation giving sediment discharge, Q_s, as:

$$\log Q_s = -10.20 + 1.64 \log Q + 0.58\ Dd + 8.84 \sin Sg \qquad (11)$$

where Dd = drainage density and Sg = average valleyside slope. Similarly Haddock, using a wider range of data from the same area, found that:

$$\log Q_s = -5.97 + 1.45 \log Q + 0.35\ Dd \qquad (12)$$

Sediment discharge in mountain rivers therefore appears to depend on geomorphic parameters, which determine the supply of sediment, as well as on hydraulic parameters.

SECTION 5 THEORETICAL APPROACH TO FLOW RESISTANCE

Flow resistance in mountain rivers is dominated by wall effects and is determined mainly by the profile drag of the elements. (Profile drag is the sum of form drag and skin friction, the latter being negligible compared with the former over the range of Reynolds numbers observed in rivers.) The drag of individual elements is determined by processes of fluid mechanics while the combined effect of the elements on the total drag of the boundary is determined by processes of wall geometry related to roughness geometry, or disposition of the elements on the bed, and channel geometry.

The profile drag, D, on a single, isolated bluff body, such as a boulder, in a uniform flow of velocity, U, is related to a drag coefficient, C_D, by the equation:

$$D = \frac{1}{2} \rho A_F U^2 C_D \qquad (13)$$

where A_F = the frontal cross-sectional area of the body projected against the flow (Duncan, Thom and Young, 1970). If the element is fully submerged, the drag coefficient varies with the position of the separation point of the boundary layer on the body. In turn that position is determined mainly by element shape and structure (surface texture and roundness) and by Reynolds number. If the element interacts with a free surface, the drag coefficient also depends on the distortions of the surface and varies with Froude number and relative submergence.

Where the flow is both through and over a closely packed layer of elements, the picture is complicated by interactions between the elements. In order to calculate the total profile drag, and thence the flow resistance, it is necessary to know how many of the elements have a significant drag and what effects neighbouring elements and the channel boundary itself have on the flow past a given element. These effects depend on the boundary roughness geometry and on the channel geometry. In addition it is necessary to know how movement of the bed material affects the drag.

The factors which determine the flow resistance and the rate of change of flow resistance with discharge may therefore be listed as:

1. Reynolds number and element structure,
2. Froude number and relative submergence,
3. roughness geometry,
4. channel geometry, and
5. bed material movement.

The relative importance of these factors alters with depth and discharge.

Factors (1) and (2) are discussed in Section 6 and factors (3), (4) and (5) are discussed in Section 7.

SECTION 6 PROCESSES OF FLUID MECHANICS

In this section the processes of fluid mechanics by which the drag of each roughness element is determined are considered.

6.1 REYNOLDS NUMBER AND ELEMENT STRUCTURE

The form drag of an element varies according to the position of the separation point of the boundary layer on the element. Generally the nearer that the separation point is to the front of the element, the bigger the wake and the larger the drag coefficient. The position of the separation point depends on the characteristics of the boundary layer and these in turn are determined by Reynolds number and element shape and structure.

At Reynolds numbers, $\bar{U}D_n/\nu$, (where D_n = the diameter of the element and ν = the kinematic viscosity of the fluid) of less than a certain value, the boundary layer is laminar, even if the external flow is turbulent. Laminar boundary layers separate relatively early so the element has a relatively high drag coefficient. As Reynolds number is increased above the critical value, transition to a turbulent boundary layer occurs. Turbulent boundary layers separate relatively late so the drag coefficient is then relatively low. In the laminar region the drag coefficient is approximately constant at Reynolds numbers between about 10^3 and the critical value. In the turbulent region the drag coefficient remains approximately constant or rises rather gradually as Reynolds number increases. Qualitatively, the magnitude of the coefficient depends on the shape of the element (e.g., Morris, 1959).

The critical Reynolds number at which transition begins, varies with the surface texture of the element. Generally the rougher the surface, the lower is the critical Reynolds number. Thus, for a smooth, infinitely long cylinder, transition occurs abruptly once the Reynolds number equals about 10^5. For a rough cylinder, transition can occur at Reynolds numbers as low as 3×10^4 (Schlichting, 1968, p. 622).

Also, greater turbulence in the main flow tends to cause transition at relatively low Reynolds numbers, perhaps as low as 5×10^4 for cylinders (Shen, 1973, p. 3.16). This is likely to be important in mountain rivers where considerable turbulence is generated.

Another factor is the influence of neighbouring objects. According to Richter and Naudascher (1976) the more concentrated the elements, the lower is the critical Reynolds number likely to be.

Finally, the effects of the wall and the finite size of natural elements in causing three-dimensional flow about the elements are likely to be important. The work of Flammer, Tullis and Mason (1970) shows that, for a hemisphere lying on a boundary and submerged in a free surface flow, transition occurs gradually over the range of Reynolds numbers of about 4×10^4 to 2×10^5. The drag coefficient therefore decreases gradually over this region.

Sensitivity to the effects of transition is reduced if an element is angular or if its shape is more cubical than spherical. The position of the flow separation point is then likely to be attached permanently to one edge with the result that the drag coefficient is practically constant.

From the foregoing it seems that the lowest critical Reynolds number marking the onset of transition is about 3×10^4. Consequently the range of Reynolds numbers in river flows (typically 10^4 to 10^6) includes the transitional region in which drag coefficient is not constant (unless the flow separation point is permanently fixed). The effect of Reynolds number should therefore be accounted for in the resistance equation.

6.2 FROUDE NUMBER AND RELATIVE SUBMERGENCE

An element which protrudes through or nearly through the free surface causes distortions in the surface which represent an energy loss and affect the drag coefficient of the element. The drag generated in this way varies with Froude number and relative submergence.

Previous studies have been concerned mainly with the wave drag related to the pattern of waves around an element and have not considered the effects of larger distortions such as hydraulic jumps. Since hydraulic jumps are a characteristic feature of mountain rivers their contribution to drag cannot be neglected. Consequently in this report the total drag caused by the distortions of the free surface around elements is considered to include both wave drag and the drag of hydraulic jumps and is referred to as free surface drag.

6.2.1 Wave Drag

Examples of wave drag on bridge piers are reported by Hsieh (1964) and Rouse (1965). In such cases depth is large enough that wall effects may be neglected and surface waves can develop freely around the piers. The waves cause differences in depth, and therefore in hydrostatic pressure, between the upstream and downstream faces of each pier and thereby create a pressure drag. The wave pattern and drag change with Froude number and the concentration of the piers.

6.2.2 Free Surface Drag of a Single Element

Studies of flows around bridge piers offer some insight into wave drag but they do not elucidate the variation of free surface drag of a roughness element lying on a surface. In that case wall effects and three-dimensional effects resulting from flow over the element need to be considered. Flammer, Tullis and Mason (1970) studied the flow about a single hemisphere on a surface and concluded that three distinct regions of free surface distortions exist (Figure 2).

Pronounced free surface effects occur at relative submergences of less than about 1.6 and Froude numbers of less than 1.5. Generally the drag coefficient depends on gravitational forces and is a function of Froude number and relative submergence. At Froude numbers in excess of 1.5, free surface distortions do not appear to contribute significantly to the drag and viscous forces may then be significant.

Moderate free surface effects occur at relative submergences of 1.6 to 4 and Froude numbers of less than 1.5. Both gravitational and viscous forces affect the drag coefficient so if the Reynolds number lies in the transitional range, the drag coefficient is a function of Froude number, Reynolds number and relative submergence.

Negligible free surface effects occur once the relative submergence exceeds a value of about 4. Viscous forces predominate so the drag coefficient varies mainly with Reynolds number. Since a relative submergence of about 4 marks the boundary between large-scale and intermediate-scale roughness, it seems likely that the physical explanation for that boundary is that it marks the relative submergence at which the effect of the elements on the free surface becomes negligible.

The data of Flammer, Tullis and Mason show that, at Froude numbers of less than 1.5, the drag coefficient, for a given Froude number, increases as the relative submergence decreases. On the other hand, for a given relative submergence, as Froude number increases, the drag

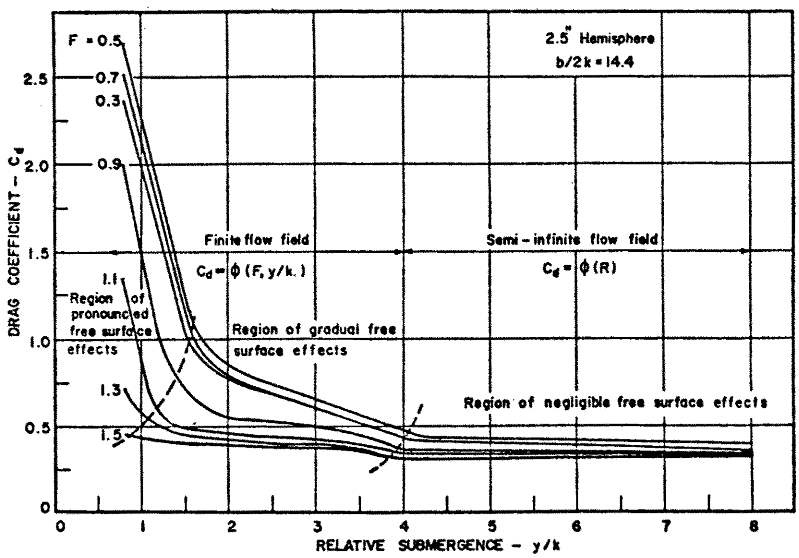

Figure 2. Variation of drag coefficient with Froude number and relative submergence for a hemisphere on a surface. (After Flammer, Tullis and Mason, 1970). For this diagram only: b = channel width; C_d = drag coefficient; F = Froude number; k = hemisphere height; R = Reynolds number; y = depth; and ϕ ( ) = a function.

coefficient first rises to a peak value and then decreases. The Froude number corresponding to the peak drag coefficient varies with relative submergence. At relative submergences of less than about 0.5 the peak coefficient occurs at a Froude number of about unity. At relative submergences of about 0.8 to 4, the peak coefficient occurs at Froude numbers of 0.5 to 0.6. Obviously the relative submergence influences the mechanism by which free surface drag develops and it is suggested here that the mechanism is related to the generation of hydraulic jumps rather than, as for bridge piers, surface waves.

6.2.3 Generation of Hydraulic Jumps

At low relative submergences (less than 0.5) the flow around an element resembles the flow about a bridge pier in that there is no flow over the element. However, the flow about a bridge pier is not greatly affected by wall effects (except at very low depths) and a surface wave pattern can develop freely. In the flow about a roughness element, wall effects are very important and depths are shallow enough that changes in depth caused by distortions of the free surface can radically alter the local Froude number.

As long as the mainstream Froude number is less than about 0.5, a free surface wave pattern can develop about the element, upstream of the point on the element at which separation of the flow occurs and the wake begins (Figure 3a and Plate 7). However, by analogy with compressible air flow mechanics (Duncan, Thom and Young, 1970, p. 437 and Chapter 9) above that limiting number there should be an abrupt increase in drag due to the localized appearance of hydraulic jumps. In this transcritical region, where the mainstream Froude number is near unity, acceleration of the flow between and around elements should cause

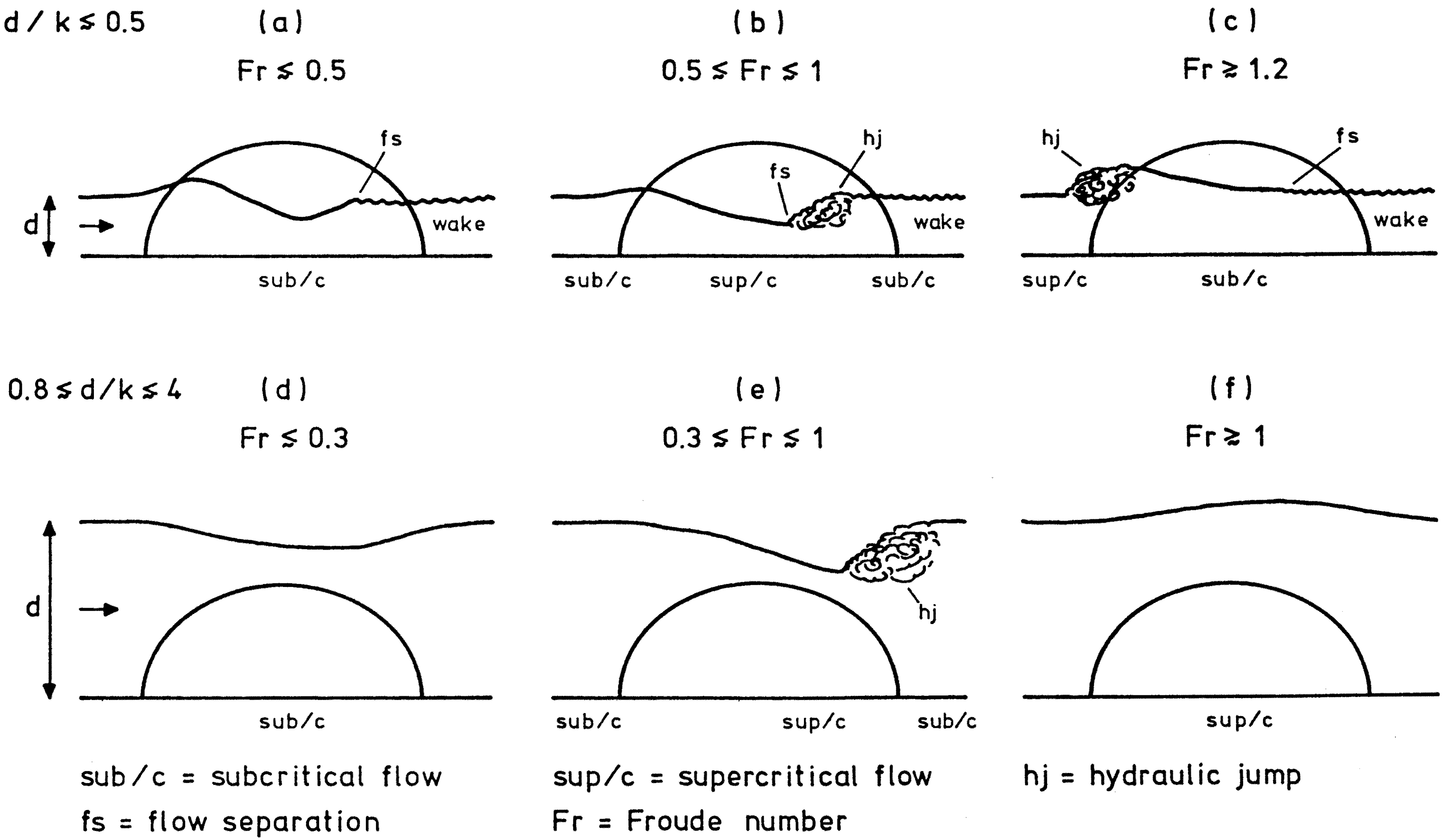

Figure 3. Theoretical free surface configurations for flow past a single roughness element of height, k, in the large-scale roughness region at various Froude numbers. Flow is from left to right.

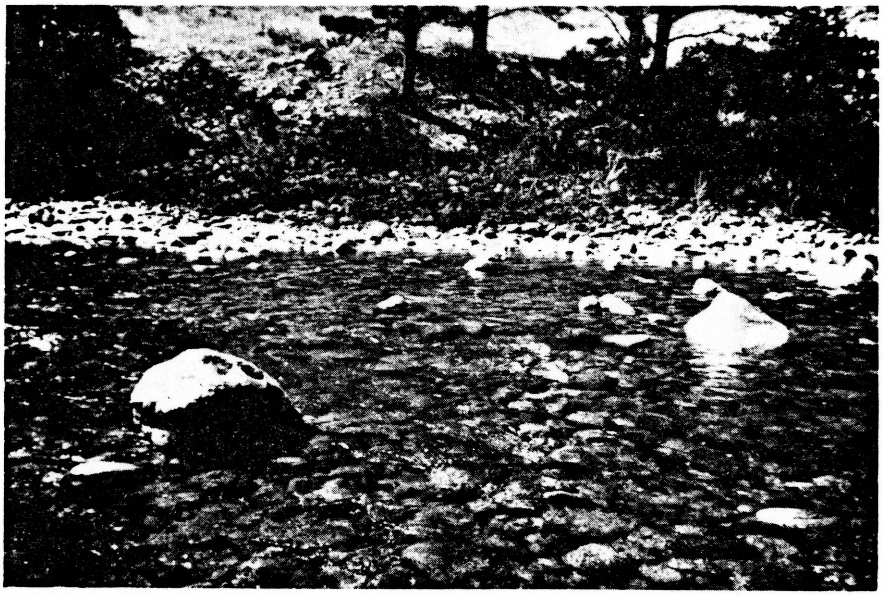

Plate 7. Subcritical, tranquil flow past protruding roughness elements: Cache La Poudre River near Ted's Place, Colorado, with flow from right to left.

the flow to become locally supercritical. However, because the mainstream Froude number is less than unity the region of supercritical flow can be maintained only next to an element. Once the flow separates from the element there is a longstream discontinuity between the supercritical flow and the relatively stationary fluid in the wake. Also the flow outside the wake decelerates as it leaves the element. Consequently a hydraulic jump forms at the discontinuity, converting the flow to subcritical (Figure 3b and Plate 8). The jump extends sideways from the element and, because of the considerable energy loss, is responsible for a high drag coefficient. By analogy with compressible air flow mechanics, the jump should increase in lateral extent and the drag coefficient should continue to increase as Froude number increases, until the mainstream Froude number becomes unity. A further increase in Froude number should result in a decline in drag coefficient, as observed by Flammer, Tullis and Mason (1970).

The upper limit to the transcritical range is determined by the mainstream Froude number at which a hydraulic jump becomes stationed directly in front of an element (Figure 3c and Plate 9). This jump (different from the jump just described) forms to facilitate the transition from the supercritical mainstream flow to the stagnation point on the upstream face of the element. In the supercritical range this jump and its associated wave train are the principal cause of the free surface drag of protruding elements.

At relative submergences of greater than about 0.8, the roughness elements can be overtopped by significant amounts. It seems probable then that, in the transcritical range, hydraulic jumps are more likely to appear above or behind the elements rather than around their sides

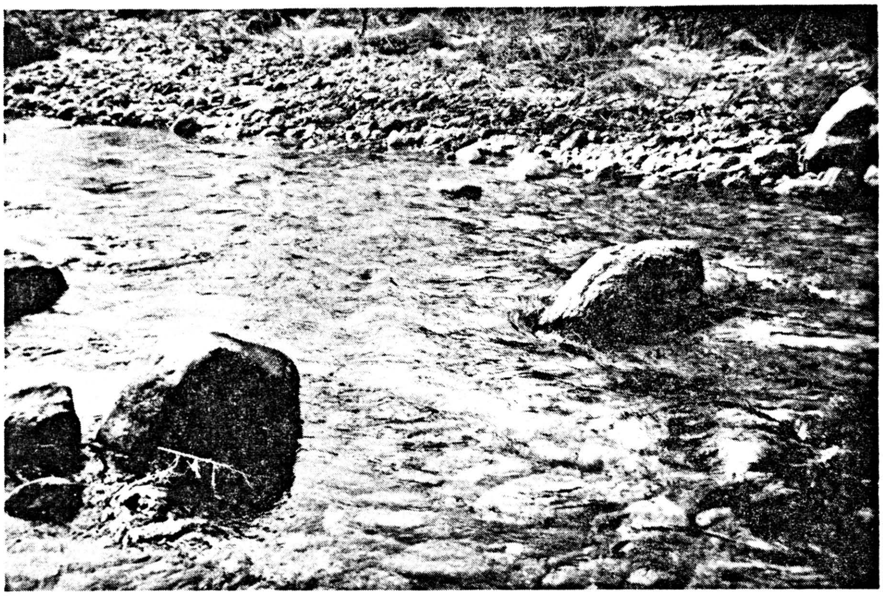

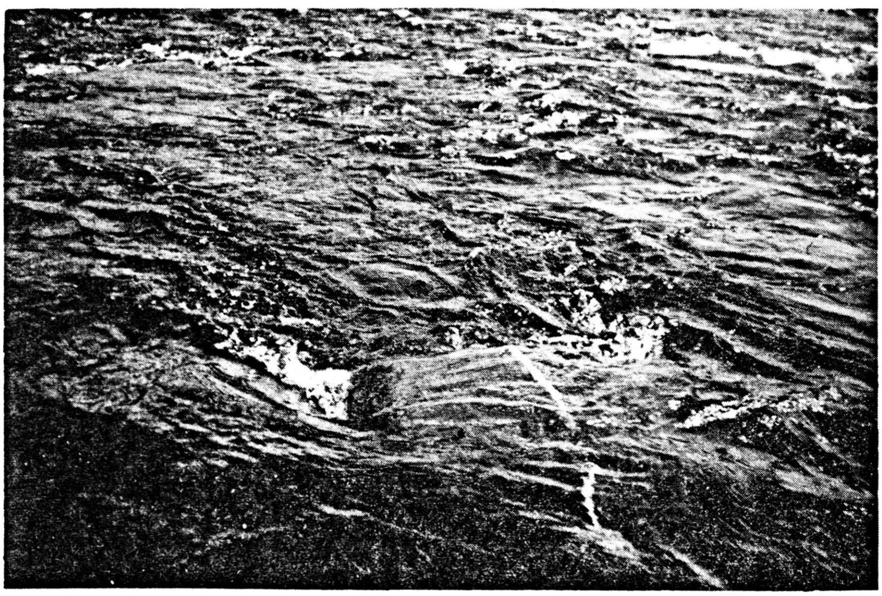

Plate 8. Transcritical flow past protruding roughness elements, with small side hydraulic jumps.
(a) Boulder at right centre: Cache La Poudre River at Poudre Falls, Colorado, with flow from left to right.
(b) River Tees at Cronkley Pasture, England, with flow into the picture.

Plate 9. (a) Transcritical flow over a submerged element, with a downstream hydraulic jump, at left foreground. Supercritical flow past a protruding element, with a bow hydraulic jump, at right centre.
(b) Supercritical flow past a protruding element, with a bow hydraulic jump, at left foreground.
Cache La Poudre River near Poudre Falls, Colorado with flow from left to right.

(Figure 3e and Plate 9a). This suggests that, by contrast with flow about protruding elements, the region of localized supercritical flow about a submerged element is likely to be limited in lateral extent to the width of the element and that consequently the hydraulic jump does not grow laterally as Froude number increases. On the other hand, because of the relatively large differences between depths over the wall and over the elements, relatively large variations in local Froude number are possible. Consequently, localized supercritical flow is likely to be induced at mainstream Froude numbers lower than those at which it would be induced in flows about protruding elements.

For a given lateral width of hydraulic jump, the lower the mainstream Froude number, the greater is the amount of energy which must be lost in the hydraulic jump to decelerate the localized supercritical flow to the subcritical mainstream flow. Consequently, as the width of a hydraulic jump over a submerged element is approximately constant, the overall free surface drag is likely to decrease as the mainstream Froude number approaches unity. The drag coefficient should therefore reach a peak value at a mainstream Froude number of less than unity, probably at the lower end of the transcritical range. This agrees with the observations of Flammer, Tullis and Mason (1970).

As the mainstream Froude number increases, the relative energy loss in the hydraulic jump decreases until, as the whole flow becomes supercritical, the jump disappears (Figure 3f). Because the elements are submerged, no jump develops at the upstream face of the element and a mainstream Froude number of unity therefore marks the upper end of the transcritical range. In the supercritical range there are likely to be severe distortions of the free surface above the element, typified by a system of standing waves (Plate 3a).

The foregoing analysis, summarized in Figures 3 and 4, shows that the roughness elements exhibit their highest drag coefficient in the transcritical range. Since the transcritical range corresponds to the region of tumbling flow, the analysis supports Morris's (1968) assertion that energy dissipation is greatest in tumbling flow.

6.2.4 Free Surface Drag of a Rough Boundary

The foregoing applies mainly to single elements. Differences are likely in the behaviour of a roughness bed of closely packed elements in which the elements can vary in shape, size and concentration. The drag coefficient of individual elements may well vary approximately along the lines described, initially increasing as Froude number increases and then decreasing. However, the same might not be true of the bed as a whole. In rivers, increases of Froude number at a section are usually caused by increases of discharge and are therefore accompanied by increases in depth and relative submergence. While the increase in Froude number might initially act to cause an increase in drag coefficient (Figure 4), that increase is likely to be masked entirely by the decrease in drag caused by the increasing relative submergence (Figure 2). Also, as Froude number continues to increase to near critical values, it acts to reduce the drag. In addition, a consequence of the increase in depth is that the number of protruding elements with significant free surface drag decreases. Thus as Froude number, or discharge, increases at a section, both the drag of individual elements and the number of significant elements are likely to decrease, with the result that the overall free surface drag should also decrease.

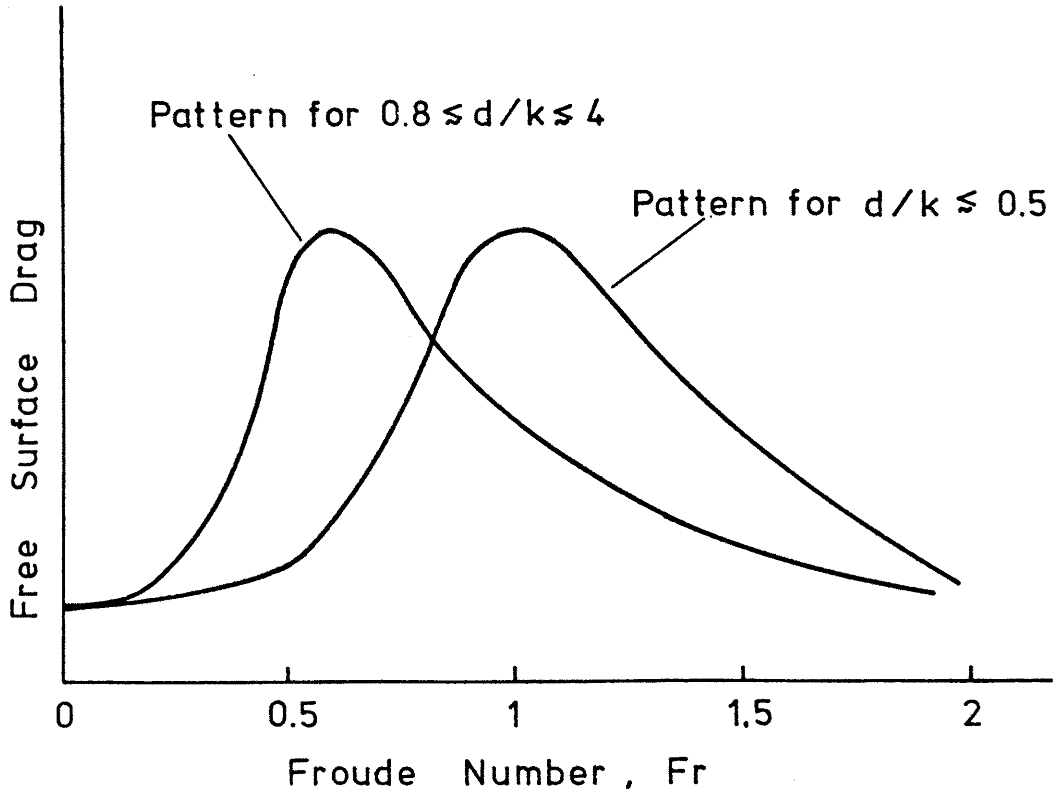

Figure 4. Theoretical variation of free surface drag with Froude number and relative submergence for a single roughness element.

6.2.5 Free Surface Instabilities

To conclude this section, brief mention is made of free surface instabilities. These are not directly connected with the distortions of the free surface around elements but appear as roll waves at high Froude numbers (Liggett, 1975). They can significantly affect local conditions by increasing depth and, probably, promoting bed material movement and presumably represent an energy loss. However, in turbulent flows, roll waves do not seem to develop until the Froude number approaches a value of two and Froude numbers of this magnitude are unusual in natural channels. Also extreme boundary roughness may further delay the onset of instability, so free surface instabilities are unlikely to be important in mountain rivers.

SECTION 7 PROCESSES OF WALL GEOMETRY

In this section the processes by which roughness and channel geometries determine the combined effect of the elements on the flow resistance are considered.

7.1 ROUGHNESS GEOMETRY

Roughness geometry, or the disposition of the elements on the boundary, determines the degree to which each element can affect the flow and consequently the proportion of the bed material which has a significant effect on the flow. It therefore determines the overall effect of the boundary on the flow. For nonuniform bed materials typical of those in rivers it depends on the areal concentration of the elements and their size distribution and shape (or sphericity).

7.1.1 Roughness Concentration

Roughness concentration can be given as the ratio of either, the average frontal cross-sectional area or, the average basal plan area of the elements, to the area of bed per element. Frontal concentration, λ_1, is:

$$\lambda_1 = \frac{\sum_{1}^{n} A_F}{A_{bed}} \tag{14}$$

and basal concentration, λ_2, is:

$$\lambda_2 = \frac{\sum_{1}^{n} A_B}{A_{bed}} \tag{15}$$

where A_F = wetted frontal cross-sectional area; A_B = basal plan area; and there are n elements on an area of bed, A_{bed}. Basal concentration is related to the number of elements per unit area. Frontal concentration, by invoking the use of frontal cross-sectional area, is related to the drag of the elements via Equation (13).

Various flume studies have shown that, for a given material, the relative influence of the roughness elements on the flow resistance depends mainly on their concentration (e.g. Rouse, 1965; Koloseus and Davidian, 1966). At low concentrations individual elements can exhibit their maximum resistance. At high concentrations the resistance of individual elements is reduced because of wake interference effects. Consequently the flow resistance of the boundary varies with roughness concentration. However, the processes by which roughness concentration was changed in the flume studies and by which it changes in rivers are different. In the laboratory studies changes in concentration depended on the operator removing or adding elements. This is not the case in rivers where, until sediment movement begins, the disposition of the elements is constant. Instead, at a site with a given bed material, concentration varies with depth. This is because the wetted frontal cross-sectional area of an element can change with depth, thereby altering the frontal concentration.

Also, in a closely packed sediment with a nonuniform size distribution, typical of river sediments, the smaller elements tend to lie in the wakes of the larger elements. Their drag is insignificant and does not contribute to the flow resistance. Consequently roughness concentration should not be calculated for all the elements on the bed (as it usually is for laboratory flows) but should be calculated as an effective concentration taking account of the differing importance of individual boulders.

7.1.2 Effective Roughness Concentration

Calculation of an effective roughness concentration can be achieved by considering the concentration of only those elements which project significantly into the flow. It may not be possible to specify such elements precisely since the criteria by which that might be accomplished are uncertain. However, the factors which determine the number of significantly projecting boulders can be isolated and a function of effective roughness concentration constructed accordingly.

At any given site, the principal determining factor is relative roughness. It can be imagined that, whatever criteria are used, the lower the depth, the greater is the number of significantly projecting elements. At depths low enough that the smaller elements can protrude through the free surface, the smaller elements project into the flow as much as do the bigger elements. As depth increases, the degree by which the smaller elements project into the flow decreases and fewer elements can be considered significant. This is tantamount to decreasing the value of n in Equations (14) and (15), so the roughness concentration falls. Eventually, at large relative submergences, even the bigger elements are insignificant and the roughness becomes small-scale, affecting the flow by boundary shear rather than by form drag. The effective roughness concentration is then negligibly small.

This concept is similar to that of Bathurst (1978) in which roughness concentration is set equal to the physical concentration of only those elements which protrude through the flow and is related directly to relative roughness (Equation (7)). However, the effective roughness concentration is a less physically obvious, more theoretical, parameter which is intended to apply to submerged as well as to protruding elements.

Effective roughness concentration at a given site should therefore vary directly with relative roughness. The rate of change, though, should vary from site to site according to the size distribution of the elements while the magnitude at any given relative submergence presumably depends on the number of elements and their shape.

7.1.3 Bed Material Size Distribution

In a bed material of uniform size distribution, each element has the same effect. Consequently, as depth increases from zero, all the elements remain equally significant, the number n in Equations (14) and (15) does not vary, so the frontal roughness concentration increases until the elements are submerged. The effective roughness concentration should also increase. As depth continues to increase, the elements have a decreasingly significant effect on the flow so the effective roughness concentration should then fall.

With a less uniform material, frontal roughness concentration would initially rise as depth increased from zero but it should begin to fall before all the elements are covered because the smaller elements become submerged and are no longer included in the calculation. Similarly, the number of significantly projecting elements decreases and so therefore does the effective roughness concentration.

The greater the size range the less steep would be the rate of fall since, for a given mean element size, a material with a wide size range would extend its effect up to a greater relative submergence than would a material with a small size range. This is demonstrated using the five roughness bed materials of this study (which are described later). For the purposes of the explanation, concentration is characterized by the frontal roughness concentration of the protruding elements. Theoretical values of concentration for the five bed materials are calculated in Appendix A and the relationship with relative submergence is presented in Figure 5. The 2.0 and 2.5 inch materials have significantly more uniform size distributions than do the 0.5, 0.75 and 1.5 inch materials and the diagram shows that, over the region where roughness concentration falls as relative submergence increases, the rate of change is greater for these more uniform materials. For a completely uniform material the fall would be instantaneous at a relative submergence of unity.

7.1.4 Bed Material Shape

Roughness shape affects the magnitude of the roughness concentration by determining the wetted frontal cross-sectional area of the elements. It can be imagined that, at any given relative submergence, an element of, say, elliptical cross section has a greater wetted frontal cross-sectional area than does, say, a triangular element of the same height and basal width (Figure 9, page 63). Consequently, at any given depth a bed of elliptical elements has a higher frontal roughness concentration than does a bed of triangular elements. In general therefore, the more cubical the element cross section, the greater is the concentration.

7.1.5 Number of Elements

Although not all the elements are included in the effective roughness concentration and the number that are included decreases as

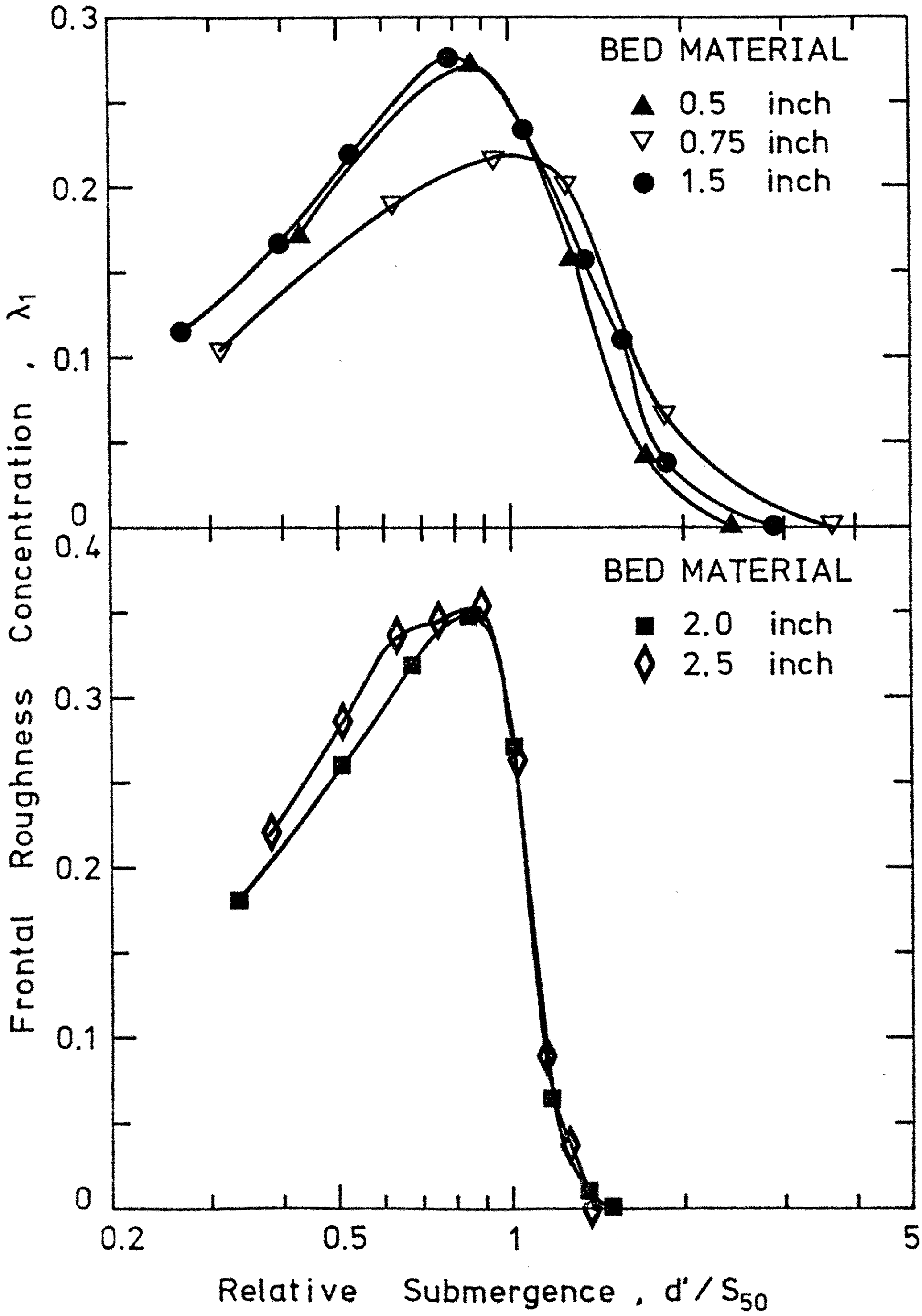

Figure 5. Variation of the theoretical frontal roughness concentration with relative submergence for the five roughness materials used in this study.

depth increases, that number is likely to be a function of the total number of elements on the bed. In other words the greater the total number of elements, the greater also is likely to be the number of significant elements at any given relative roughness and the greater therefore is the effective roughness concentration.

The total number of elements on the bed is a direct function of the ratio of the area of the bed to the average basal plan area of the element. In turn the basal plan area is a function of the product of two axes of the element base, such as the longstream axis, X_n, and the cross-stream axis, Y_n. Thus in a section of channel of width, w, and length, Δx, the total number of boulders is a function of N where:

$$N = \frac{w\ \Delta x}{X_n\ Y_n} \tag{16}$$

Setting Δx equal to X_n gives a number characteristic of, but not necessarily equal to, the number of elements at a section:

$$N = \frac{w}{Y_n} \tag{17}$$

It should therefore be possible to give an effective roughness concentration as some function varying directly with relative roughness, the rate of variation depending inversely on the roughness size distribution and the magnitude varying with roughness shape and w/Y_n

7.1.6 Quantification of Roughness Geometry

In order to mathematically describe the roughness effects, quantitative measures of roughness size distribution and shape are required.

Past attempts to account for size distribution have largely been empirical in approach and have concentrated on finding some size which was deemed to be characteristic of all the size effects of the roughness (e.g., Limerinos, 1970). However, in a process-based approach it is more appropriate to separate the various effects. The size distribution of an element axis should therefore be described in the same way as is any statistical distribution: by a characteristic size of statistical significance, such as the mean or median, by a standard deviation and, if the distribution is not normal, by a coefficient of skewness.

The precise axis of an element which is measured depends on the method by which samples of bed material are gathered. The most practical and widely used method is that of Wolman (1954) in which individual elements are collected on a random basis from the surface layer of the bed material and their median axes measured. Once the sample is complete, the elements can be ranked by size, a cumulative percentage frequency curve is constructed and the median size of the median axis, D_{50}, extracted. If the long and short axes are also measured, their median axes (L_{50} and S_{50}, respectively) can be similarly derived.

The method is relatively simple to apply and is equivalent to bulk sieve analysis (Kellerhals and Bray, 1971). Leopold (1970) criticizes the method for concentrating on the larger elements of the distribution and proposes a weighting technique that would allow the distribution to be more closely represented. However, this does not mean that the Wolman technique is inconsistent.

A more serious defect is that the long, median and short axes so measured, while of sedimentological significance, may not be relevant to hydraulic processes (D. Doehring, 1979, Colorado State University, personal communication). For example, the lengths required to characterize the roughness geometry are really element height, for the relative roughness, and element cross-stream axis, for the parameter N in Equation (17). While, in natural sediments, these lengths are often equal to, respectively, the short and long axes of an element (Johansson, 1963; Judd and Peterson, 1969), this is not always so. Attempts have been made to overcome this defect by sampling only the larger elements, deemed to have the most hydraulic significance (Calhoun, 1975), or by using fabric analysis, to account for the three-dimensional disposition of the elements on the bed (Briggs, 1977, Chapter 5; Simpson, 1978; Haddock, 1978), but these techniques have not yet reached the stage where they have wide, practical utility. Consequently it will be assumed for this study that in natural channels the long, median and short axes of an element correspond respectively to the cross-stream axis, longstream axis and height. Support for this assumption is provided by the aforementioned studies and by the photographs of Miller (1958) and Barnes (1967).

Size distributions of natural sediments are often log-normal or nearly so (Miller, 1958; Mahmood, 1973; Calhoun, 1975; Bathurst, 1977). The simplest representation of the standard deviation, σ, is therefore:

$$\begin{aligned}\sigma &= \log (D_{84}) - \log (D_{50}) \\ &= \log \left(\frac{D_{84}}{D_{50}}\right)\end{aligned} \tag{18}$$

(The median axis is used here for the purposes of illustration but Equation (18) applies to any axis with a log-normal size distribution.)

Although more complex formulae based on additional percentile values of the size distribution are available, Equation (18) is used in this report since some of the data in the literature, which are referred to for purposes of comparison, include only the 84 and 50 percentile values of the size distribution. It should be noted that as the standard deviation is given as a logarithm it can not be directly related to the roughness size which has dimensions of length.

The standard deviations of size distributions of natural sediments seem to vary within a characteristic range. This is illustrated in Figure 6 using data from a wide range of river sites in North America and Great Britain. In each case sampling was carried out using the Wolman technique. The data of Thorne are currently unpublished and were supplied by personal communication (C. R. Thorne and R. D. Hey, 1979, University of East Anglia, Norwich, United Kingdom). There seems to be a consistent lower limit to the value of σ, equal to about 0.13, but the upper limit varies in value from approximately 0.3 to 0.6, being higher for sediments with smaller values of D_{50}. In general, though, most of the points fall within the range of 0.2 to 0.4.

Roughness shape or sphericity can be quantified most simply by some ratio of the long, median and short axes of the elements. A commonly used parameter is Krumbein's (1941) intercept sphericity, ψ:

$$\psi = \sqrt[3]{\frac{D_n S_n}{L_n^2}} \tag{19}$$

While this parameter provides a consistent mathematical description of shape it may not necessarily have a precise hydraulic meaning. Various other parameters are also available (Briggs, 1977, Chapter 4).

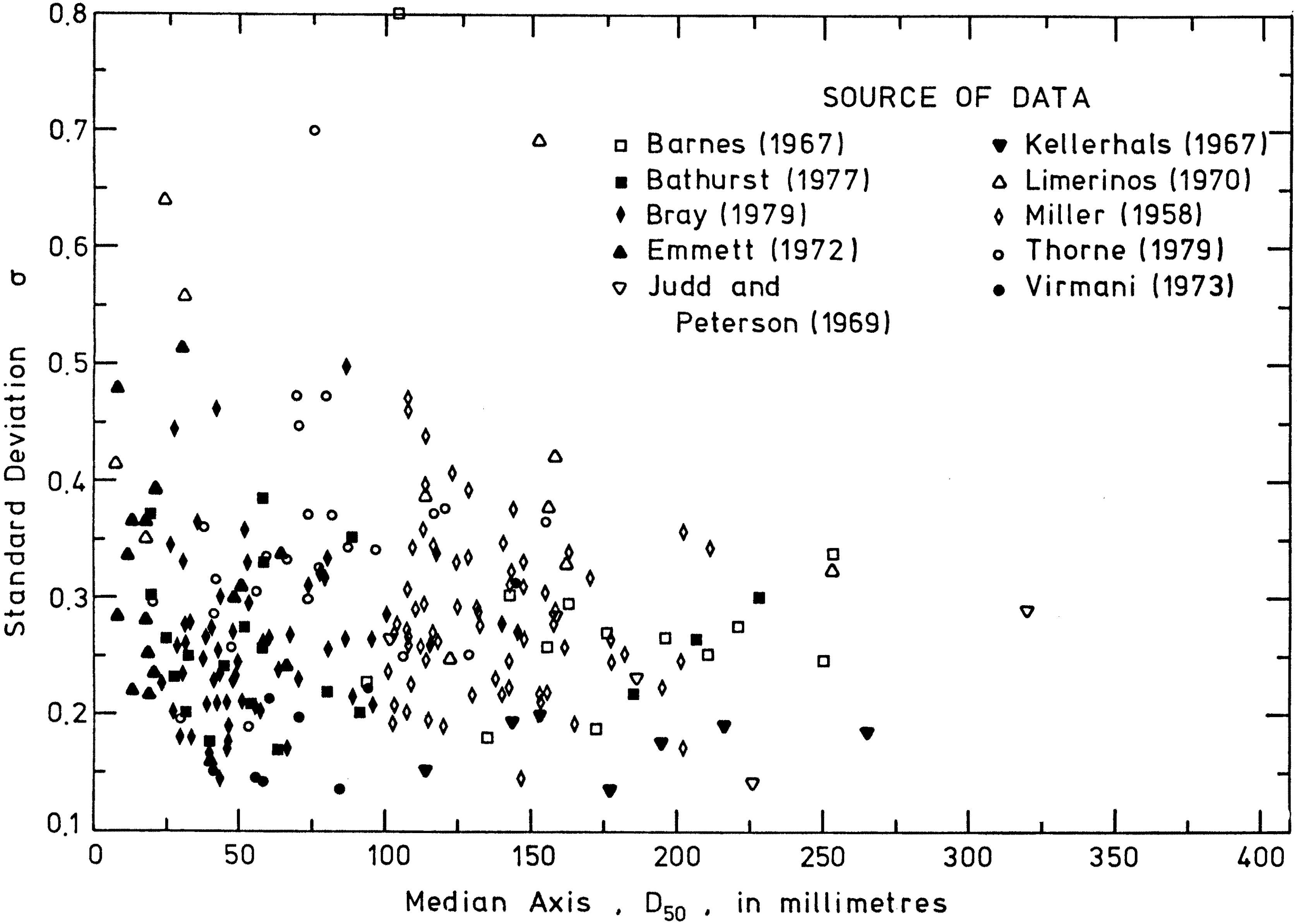

Figure 6. Variation of bed material standard deviation of size distribution with size for samples of bed material from selected rivers.

Figure 7 shows the variation of roughness shape between various river sites. (The materials used in this study are also included.) Because the long axes are not given in all the published data, shape is characterized by the ratio of short axis to median axis. Significant differences between sites are apparent which, it might be expected, would be geological in origin. However, Miller (1958) found that although geology affects the size and lithologic composition of bed material it does not necessarily affect the shape. Also examination of published photographs (Miller, 1958; Barnes, 1967; Judd and Peterson, 1969; Bathurst, 1978) shows that the bed materials of mountain rivers in regions of different geology are consistently blocklike (rather than platelike). Presumably therefore bed material in mountain rivers should have relatively high values of the ratio of short axis to median axis. This appears to be borne out by the data of Figure 7.

Surface texture and roundness of bed material are more difficult to quantify. Various sedimentological techniques have been devised (Briggs, 1977, p. 117) but qualitative descriptions are retained in this study.

7.2 CHANNEL GEOMETRY

Channel geometry is not as important in channels with large-scale roughness as it is in channels with small-scale roughness. Extreme wall roughness and shallow depths do not permit the development of secondary circulation at bends or changes of cross-sectional shape and the longitudinal bed profile is usually uniform (Miller, 1958; Judd and Peterson, 1969). Consequently the effects of channel pattern or planform and bed profile can be neglected. According to the studies of Judd and Peterson (1969) and Bathurst (1978), though, channel cross-sectional shape can

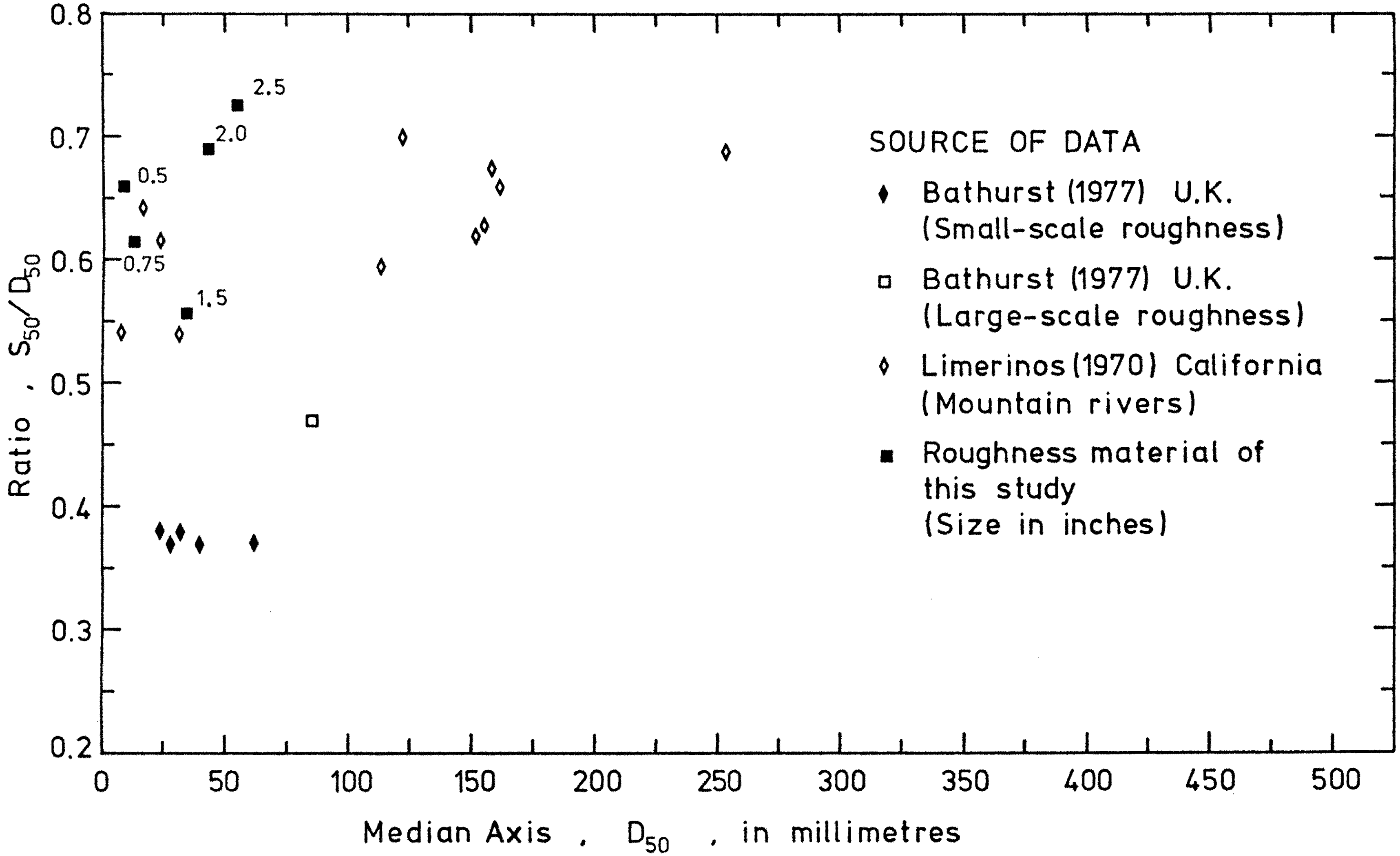

Figure 7. Variation of a parameter of bed material shape, S_{50}/D_{50}, with size for samples of bed material from selected rivers.

influence the variation of resistance with discharge. It is suggested here that this shape effect in fact acts via a relationship with the proportion of a channel cross-section which is occupied by roughness elements, that proportion having a direct effect on the manner in which the flow loses energy.

Herbich and Shulits (1964) showed that, with large-scale roughness and a high concentration of elements, the flow is funnelled between the elements in jets and then impacts against downstream elements. The resulting energy losses and the distortions of the free surface, typical of tumbling flow, must considerably affect the flow velocity and resistance. However, the strength of the funnelling effect must be a function of the proportion of the channel cross-section occupied by elements at a given discharge. Thus, at any given discharge, the greater the proportion, the less the flow cross-sectional area and the more intense the funnelling effect. As a corollary, at any given section it would be expected that as discharge increases and the roughness elements are submerged, the proportion of channel occupied by elements would decrease and the funnelling effect become less intense.

This concept is illustrated using Figure 8 which shows a cross section of a channel with large-scale roughness. The shaded area represents that part of the roughness which lies below water. Total channel cross-sectional area (flow area plus wetted roughness area) is wd', where d' = depth from the free surface to the bed. (With large-scale roughness the mean depth, d, used for relative submergence, is equal to the flow cross-sectional area, A, divided by the channel width, w, and is smaller than the depth, d', against the elements.) If A_w is the total wetted cross-sectional area of the roughness, the proportion

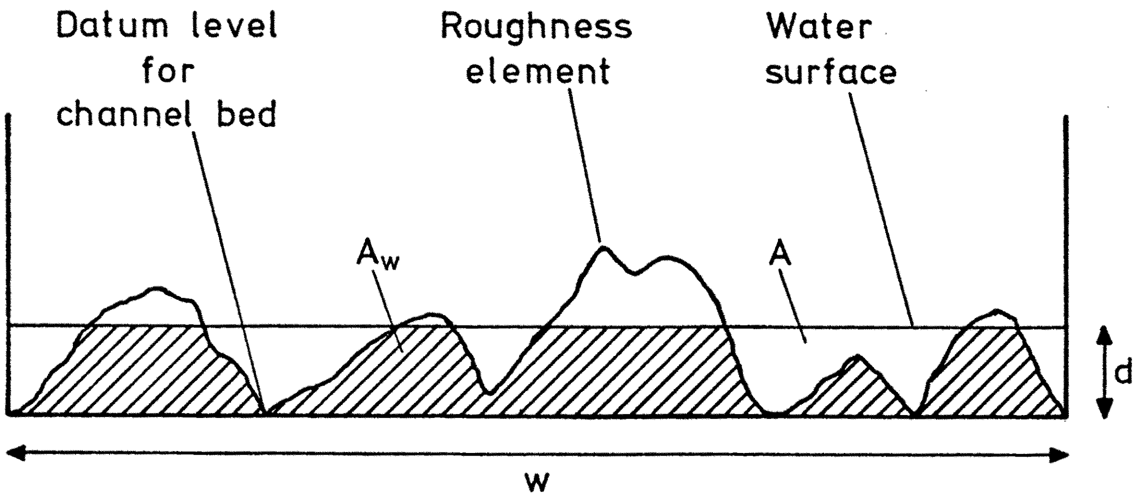

A = flow cross-sectional area

A_w = wetted roughness cross-sectional area

$A + A_w = wd'$

A_w / wd' = relative roughness area

Figure 8. Definition diagram for relative roughness area.

of the channel cross section occupied by roughness is A_w/wd'. This parameter, here defined as the relative roughness area, is a two dimensional relative roughness.

Relative roughness area at a section decreases as depth increases but the relationship with depth must be different at different channel sections. Usually, although not always, as depth increases at a section, width also increases but the ratio of width to depth decreases. It can be imagined that the increase in width acts to counter the decrease in relative roughness area, caused by the increase in depth, by bringing into play more elements from the channel sides. Consequently the relative roughness area should vary directly with the ratio of width to depth.

For a given roughness geometry the relationship depends only on channel cross-sectional shape. In a channel which has a gently varying, saucer-shaped section, a given increase in discharge produces a relatively small increase in depth and a relatively large increase in width. Consequently the ratio of width to depth decreases by a relatively small amount, as should also the relative roughness area. Conversely, in a channel of more semicircular cross section, a given increase in discharge produces a relatively large increase in depth and a relatively small increase in width. As a result both the ratio of width to depth and the relative roughness area decrease by relatively large amounts.

At a site of given cross-sectional shape, a given change in discharge produces a given change in the ratio of width to depth. Presumably the rate of change of relative roughness area with the ratio of width to depth then depends on the roughness geometry, particularly the degree to which the roughness elements project into the flow at any given depth. This in turn depends on the effective roughness concentration. The smaller the effective roughness concentration at any given depth, the smaller is the degree to which the elements project into the flow and the less is the funnelling effect. Thus, if the effective roughness concentration decreases rapidly as depth increases, so should the relative roughness area. If it decreases slowly, the relative roughness area should also decrease slowly.

If the foregoing is correct, then for channels in which relative roughness area cannot be measured directly, it should be possible to derive a relationship in which relative roughness area changes with the ratio of width to depth and in which the rate of change is a function of the effective roughness concentration. If the relationship is shown to be a power law, relative roughness area is likely to be given by a term very similar to the modified Judd and Peterson (1969) channel parameter, $(w/d)^{7(\lambda_1 - 0.08)}$ (Bathurst, 1978).

The effect of relative roughness area on the flow should be negligible once the roughness cross-sectional area, A_w, becomes small compared with the flow cross-sectional area, A. A rough idea of the relative submergence at which this occurs can be gained with the aid of Figure 9. Assuming for the purposes of the argument that the bed is composed of elements which are uniform in size, the area of flow, A, above each element is:

$$A = wd' - A_w$$

(The symbols are defined in Figure 9.)

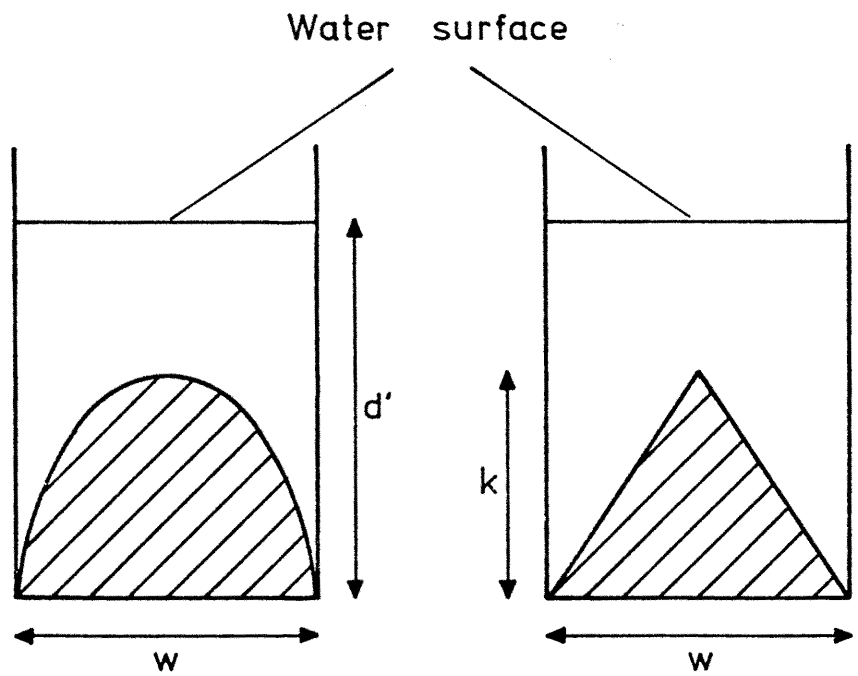

A_w = wetted roughness cross-sectional area

For semiellipse $A_w = w k \pi / 4$

For triangle $A_w = w k / 2$

Figure 9. Diagram used in illustrating the effect of bed material shape on relative roughness area.

If it is also assumed that the limiting relative submergence is that at which the difference between A and wd' is, say, five percent of A, then the limiting relationship is:

$$0.05\ A = A_w$$

or

$$0.05\ d = \frac{A_w}{w}$$

For triangular elements this becomes:

$$0.05\ d = \frac{k}{2}$$

and for semielliptical elements:

$$0.05\ d = \pi\ \frac{k}{4}$$

The limiting relative submergence for triangular elements is therefore 10 and for semielliptical elements it is 15.7.

It was shown earlier that relative submergences of 10 to 15 mark the boundary between the regions of small-scale and intermediate-scale roughness for natural river sediments (Figure 1). A possible physical explanation for that boundary, therefore, is that it marks the relative submergence at which the effect of relative roughness area becomes negligible.

7.3 BED MATERIAL MOVEMENT

There does not appear to have been any research on the effect of bed load on flow resistance in cobble-bed rivers. It is uncertain, therefore, whether the flow uses more or less energy in transporting bed material over a loose bed than it does in overcoming the resistance of an identical fixed bed.

At low rates of bed material movement, the effect is likely to be small. The material would then be rolling along the bed and would travel with a speed at least an order of magnitude less than the speed of the flow. Consequently, the moving elements would affect the flow in much the same way as would fixed elements.

At high rates of bed material movement it might be possible for elements to saltate and leave the bed for short periods. They would then be supported by the fluid and would extract momentum from the flow at some distance from the boundary. The resistance to flow might then be greater than it would be if there were no bed material movement.

SECTION 8 EXPERIMENTAL WORK

In order to provide data with which to develop a flow resistance equation, a flume study was carried out. Measurements were made of flows over five different roughness beds at a variety of slopes and discharges. Most of the measurements were made with fixed beds but a few measurements were made using loose beds in order to study the effect of bed material movement on flow resistance.

8.1 ROUGHNESS CHARACTERISTICS

The five roughness materials are classified as 0.5, 0.75, 1.5, 2.0, and 2.5 inch (respectively, 12.7, 19.05, 38.1, 50.8, and 63.5 mm) these figures referring rather approximately to the maximum size of each material. The 0.5, 0.75 and 1.5 inch materials were commercially available gravels, consisting of chips derived by crushing larger cobbles. The 2.0 and 2.5 inch materials consisted of cobbles which were collected by hand.

The size distributions of the materials were determined before the roughness beds were constructed. In an attempt to simulate as closely as possible Wolman's (1954) method of sampling coarse bed material, a sample of a hundred elements was collected on a random basis from a heap of each material, lying where it was dumped from the delivery truck. The long, median and short axes of each element were measured by ruler and the relevant class size interval to which each axis corresponded was noted. The class size intervals are indicated with the results in Appendix C. The arrangement of the interval widths is one which has been found to be useful for river sediments (Bathurst, 1977).

Cumulative percentage frequency curves were plotted on log-probability paper (Appendix C). The distributions are approximately log-normal so the standard deviations of the distributions were calculated using Equation (18). Generally the distributions are more uniform than those of natural river sediments (Figure 6 and Appendix C).

Intercept sphericity of each material was calculated using Equation (19) based in turn on the 84, 50 and 16 percentile sizes of each axis. The ratios of long to short and median to short axes were also calculated (Figure 7 and Appendix C). There are differences in shape between the chips and the cobbles but both have intercept sphericities similar to those measured by Miller (1958) in mountain rivers.

Densities of the packed materials (voids plus elements) were obtained by measuring the weight of a given volume of each material (Appendix C). Surface texture of the material was rough. The chips were angular and the cobbles were well rounded.

8.2 EXPERIMENTAL EQUIPMENT

The experiments were carried out using the steep stream flume of the Engineering Research Center of Colorado State University. The flume is 9.54 m (31.33 ft) long and 1.168 m (3.833 ft) wide. Slopes can be adjusted over the range of zero to 30 percent. Discharge is measured by a V-notch weir in the sediment settling tank at the end of the flume. Maximum discharge is about 0.087 $m^3\ s^{-1}$ (3.072 $ft^3\ s^{-1}$) but, during the period of research, difficulties with pumps often reduced that limit to about 0.05 $m^3\ s^{-1}$ (1.766 $ft^3\ s^{-1}$). The flume is an open recirculating flume and draws its water from an underground reservoir. Further details are given by Li et al., (1977).

Each roughness bed was constructed by gluing the material to masonite boards with fibreglass resin. In the case of the chips, one face of the board was smeared with resin and the board was laid, gluey face down, on top of a level deposit of the material. The material adhered to the board, resulting in a fixed roughness bed of one layer of closely packed elements. The boards were then screwed to the bed of the flume.

In the case of the cobbles, roughness beds constructed in this way would have been too heavy to lift. Consequently the boards were first screwed to the flume, then their upper faces were smeared with resin and the cobbles were laid on top, again in a closely packed pattern one layer deep. In none of the five beds were there obvious patches of smooth board visible between the elements, so the beds were good approximations to natural river beds (Plates 10 to 14).

Between four and five boards were needed to cover the bed of the flume. The flume side walls (one perspex, the other painted wood) were not covered. It was expected that, because of the extreme bed roughnesses and high ratios of width to depth, side wall effects would be insignificant.

For the experiments with loose beds, a layer of material about 76 mm (0.25 ft) thick was laid on top of the fixed bed (Plates 15 and 16). Material was delivered to the upstream end of the flume by a conveyor belt from a hopper, the rate of delivery being regulated as required. Rate of transport of bed material was measured by collecting all the material falling off the downstream end of the flume during a given period in a specially constructed basket. Further details of this equipment are given by Li et al., (1977).

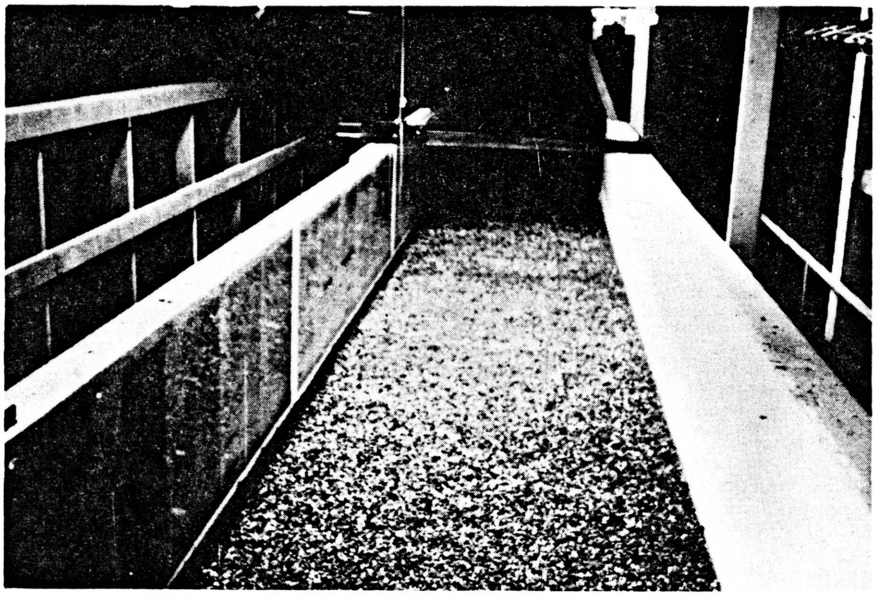

Plate 10. View of the 0.5 inch fixed roughness bed, looking down the flume. Measuring section is shown in this and subsequent photographs by the rail across the flume.

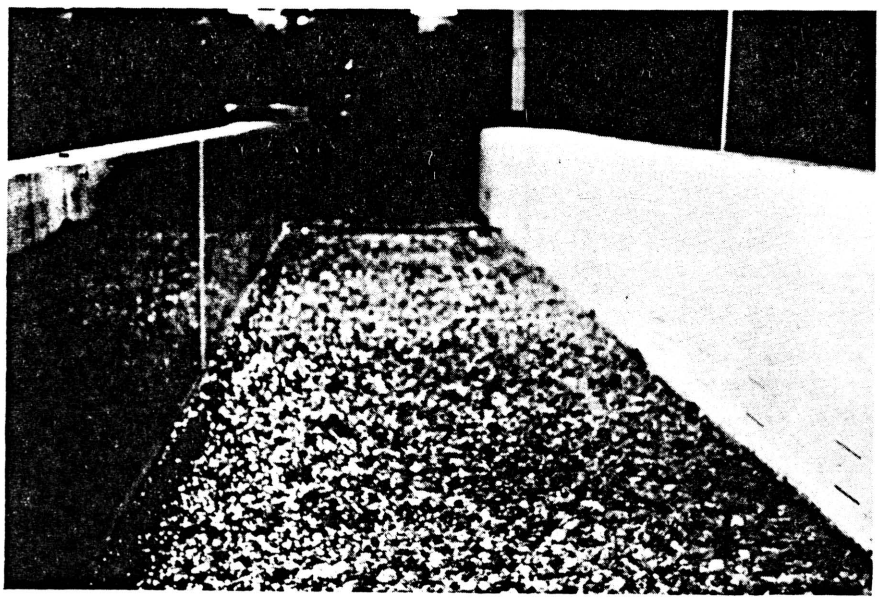

Plate 11. View of the 0.75 inch fixed roughness bed, looking down the flume.

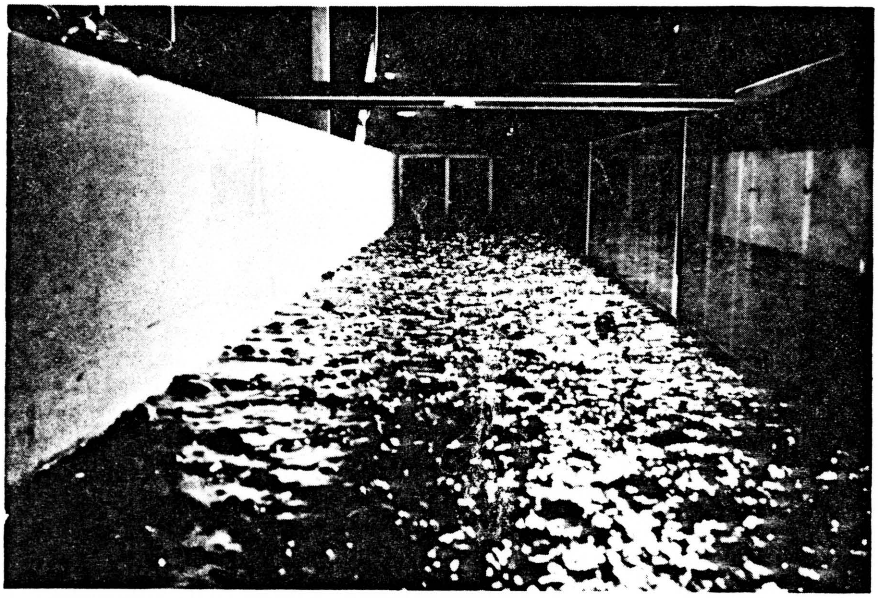

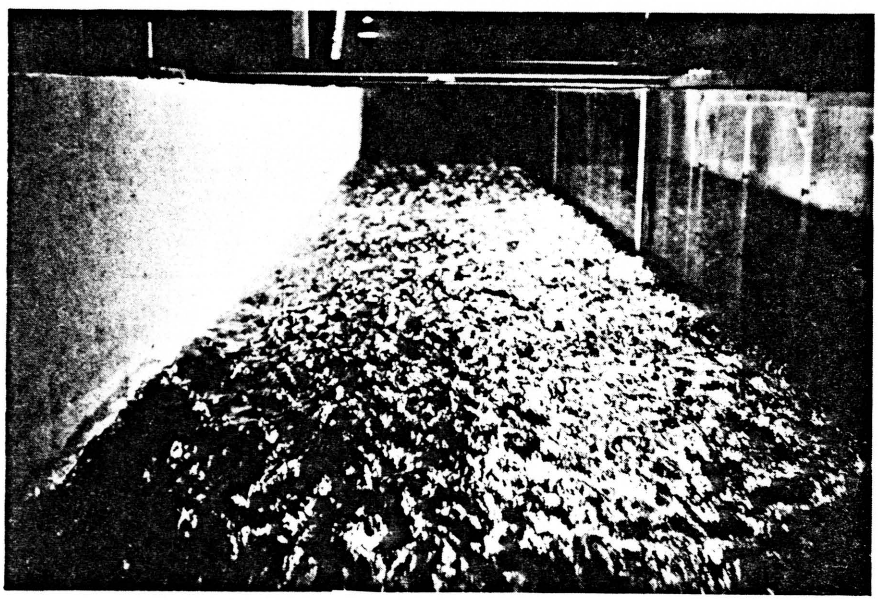

Plate 12. Views of the 1.5 inch fixed roughness bed, looking up the flume. (a) With a discharge of 0.00181 $m^3 s^{-1}$ at a slope of 5 percent. (b) With a discharge of 0.0742 $m^3 s^{-1}$ at a slope of 5 percent. Note the surface wave pattern.

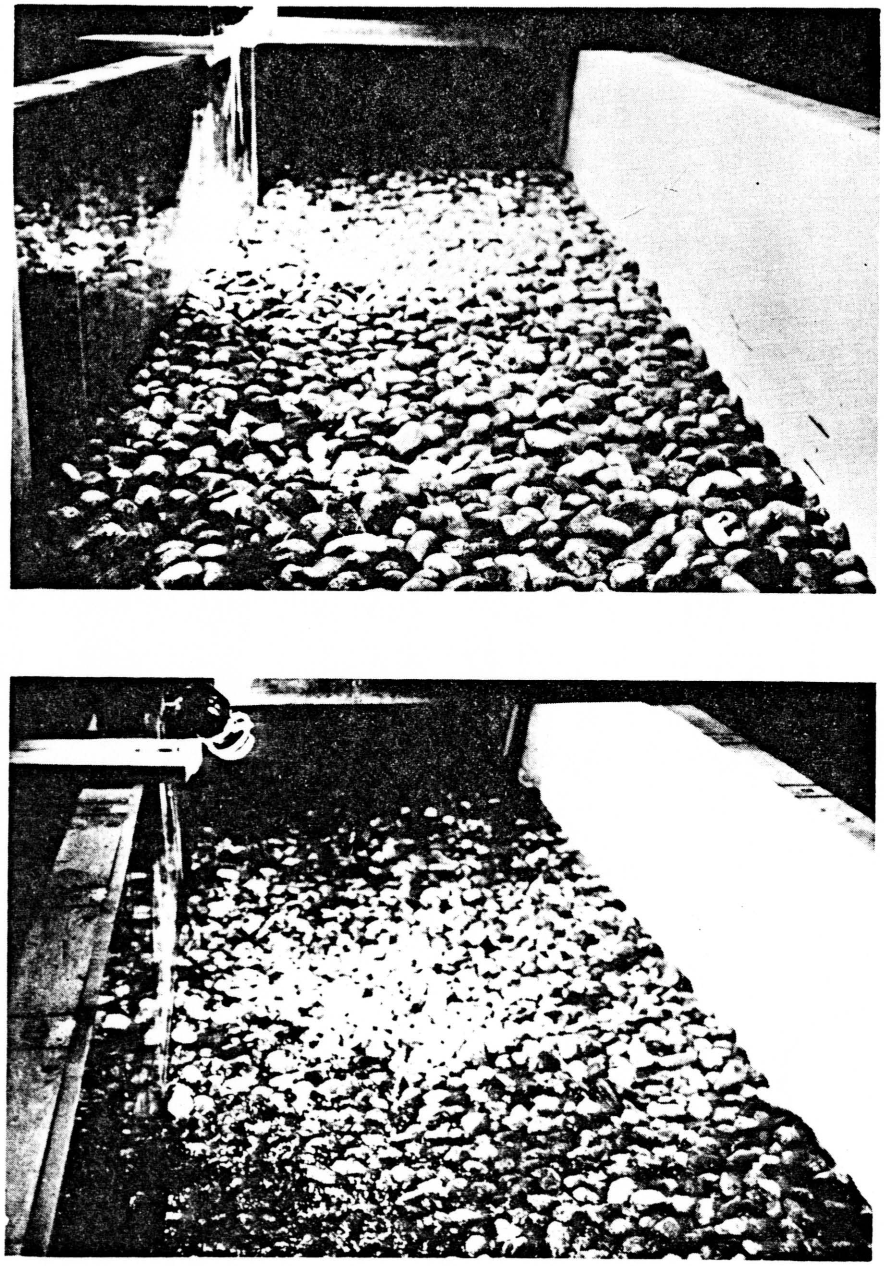

Plate 13. Views of the 2.0 inch fixed roughness bed, looking down the flume.
(a) With no discharge.
(b) With a low discharge, with protruding elements, at a slope of 8 percent.

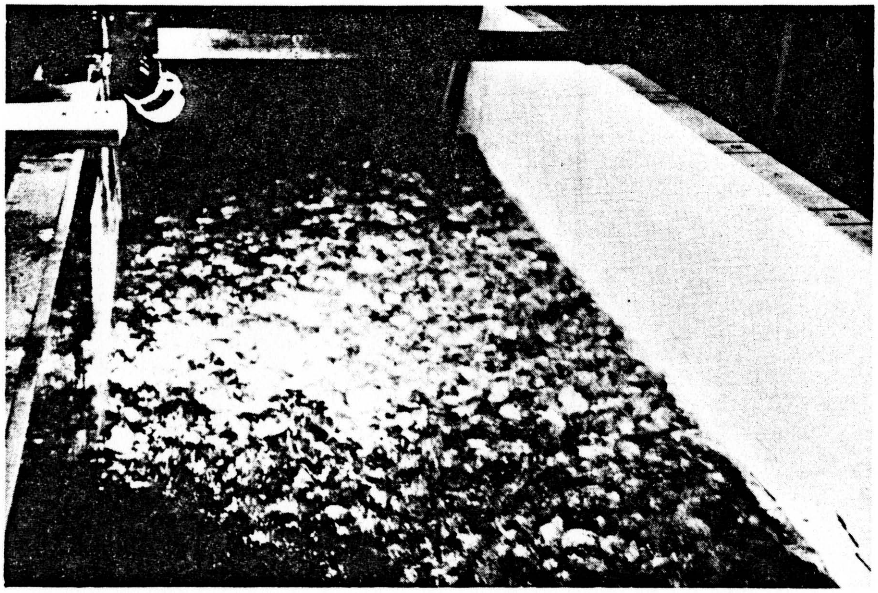

Plate 13. Views of the 2.0 inch fixed roughness bed, looking down the flume (continued).
(c) With a high discharge, with surface wave pattern, at a slope of 8 percent.

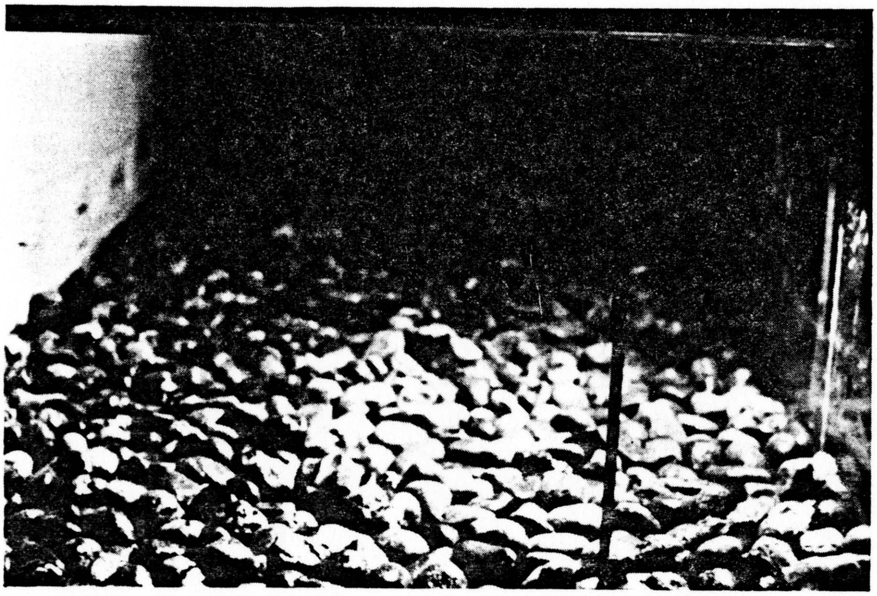

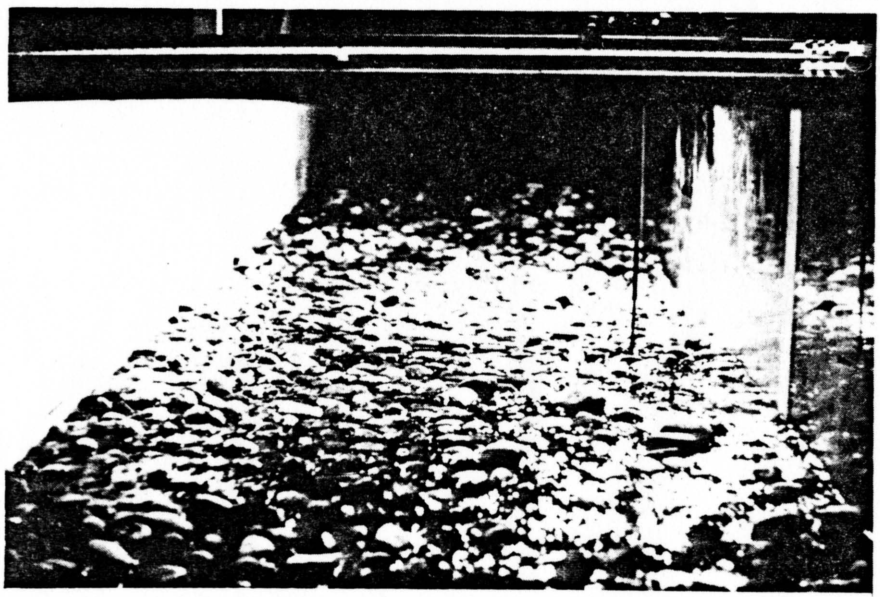

Plate 14. Views of the 2.5 inch fixed roughness bed, looking up the flume.
(a) With no discharge.
(b) With a low discharge, with protruding elements, at a slope of 5 percent.

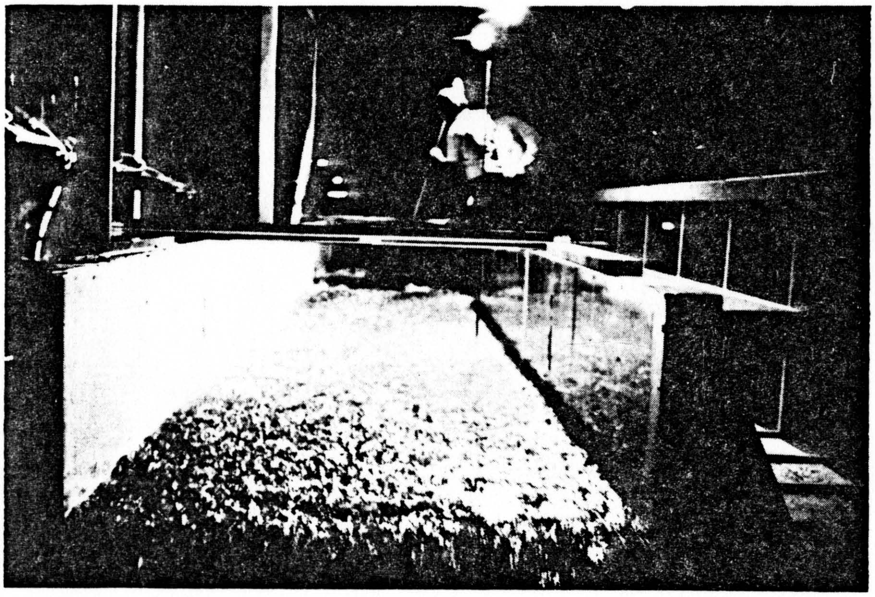

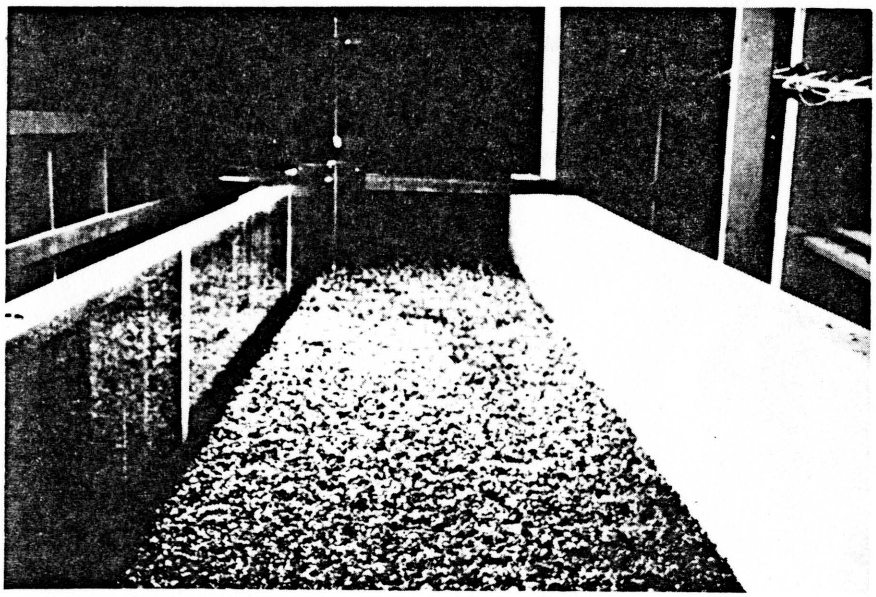

Plate 15. Views of the 0.5 inch loose roughness bed.
(a) Looking up the flume, with a water discharge of 0.0698 $m^3\ s^{-1}$ at a slope of 8 percent. Note the surface wave pattern.
(b) Looking down the flume, after the discharge of (a).

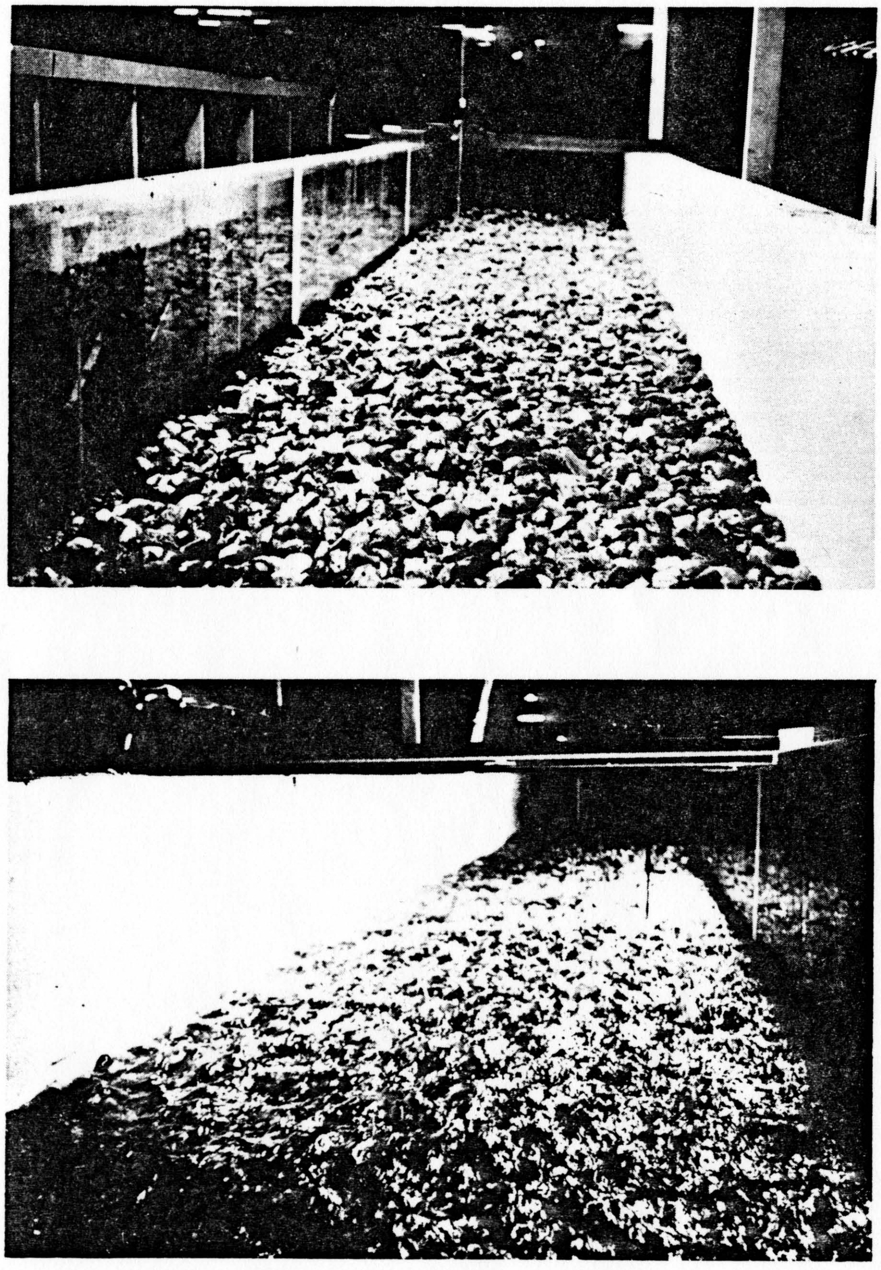

Plate 16. Views of the 1.5 inch loose roughness bed.
(a) Looking down the flume.
(b) Looking up the flume, with a water discharge of $0.0275\ m^3\ s^{-1}$ and no sediment movement at a slope of 8 percent. Note the surface wave pattern.

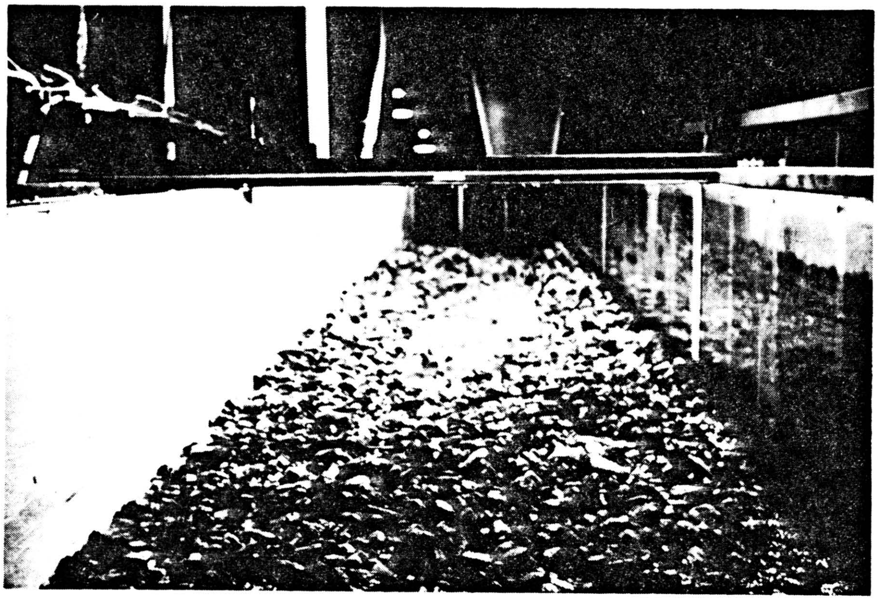

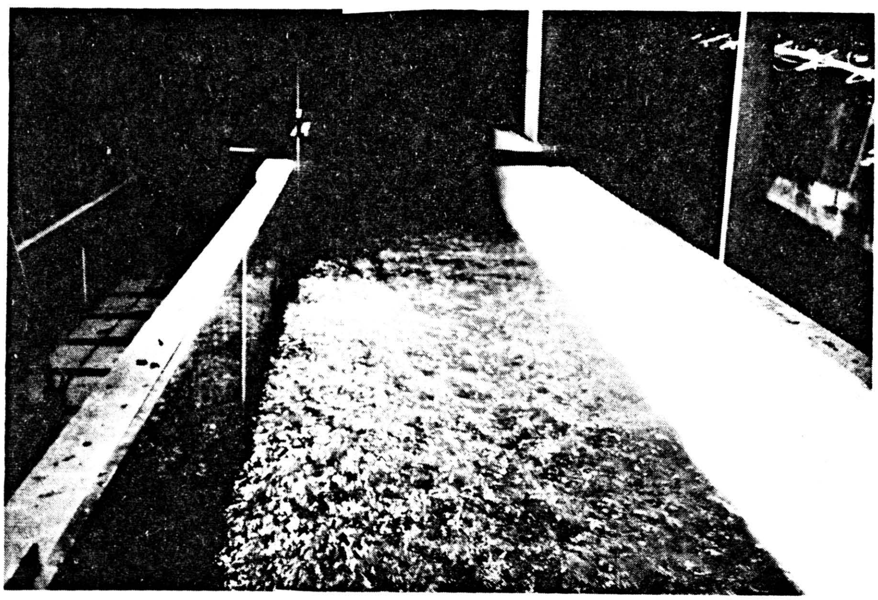

Plate 16. Views of the 1.5 inch loose roughness bed (continued).
(c) Looking up the flume, after a water discharge of $0.0687\ m^3\ s^{-1}$ at a slope of 8 percent. Note the channelization at the flume centre.
(d) Looking down the flume, with a water discharge of $0.0655\ m^3\ s^{-1}$ and no sediment movement at a slope of 5 percent. Note the surface wave pattern.

8.3 EXPERIMENTAL PROCEDURE FOR FIXED BEDS

For each of the five roughness beds measurements were made at slopes of 2, 5 and 8 percent, this range being typical of mountain rivers. At each slope, measurements were made at five to seven discharges distributed over the available range. Thus about eighteen sets of measurements were carried out for each bed, the total for the five beds being eighty-eight sets.

In each set of measurements, depth was gauged at a single section across the flume so that the cross-sectional properties of the flow could be determined. A single section was thought to be representative of the entire bed because of the uniform construction of the bed, the large ratio of flume width to bed material size (which ensured that the flow pattern at the section would be determined by the average properties of the bed and not by individual elements) and the uniform rectangular cross section of the flume. On average, in a macroscopic sense, there was unlikely to be any variation in conditions from one section to another for a given flow. This can not be assumed so freely for river channels where longstream changes in channel geometry are apparent.

The section was situated about 7.1 m (23.3 ft) downstream of the flume entrance and about 2.4 m (7.9 ft) upstream of the exit to the sediment settling tank. Because of the steep slopes, rough beds and shallow depths and the extreme turbulence of the flow, it could be assumed that the balance between the resistive and propulsive forces on the flow was achieved far upstream of the section. Steady, uniform flow therefore prevailed at the section and until just upstream of the flume exit.

The method of gauging depth followed Bathurst's (1978) field technique as closely as possible. That technique required that bed and water surface elevations be taken at every change of bed elevation across the channel. In this case similar results were achieved by measuring the elevations at intervals of 12.7 mm (0.0417 ft or 0.5 inch) across the channel, that interval being equal to the smallest size of bed material. Elevations were therefore obtained at ninety-three verticals in the section. The measurements were made with a point gauge which was mounted on a rail across the flume and the elevations were read to three decimal places in feet, using a vernier scale. Completion of each section took about one hour, over which period the discharge was kept constant. At the end of each gauging the temperature of the water was measured.

Total cross-sectional area of the flow, A, was calculated from the bed and free surface elevations by computer integration using the trapezoidal rule. Cross-sectional area of the roughness, A_w, was calculated from the bed elevations by the same method, the datum for the depth, d', being the elevation of the top of the boards on which the elements were laid (Figure 8). Knowing A and A_w, the total channel cross-sectional area, wd', could be calculated, leading to d' and the relative roughness area, A_w/wd'.

As with Bathurst's technique, wetted perimeter is based on the datum level of the bed, neglecting the projections of the roughness elements. This is because wetted perimeter should define the area of bed over which the resistive shear acts. In this case the main resistive shear of the bed is given by the total form drag of the elements divided by the area of bed on which the elements lie and is not, as in small-scale roughness, the frictional shear divided by the surface area of the elements. Consequently the area of bed is given by the product of unit longstream length and the wetted perimeter based on the datum level of the bed, neglecting the projections of the elements. For the flume experiments, because of the high ratios of width to depth and negligible sidewall effects, wetted perimeter is considered to be equal to channel width. Hydraulic radius is therefore equal to the mean depth, given by the ratio of flow cross-sectional area to width.

The measured data and their derivatives are given in Appendix D. Examples of the flows are shown in Plates 12 to 14.

8.3.1 Errors

Because of the accuracy with which the measurements were made, it is not thought that the data and their derivatives have significant errors. However, it is possible that they are slightly misrepresentative in certain cases. For example, warping of the masonite boards occasionally occurred, creating a series of minor undulations along the bed. These caused local backwater conditions, particularly at the lower discharges, but it was usually possible to alter the position of the measuring section and avoid these effects.

Another problem was that the cobbles, being larger and more spherical than the chips, did not fit as closely to the bed as did the chips (Plates 10 to 14). Consequently a certain amount of flow could have occurred beneath the cobbles and might not therefore have been included in the measurements of depth. It is uncertain whether the amount involved could have been significant but generally the proportion relative to the total flow would have been small except at the lowest discharges.

On a few occasions, generally with the finer bed materials, roll waves were observed. However, they were not excessive and did not seem to disturb the free surface sufficiently to hamper the measurements. On the whole the roughness of the bed more than compensated for the destabilizing effect of the steep slopes and high Froude numbers.

8.4 EXPERIMENTAL PROCEDURE FOR LOOSE BEDS

Loose bed experiments were carried out using the 0.5 and 1.5 inch chips. These materials were the only ones available in quantities sufficient to allow their delivery to the flume at a rate adequate to prevent degradation of the bed during a period of bed material movement. Also, it was found that the 2.0 and 2.5 inch material could not be moved by any of the flows. Even with the 1.5 inch material no significant movement occurred at the two lower slopes.

Procedure for the loose beds involved greater inaccuracies than did the procedure for the fixed beds. Because an adequate sediment supply could not be maintained for long periods, and in order to avoid difficulties related to changing bed form and channelization, each set of measurements had to be completed within about five minutes. Consequently detailed gaugings were not possible.

At the measurement section, bed and free surface elevations were measured at ten verticals spread equidistantly across the flume. Bed elevation was also measured before and after each flow to check that the average bed level had not degraded significantly and after each experiment the bed was smoothed to its original form and thickness. The various flow parameters were calculated as for the fixed beds.

During each experiment, the rate of supply of sediment to the flume was kept at a level sufficient to prevent degradation of the bed. This was judged by eye, a method which seemed to be quite acceptable. As the sediment was poured into the flume it was raked level so that it would not pile up.

Rate of transport of sediment was measured from one to three times during each experiment, depending on the time taken to fill the basket. This varied from 15 to 300 seconds. The volume (voids plus material) of the collected sediment was measured and the sediment discharge calculated.

In order to enable comparison with the results of the fixed beds, one set of measurements was made with each loose bed at each slope at a discharge below that at which sediment transport began. The technique employed was exactly the same as for the fixed beds. This check was necessary because it was not expected that the flows over the fixed and the loose beds would be directly comparable. The fixed beds were essentially impermeable while with the loose beds it was possible that a significant proportion of the flow could occur through the bed. (The fixed beds were therefore more representative of natural river beds which, because of sediment packing and cementing, tend to be relatively impermeable.) Also the loose beds were probably rougher than the fixed beds since it was possible for there to be deeper gaps between neighbouring elements in the loose beds than in the fixed beds.

Twenty-eight sets of data were obtained. The measurements and their derivatives are given in Appendix E and examples of the flows are shown in Plates 15 and 16.

8.4.1 Errors

The measurements of bed and water surface elevations suffered from the changes in cross-sectional shape caused by channelization which occurred during the experiments, particularly at the higher discharges (Plate 16c). However, although individual cross-sectional measurements are likely to contain errors, the variation of the data from discharge to discharge should be essentially correct. Consequently the trends in the results should be correct although individual data points may be scattered about the trend line.

The main problem in measuring the rate of sediment transport was to obtain the average rate and avoid errors related to pulses of movement associated with channelization. With the longer sampling periods an average rate could be assured. With the shorter sampling periods some temporal variation in the rate of transport is evident (Appendix E). However, by taking the collective average of the samples of each experiment, an average rate of sediment transport could be calculated.

SECTION 9 EXAMINATION OF RESULTS

9.1 FLOW CHARACTERISTICS

At the lowest discharges, with relative submergences of less than unity, the flow was subcritical everywhere, characteristic of the tranquil regime. Increases in discharge raised the mainstream Froude number to the level (still subcritical) where funnelling of the flow between roughness elements was sufficient to produce localized regions of supercritical flow and the subsequent hydraulic jumps. Supercritical flow was also noticed over the tops of submerged elements, again terminating in hydraulic jumps. These conditions are typical of the tumbling regime. With further increases of discharge the elements were completely submerged. Depending on the channel slope and roughness size, the mainstream Froude number was able to exceed a value of unity and conditions of rapid flow then prevailed. Generally, these conditions were not achieved at the 2 percent slope or with the 2.0 and 2.5 inch materials.

Once the elements were submerged there were no obvious indications of free surface drag related to individual elements. However, a pattern of standing waves developed over the whole surface (Plates 12b, 13c, 15a, 16b, and 16d).

Relative submergence, d/S_{50}, varied from 0.41 to 12.10, adequately covering the regions of large-scale and intermediate-scale roughness. (d is the mean depth of flow, equal to A/w, and is smaller than the actual depth, d', against the elements (Figure 8). d' would probably give a closer representation of the actual relative submergence but there is no inconsistency in using d and that parameter is also the more convenient.) The ratio of width to depth varied from 13 to 153.

Because of these high ratios and the low relative submergences, side wall effects were unimportant and the flows were laterally uniform. As the flows were also longitudinally uniform, it is possible to assume that they were one-dimensional on the average.

Froude number, $\bar{U}/(gd)^{0.5}$, varied from 0.189 to 1.927, covering the regions of subcritical, transcritical and supercritical flow. Reynolds number, $\bar{U}\ D_{50}/\nu$, varied from about 10^3 to 4.4×10^4. This range lies below the critical Reynolds number marking the transition from laminar to turbulent boundary layers on the elements and, also, in this range drag coefficient varies little with Reynolds number. Some of the flows with higher Reynolds numbers may have occupied the transitional range but these flows happened also to be those with low relative submergences and Reynolds number effects would then have been insignificant compared with free surface drag. Reynolds number effects were therefore negligible.

In calculating relative submergence it is assumed that the height of an element on the bed was equal to its short axis. This is the disposition most likely to have been adopted by the elements during construction of the beds. However, because the beds were not laid down by hydraulic processes it cannot be assumed (as it is for river sediments) that the cross-stream axis, Y_n, of an element was equal to its long axis, L_n. More probably it was nearer to the average of the long and the median, D_n, axes. Consequently for the flume beds it is assumed that:

$$Y_n = \frac{L_n + D_n}{2} \tag{20}$$

Values of Y_n and the ratio, N, of channel width to Y_n (Equation (17)) are given, together with a resumé of the roughness characteristics, in Table 2.

TABLE 2.--Roughness Geometry of the Flume Beds

Bed material size in inches (1)	Median size of short axis S_{50} in millimetres (2)	Standard deviation of distribution of short axis (3)	Median size of cross-stream axis Y_{50} in millimetres (4)	Ratio N of channel width to cross-stream axis (5)
0.5	5.8	0.129	11.2	104.29
0.75	8.0	0.187	16.4	71.33
1.5	19.0	0.153	40.5	28.84
2.0	29.75	0.058	51.0	22.90
2.5	39.5	0.047	63.6	18.36

9.2 FLOW RESISTANCE

Variation of the resistance function, $(8/f)^{0.5}$, with relative submergence is shown in Figures 10 to 14. The data are plotted on semilogarithmic graphs in order to allow comparison with the results shown in Figure 1. There is a general decrease in resistance as relative submergence increases and the straight lines plotted by eye through the data show that, if the semilogarithmic Equation (4) for small-scale roughness were to apply, the rate of change, equal to parameter A, could be 5.62. This is exactly the figure suggested by the boundary layer theory on which Equation (4) is based. However, this

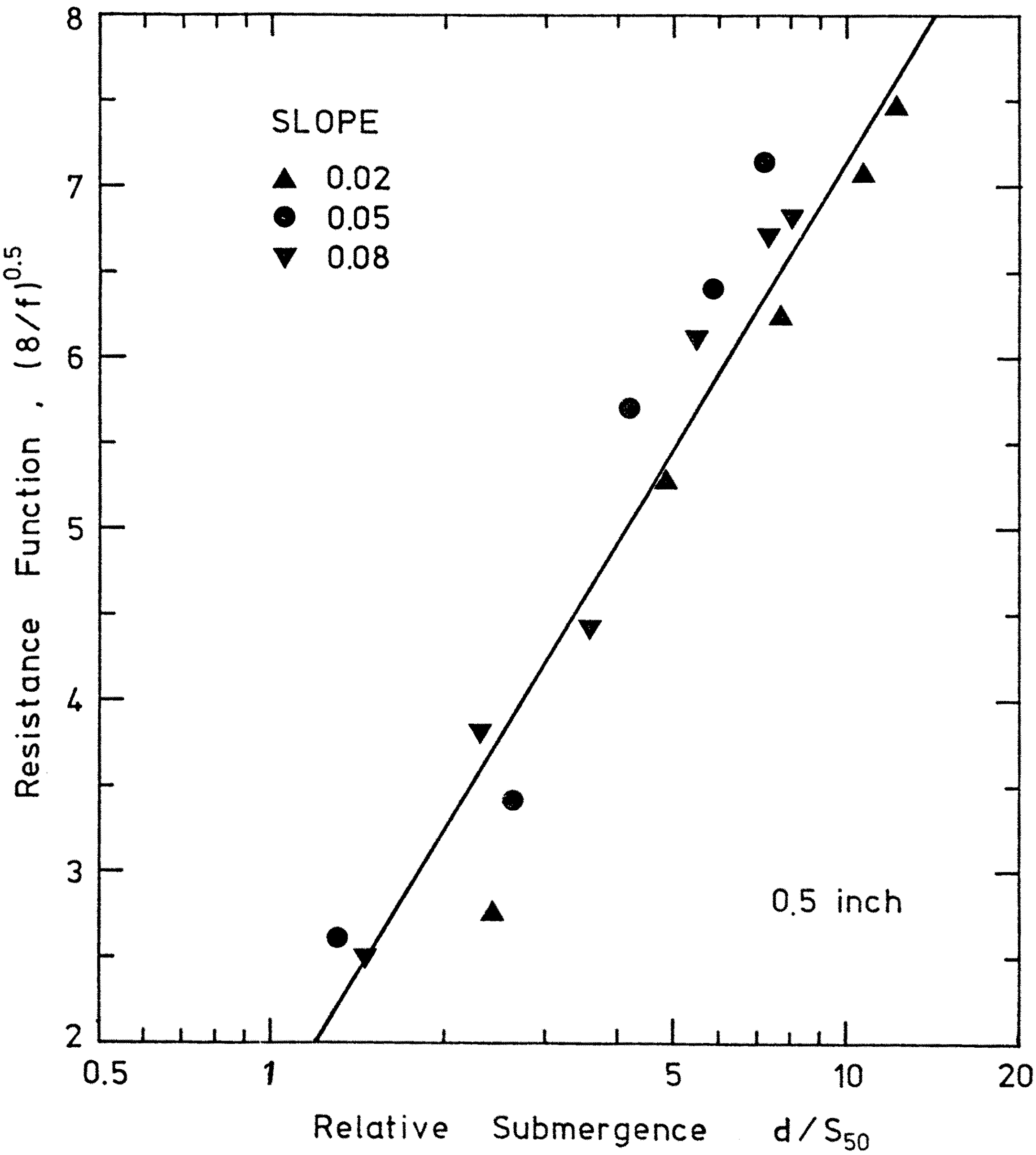

Figure 10. Variation of the resistance function with relative submergence for the flows over the 0.5 inch fixed roughness bed. The line, fitted by eye, has a gradient of 5.62.

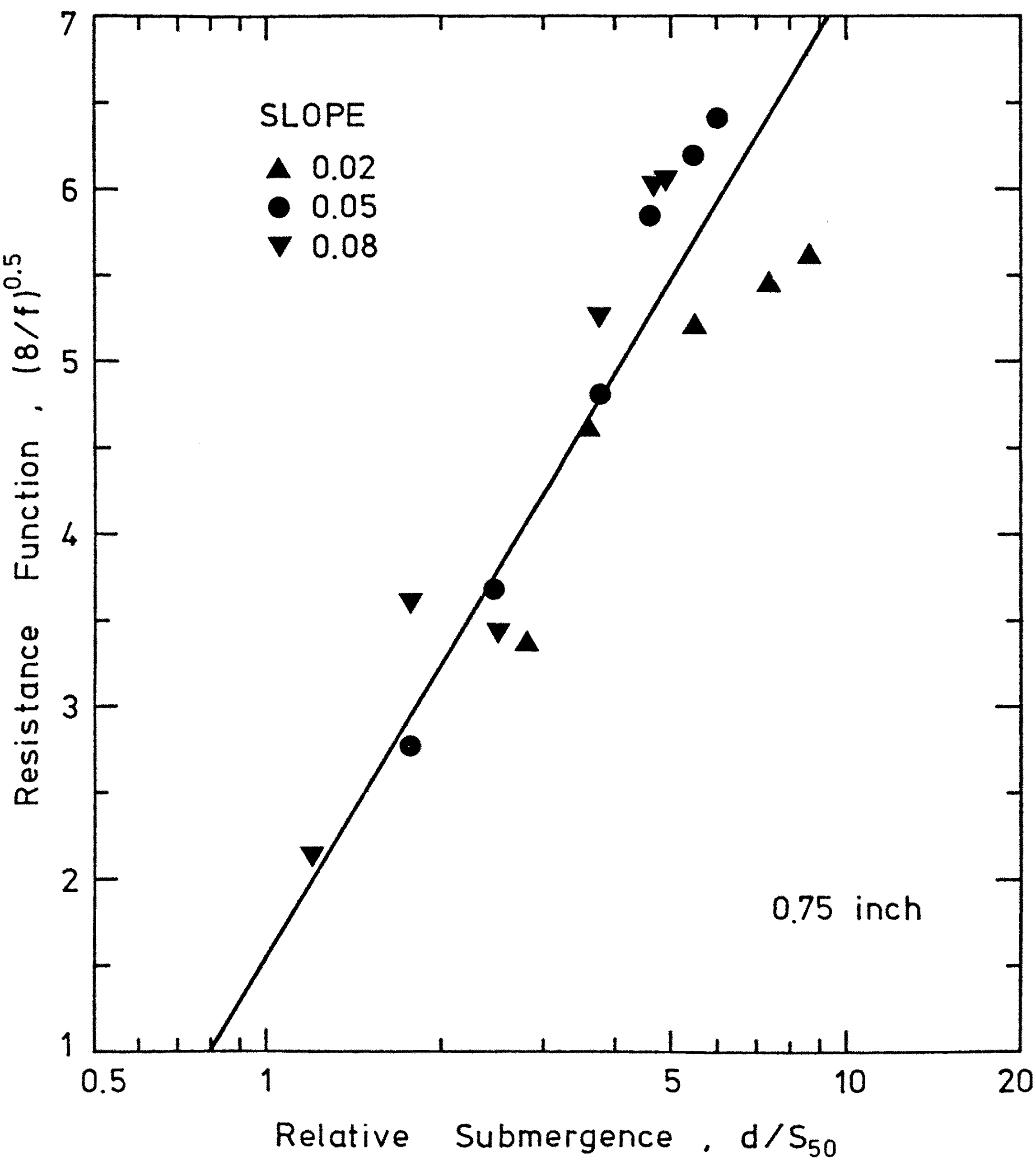

Figure 11. Variation of the resistance function with relative submergence for the flows over the 0.75 inch fixed roughness bed. The line, fitted by eye, has a gradient of 5.62.

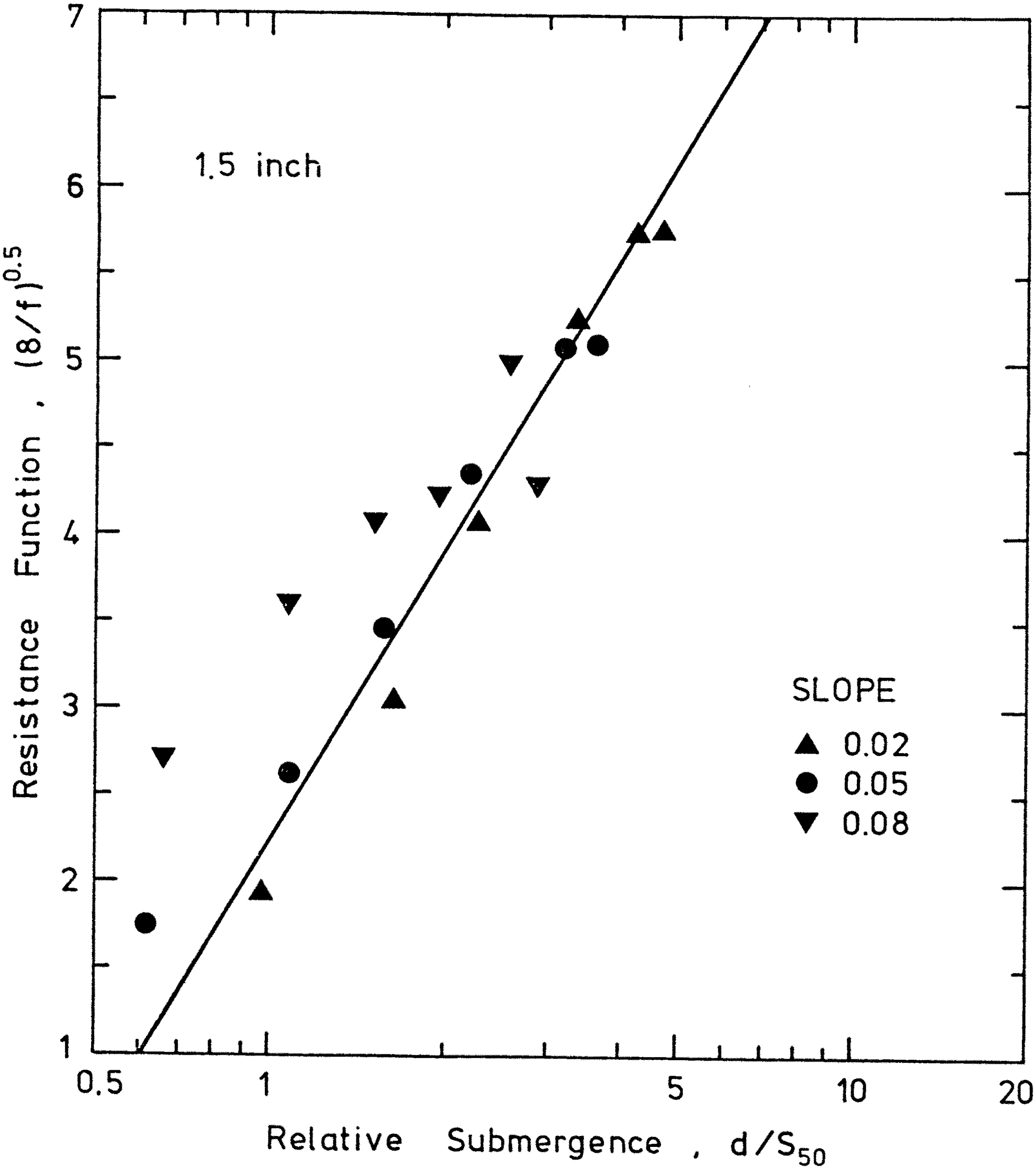

Figure 12. Variation of the resistance function with relative submergence for the flows over the 1.5 inch fixed roughness bed. The line, fitted by eye, has a gradient of 5.62.

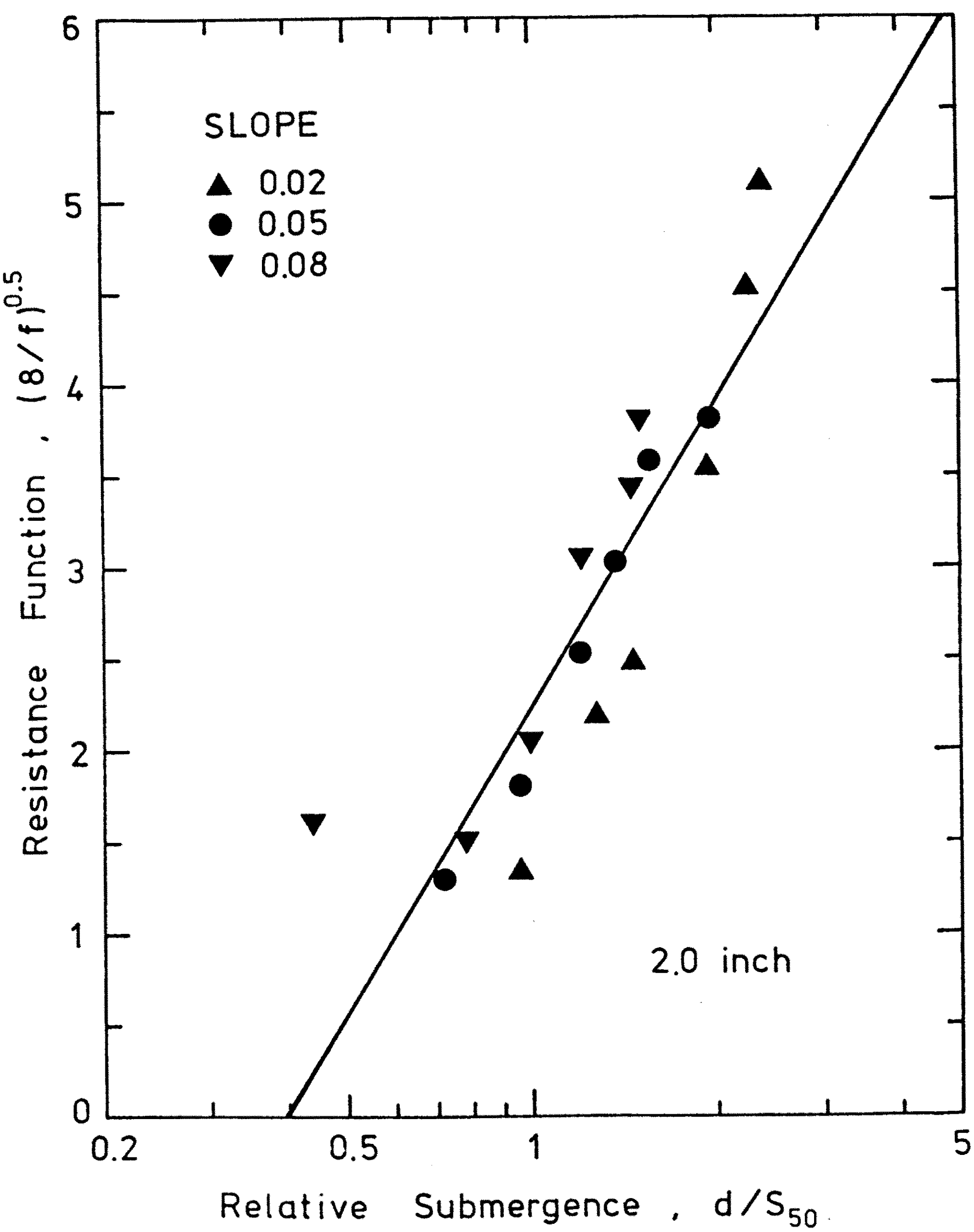

Figure 13. Variation of the resistance function with relative submergence for the flows over the 2.0 inch fixed roughness bed. The line, fitted by eye, has a gradient of 5.62.

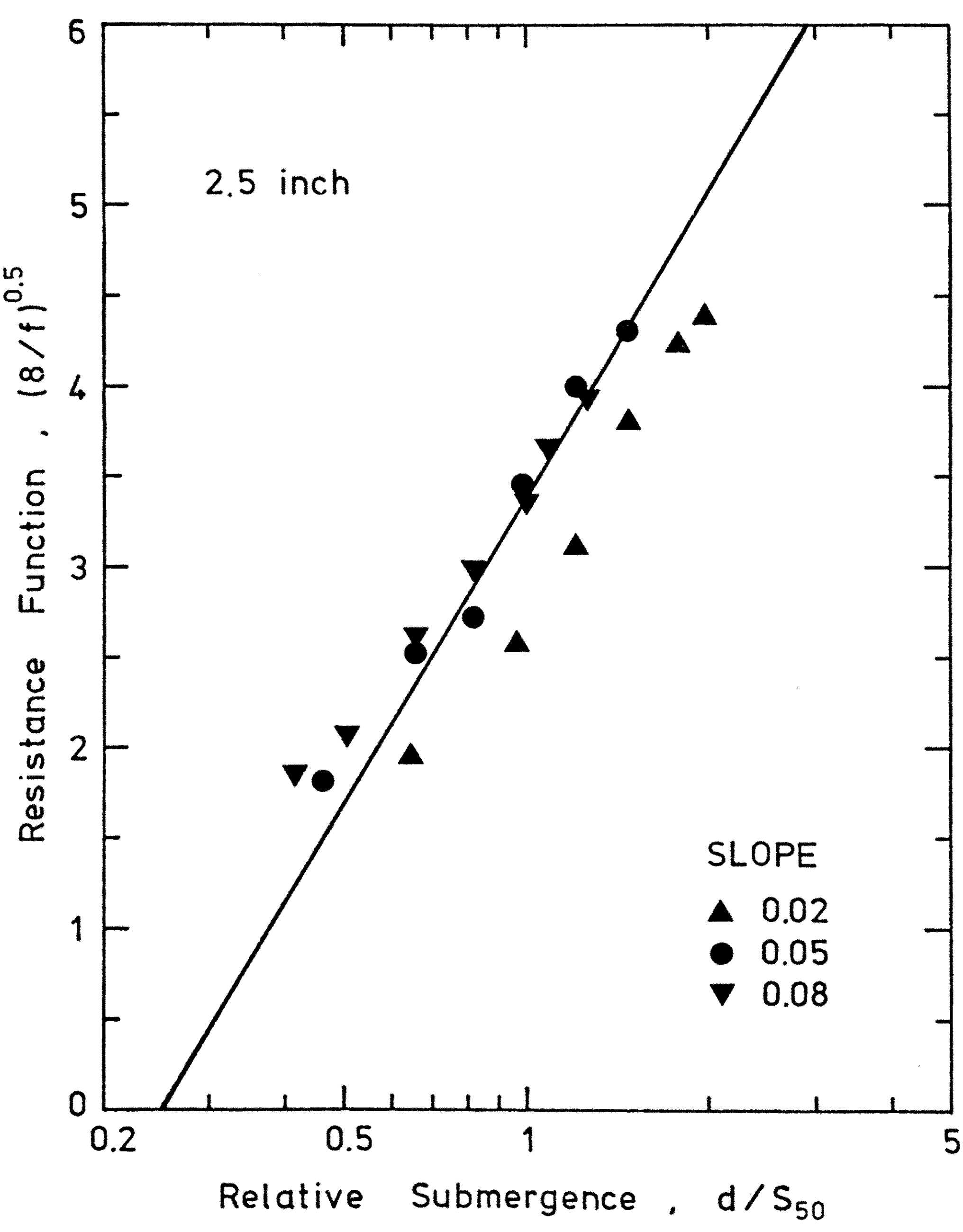

Figure 14. Variation of the resistance function with relative submergence for the flows over the 2.5 inch fixed roughness bed. The line, fitted by eye, has a gradient of 5.62.

agreement may be just coincidence since there is no theoretical reason why the equation for small-scale roughness should apply at the low relative submergences indicated.

It was noted that, for the range of data, straight lines could also be fitted to the plots if logarithmic scales were used. It can not therefore be determined without further analysis whether the flow resistance function is more accurately portrayed as varying logarithmically or semilogarithmically with relative sumbergence in the regions of large-scale and intermediate-scale roughness. It can be seen, though, that there are differences between the plots for the five different beds and that there is a certain amount of scatter among the data of individual beds. This indicates that the flow resistance depends on more than the relative submergence.

9.3 COMPARISON OF DATA WITH PREVIOUS FLOW RESISTANCE EQUATION

The theory of this study is based partly on the theory developed by Bathurst (1978). The data were therefore used to check the validity of the earlier theory, which is embodied in Equation (8). With roughness concentration, λ_1, calculated using Equation (7), the ratio

$$[\bar{U}/(gdS)^{0.5}]/[(w/d)^{7(\lambda_1 - 0.08)}]$$

is plotted against d/D_{84} on logarithmic scales in Figure 15. Also shown is the line of Equation (8). Agreement is good which is somewhat remarkable considering the differences in roughness and channel characteristics between the flume and the river for which Equations (7) and (8) were derived.

As noted by Bathurst there is a tendency for Equation (8) to diverge from the data points at values of d/D_{84} greater than about

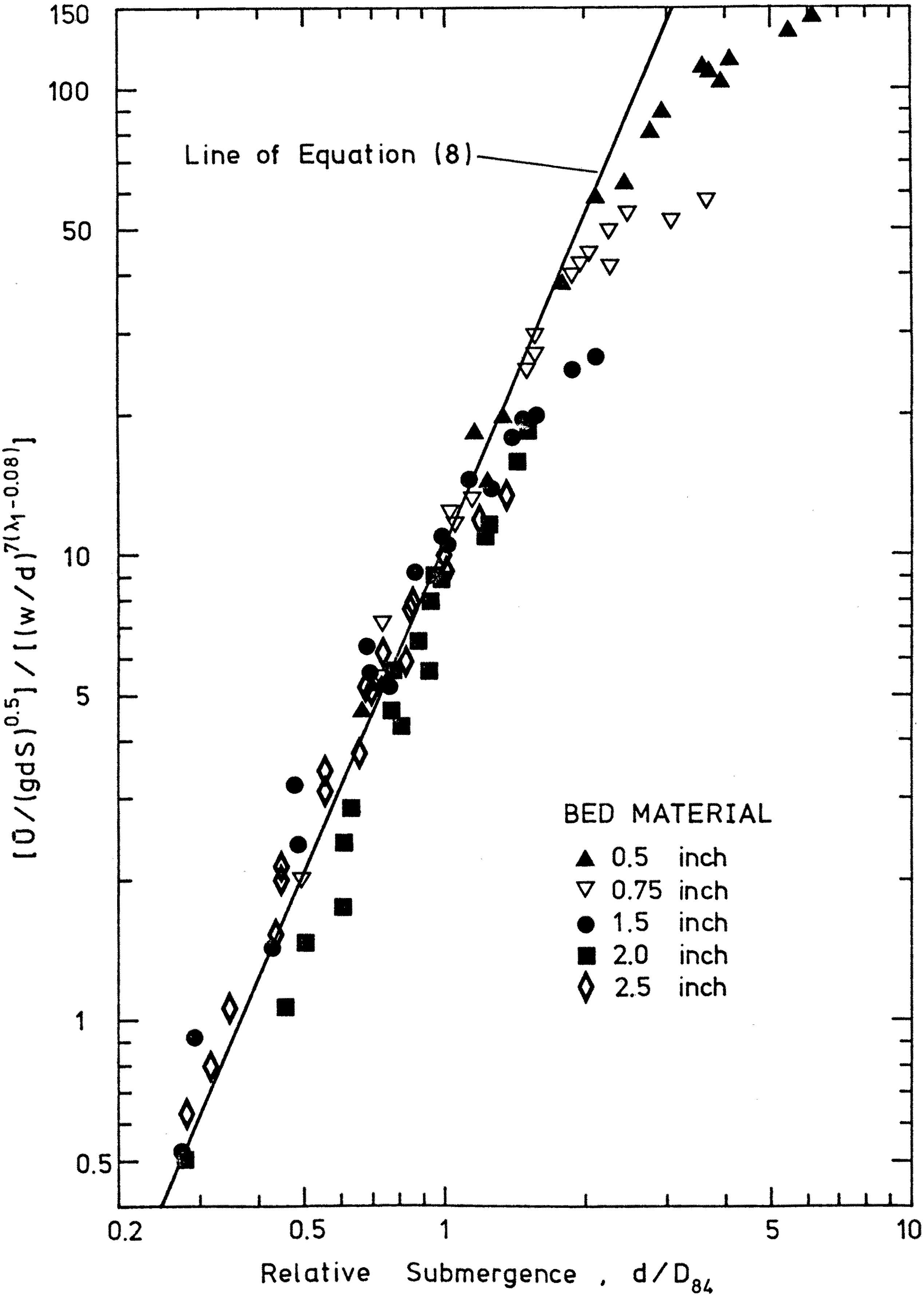

Figure 15. Variation of $[\overline{U}/(gdS)^{0.5}]/[(w/d)^{7(\lambda_1 - 0.08)}]$ with relative submergence for all the flows over the fixed roughness beds.

unity, possibly as a result of changes connected with the transition from large-scale to intermediate-scale roughness. The trend is not illustrated by the data for the 2.0 and 2.5 inch beds since relative submergence did not extend much beyond unity for those beds. At the higher relative submergences the data appear to vary in a semilogarithmic manner (Figure 16). Separate plots (fitted by eye) apply to the different roughness beds but it was found that (for the limited range of data) the differences could be resolved, and a single equation constructed, by introducing a parameter, w/D_{84}, similar to N in Equation (17), so that:

$$\frac{\bar{U}}{(gdS)^{0.5}} = \left(\frac{8}{f}\right)^{0.5} = \left[1.842\ \frac{w}{D_{84}} \log\left(\frac{d}{1.2\ D_{84}}\right) + 14.66\right] \times \left(\frac{w}{d}\right)^{7(\lambda_1 - 0.08)} \qquad (21)$$

This equation applies to the flume flows for values of d/D_{84} greater than 1.2.

In the logarithmic region (Figure 15) there is a definite scatter of data points which is based partly on differences between the roughness beds and partly on Froude number. Values of Froude number are not given in the diagram but examination of the data shows that, at a given relative submergence and for a given roughness bed, the flow resistance decreases as Froude number increases. The scatter is not so obvious in the semilogarithmic region (Figure 16) suggesting, as expected, that the effect depends on a free surface drag which is present only while the roughness elements protrude through or nearly through the free surface.

It seems then that the basic theory developed by Bathurst (1978) is correct so far as it goes. Equation (8) should therefore apply to river

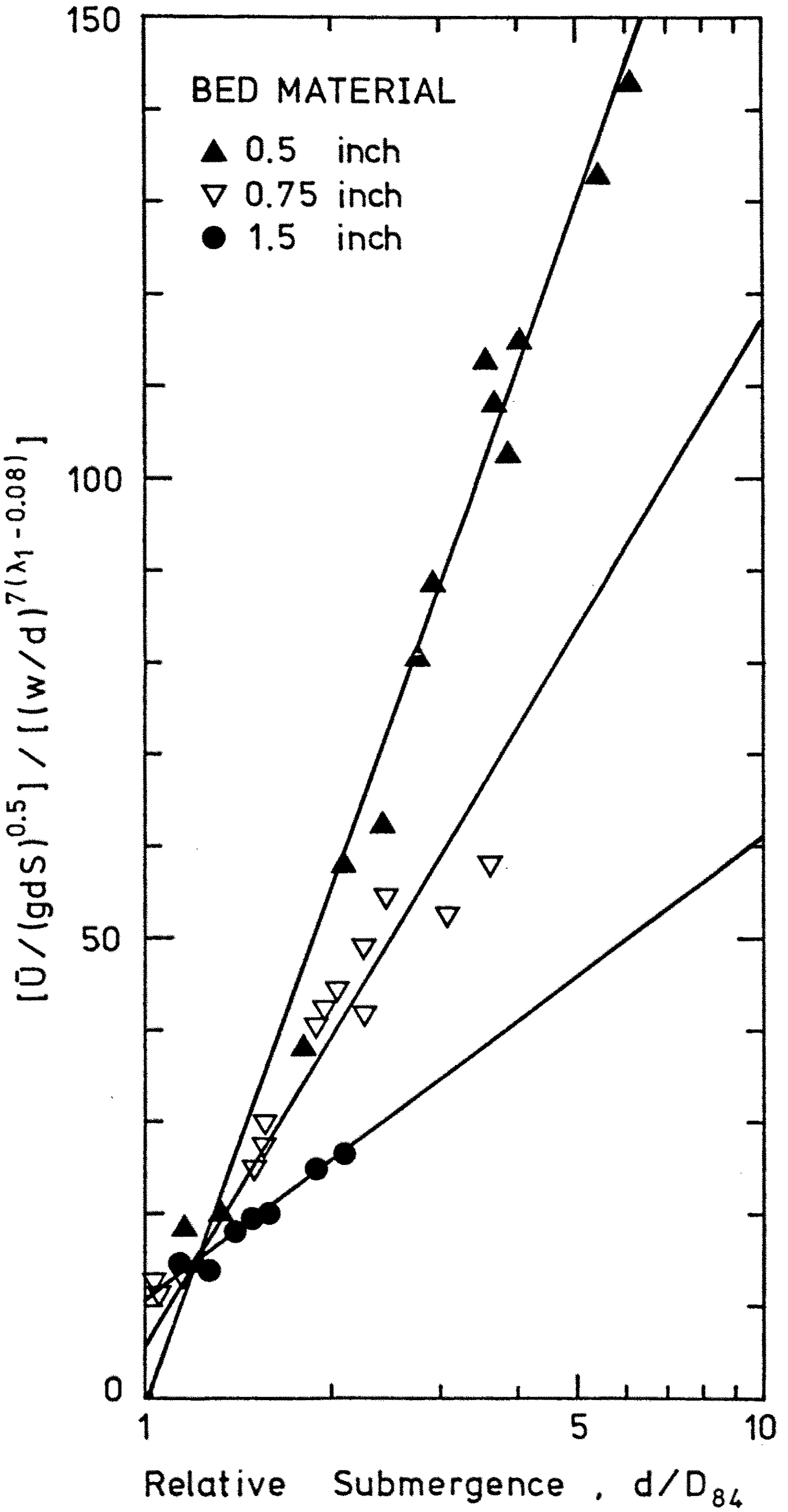

Figure 16. Variation of $[\overline{U}/(gdS)^{0.5}]/[(w/d)^{7(\lambda_1 - 0.08)}]$ with relative submergence for all the flows over the fixed roughness beds with relative submergence of greater than unity.

flows although the constants have to be empirically calibrated for individual sites. A more general equation should include additional terms to account for free surface drag and variations in roughness geometry. Also a replacement for the roughness concentration, λ_1, is required. Although values of λ_1 calculated by Equation (7) are used in the plots of Figures 15 and 16, some of those values are negative. Strictly a negative value of λ_1 is physically meaningless since the elements are then submerged and should have zero frontal concentration. However, successful application of the negative values in the diagrams indicates that some representation of roughness concentration is needed even when the elements are submerged. This can be provided by the effective roughness concentration.

SECTION 10 DEVELOPMENT OF THE FLOW RESISTANCE EQUATION

Analysis has shown that the flow resistance of large-scale roughness is likely to vary with relative roughness area, roughness geometry, Froude number and, possibly (if in the transitional boundary layer region) Reynolds number, while the flow resistance of intermediate-scale roughness should vary with relative roughness area, roughness geometry and Reynolds number. The experimental data are used to quantify these relationships in a semiempirical fashion. The relationships are derived with river channels in mind but because of the one-dimensional nature of the flume flows the results should be applicable to any given vertical in a flow and therefore to overland flow.

10.1 RELATIVE ROUGHNESS AREA AND EFFECTIVE ROUGHNESS CONCENTRATION

According to the theoretical analysis, the relative roughness area in a channel, A_w/wd', should vary directly with the ratio of width to depth, the rate of change being a function of the effective roughness concentration. That function is here denoted by the symbol b. Using Bathurst's (1978) modification of the channel parameter of Judd and Peterson (1969) as a model, the relationship can be expressed as a power law:

$$\frac{A_w}{wd'} = \left(\frac{w}{d}\right)^{-b} \tag{22}$$

The negative power is introduced now for mathematical convenience since, as was found during the analysis, the function, b, can then take positive values.

If the relationship is correct then the function, b, should vary with relative submergence since the proposed effective roughness concentration varies with relative submergence. Accordingly values of b were calculated from the measured values of A_w/wd' and w/d using Equation (22) (Appendix D) and are plotted against d/S_{50} for each roughness bed in Figure 17. To a good accuracy of fit the relationship is:

$$b = a \left(\frac{d}{S_{50}}\right)^{c} \tag{23}$$

where a and c are constants dependent on roughness geometry. Values of a and c and the accuracies of fit of the relationship for each roughness bed are given in Table 3.

TABLE 3.--Parameters of Equation (23) for the Flume Data

Bed material size in inches (1)	Constant c (2)	Constant a (3)	Constant $a^{1/c}$ (4)	Accuracy of fit of Equation (23) in percent* (5)
0.5	0.759	0.158	0.0879	1.04
0.75	0.812	0.166	0.1095	0.53
1.5	0.835	0.235	0.1765	0.37
2.0	0.929	0.229	0.2046	0.69
2.5	0.994	0.240	0.2379	0.29

*The smaller the percentage, the greater the accuracy of fit.

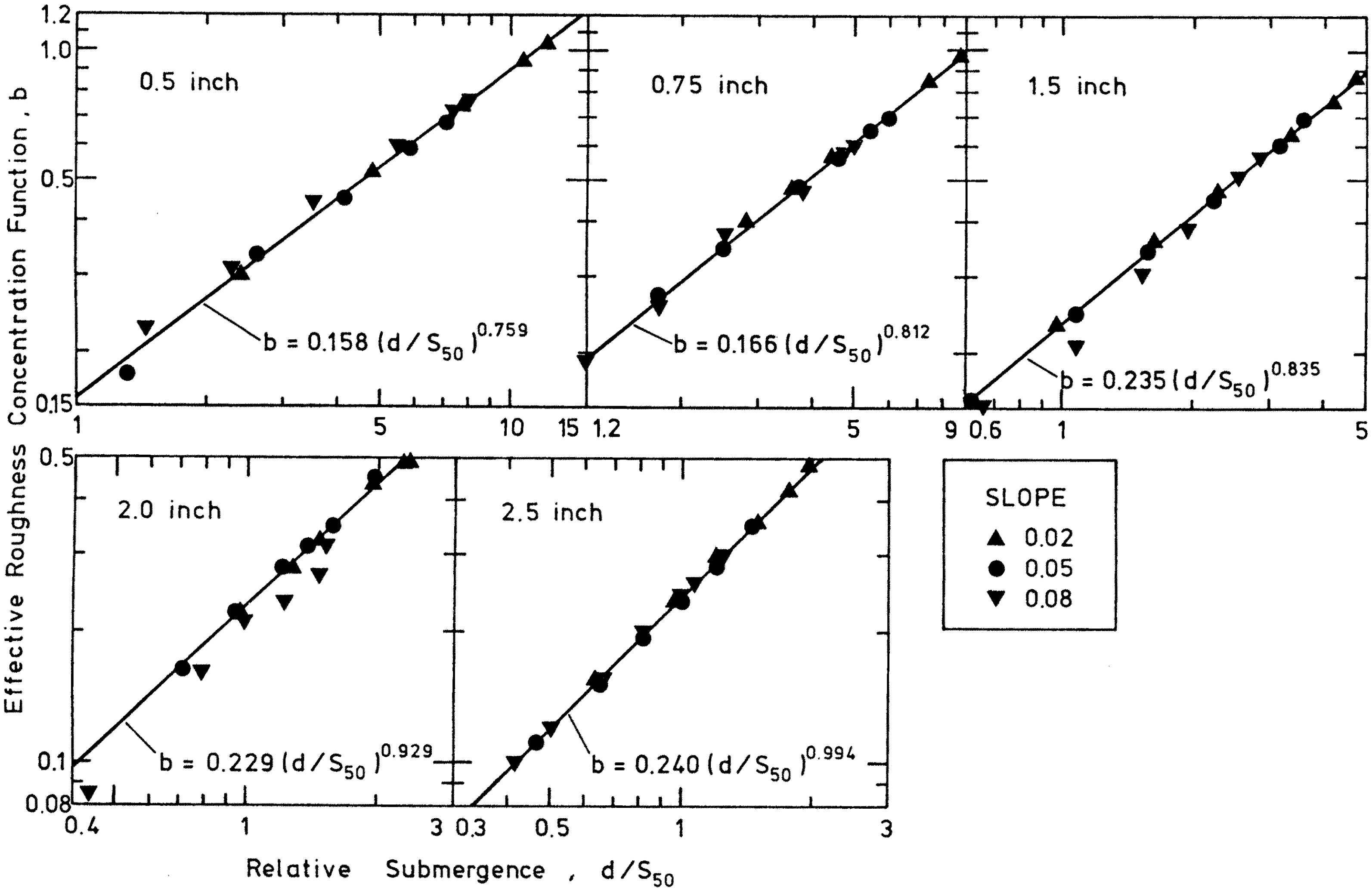

Figure 17. Variation of the effective roughness concentration function with relative submergence for all the flows over the fixed roughness beds.

This and subsequent equations were fitted to the data by computer using a direct search optimization technique (Monro, 1971). Starting with guessed values of the unknown constants in the equation, the technique improves those values according to a specified evaluation criterion so that a more accurate fit of the equation to the data is achieved. In this way the fit of the equation is optimized.

When fitting Equation (23) the data points corresponding to the following discharges were ignored: the lowest discharge at the 5 percent slope for the 0.5 inch bed; the four lowest discharges at the 8 percent slope for the 1.5 inch bed; and all discharges at the 8 percent slope for the 2.0 inch bed. These points show significant scatter compared with the remaining points (Figure 17), so by ignoring them a more accurate optimization of the equation is possible. It is thought that the scatter is caused by experimental difficulties related to the shallow depths at the steeper slopes rather than by any physical processes of resistance.

As explained earlier the rate of change of the effective roughness concentration with relative submergence should be a function of the roughness size distribution, while the magnitude should vary with roughness shape and the ratio, w/Y_n. The constant, c, represents the rate of change so it is plotted against the standard deviation, σ, of the size distribution of the short axis of each bed material (Table 2) in Figure 18. The relationship takes the form:

$$c = 0.648\ \sigma^{-0.134} \tag{24}$$

This equation, determined with an accuracy of fit of 0.7 percent, was fitted by ignoring the data point for the 0.5 inch material. It is not certain whether the scatter of that point is significant.

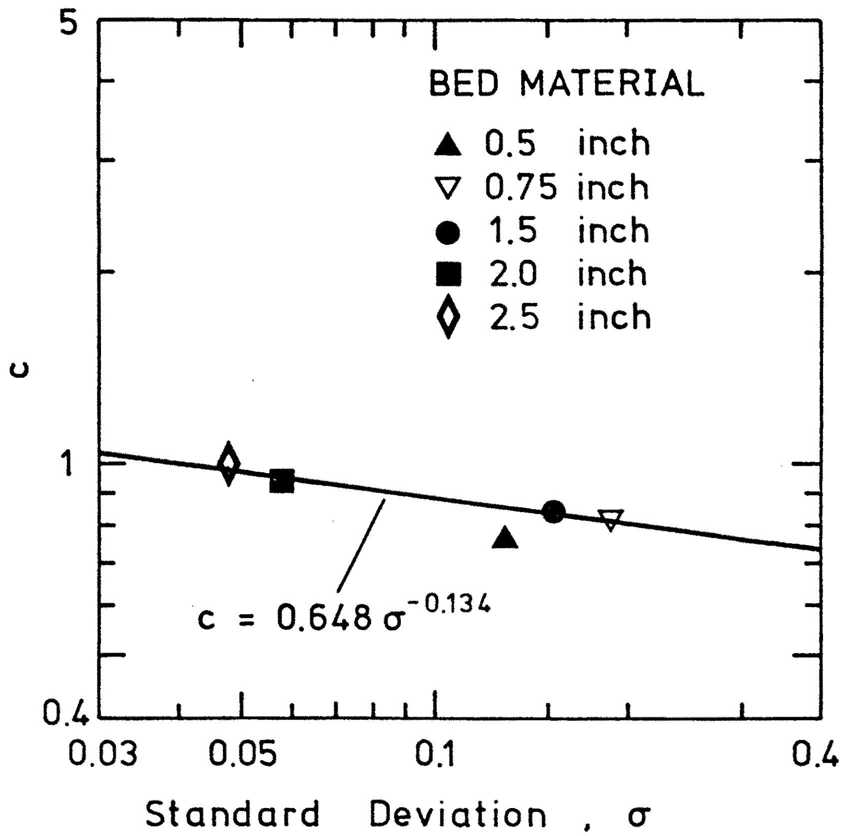

Figure 18. Variation of the parameter, c, with the standard deviation of size distribution for the fixed roughness beds.

Roughness shape is assumed to be approximately constant despite the variations in intercept sphericity between the chips and the boulders. Lying on the bed the chips presented an approximately semielliptical cross section to the flow. The cobbles, although more elliptical in cross section, probably also presented a semielliptical cross section because their lower halves were effectively shielded from the flow by their neighbours. Consequently the parameter, a, which affects the magnitude of the function, b, is tested only against the parameter w/Y_{50}, values of which are given in Table 2. Figure 19 shows that:

$$a^{1/c} = 1.175 \left(\frac{Y_{50}}{w}\right)^{0.557} \tag{25}$$

the accuracy of fit being 0.675 percent. (It should be noted that although the fit is very good, the relationship has not really been tested against changes in channel width since the flume width was constant.)

The analysis of this section therefore supports the theory developed earlier. For a channel flow, relative roughness area can be related to the ratio of width to depth and a function of effective roughness concentration and that function, b, appears to account for several of the resistive effects of roughness geometry. The function is given by:

$$b = \left[1.175 \left(\frac{Y_{50}}{w}\right)^{0.557} \left(\frac{d}{S_{50}}\right)\right]^{0.648} \sigma^{-0.134} \tag{26}$$

The function must in fact vary inversely with the effective roughness concentration since that concentration is a direct function of w/Y_{50} and S_{50}/d. This appears to be contrary to the theory developed

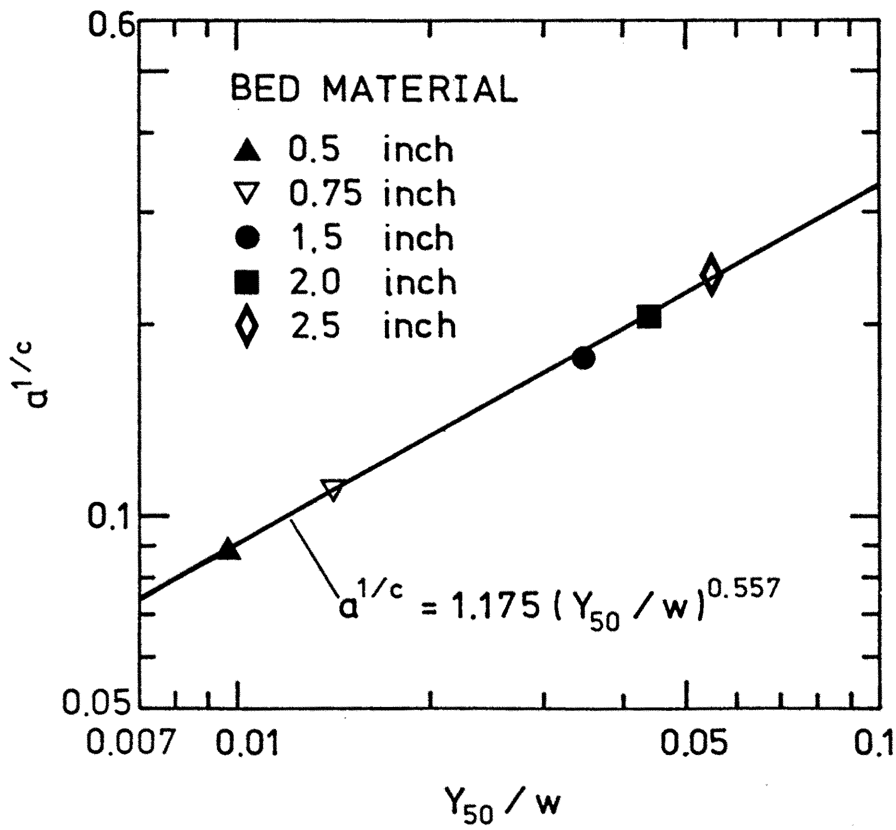

Figure 19. Variation of the parameter, $a^{1/c}$, with the parameter, Y_{50}/w, for the fixed roughness beds.

earlier which supports the form of the Judd and Peterson channel parameter, modified by Bathurst, in which the ratio of width to depth is raised to a power dependent directly on the roughness concentration. The difference is resolved in Equation (22), though, by the presence of the negative power which ensures that the right side of the equation varies correctly.

Equation (26) does not apply to uniform material, where the standard deviation of the distribution is zero. Physically this is because the theory behind the effective roughness concentration requires that the roughness concentration, λ_1, of the protruding elements should decrease as relative submergence increases. With uniform material this does not occur except over the infinitely small range where relative submergence equals unity. Mathematically the exclusion is necessary since the term accounting for the effect of size distribution, Equation (24), is derived from Figure 18 in which the scales are logarithmic and which does not therefore apply when the standard deviation of the size distribution, σ, is zero.

10.2 ROUGHNESS GEOMETRY

The analyses of Judd and Peterson (1969) and Bathurst (1978) (Equations (5) and (8)) indicate that, in the absence of Froude and Reynolds numbers effects, the flow resistance of a fixed bed should depend on the relative roughness area and some function of roughness geometry which should vary with relative submergence. It is suggested here that the function can most usefully be represented by the function of effective roughness concentration, b, since that function indicates the effect of the roughness geometry at any given relative submergence.

In order to determine the function of b to be included in the equation, the ratio $[\bar{U}/(gdS)^{0.5}]/[A_w/wd']$ is plotted against b for each roughness material in Figures 20 to 24. This particular format and the logarithmic scales are chosen since the analyses of Judd and Peterson (1969) and Bathurst (1978) show that the resistance equation can be represented by a power law.

Generally the data points lie about one line for each roughness. However, there is a certain amount of scatter, particularly at the lower values of b. As in Figure 15, the scatter is probably due to the free surface drag of elements protruding through the free surface. The given Froude numbers in Figures 20 to 24 show that for each roughness bed, the lower the Froude number at a given value of b, the higher the flow resistance. The scatter is less obvious at the higher values of b where the elements are submerged and free surface drag is negligible.

To define the function of roughness geometry, only those data points representing flows unaffected by Froude number can be used. These points were identified, using Figure 2, on the basis of Froude number and relative submergence d/S_{100}, where S_{100} = the maximum size of the short axis, or height, of the material. S_{100} is used instead of S_{50} because only when depth exceeds S_{100} can it be said that the elements are all submerged and direct comparison with Figure 2 be made. (In fact because mean depth, d, is less than the actual depth, d', against the elements, a value of d/S_{100} equal to unity means that the elements do not in fact quite reach the free surface.)

Approximate values of S_{100} were calculated by assuming that all the points of a size distribution lie within three standard deviations of the mean. (Strictly that range includes only 99.9 percent of the

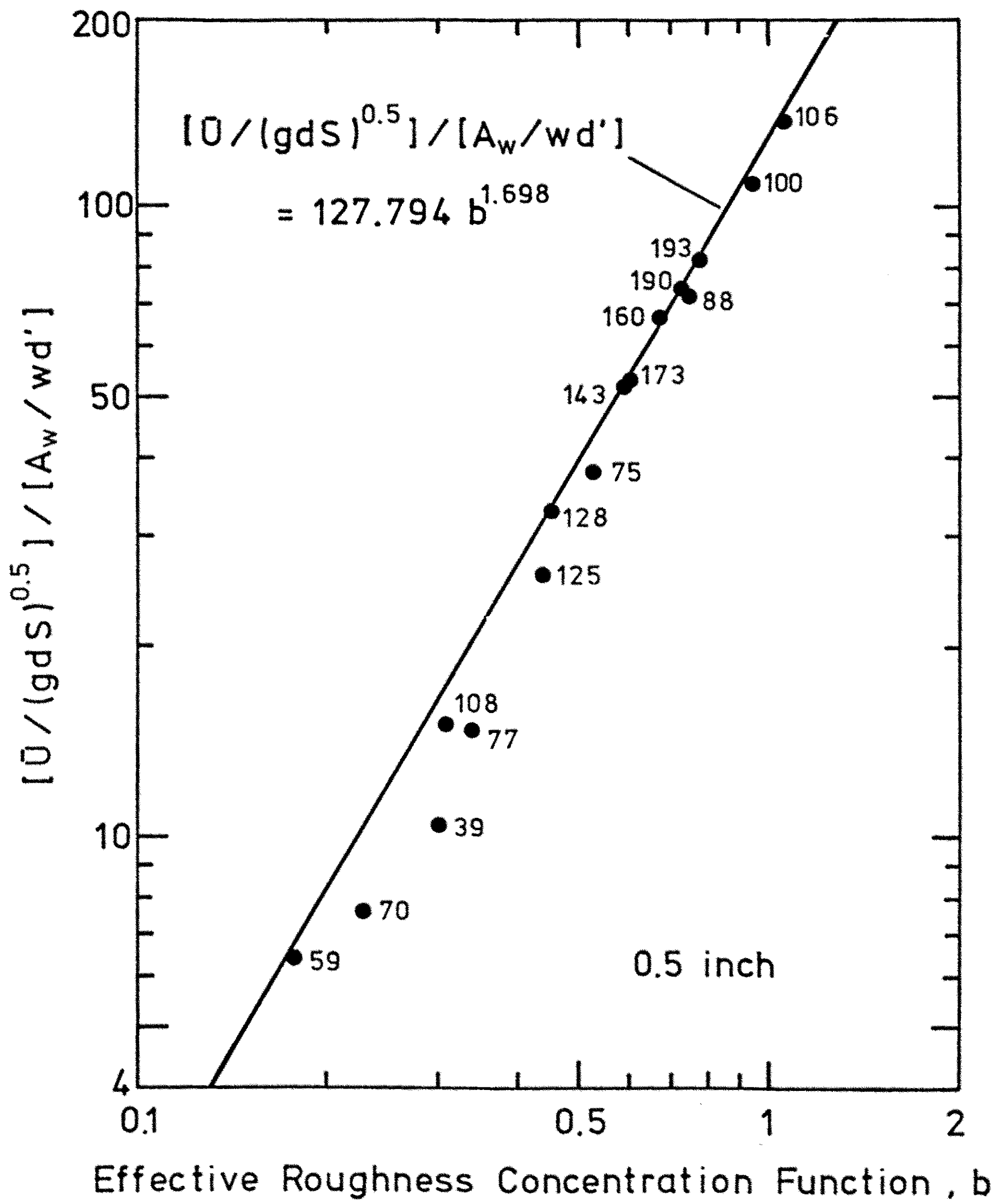

Figure 20. Variation of $[\bar{U}/(gdS)^{0.5}]/[A_w/wd']$ with the effective roughness concentration function for the flows over the 0.5 inch fixed roughness bed. Corresponding Froude numbers, multiplied by 100, are given by each data point.

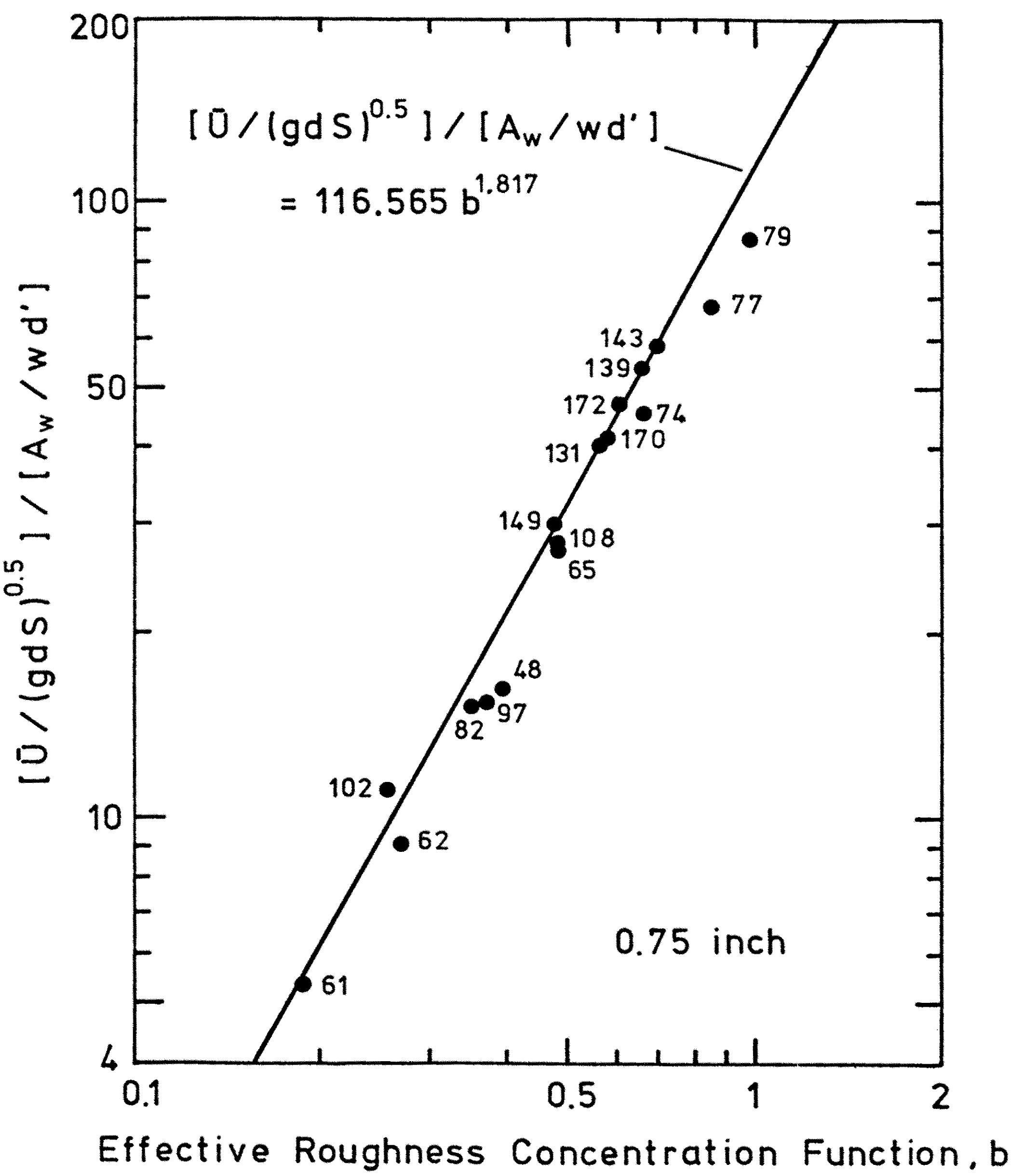

Figure 21. Variation of $[\overline{U}/(gdS)^{0.5}]/[A_w/wd']$ with the effective roughness concentration function for the flows over the 0.75 inch fixed roughness bed. Corresponding Froude numbers, multiplied by 100, are given by each data point.

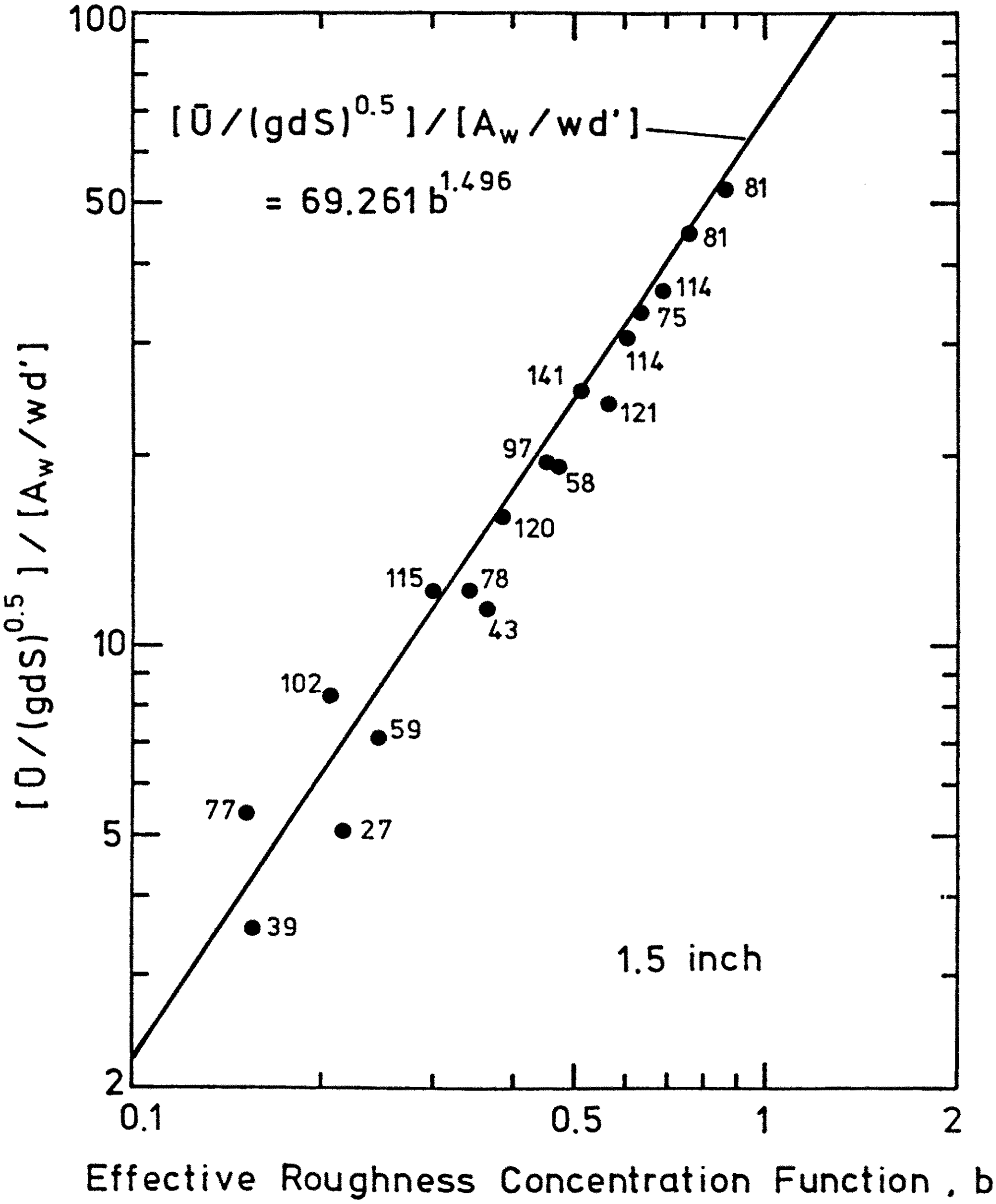

Figure 22. Variation of $[\bar{U}/(gdS)^{0.5}]/[A_w/wd']$ with the effective roughness concentration function for the flows over the 1.5 inch fixed roughness bed. Corresponding Froude numbers, multiplied by 100, are given by each data point.

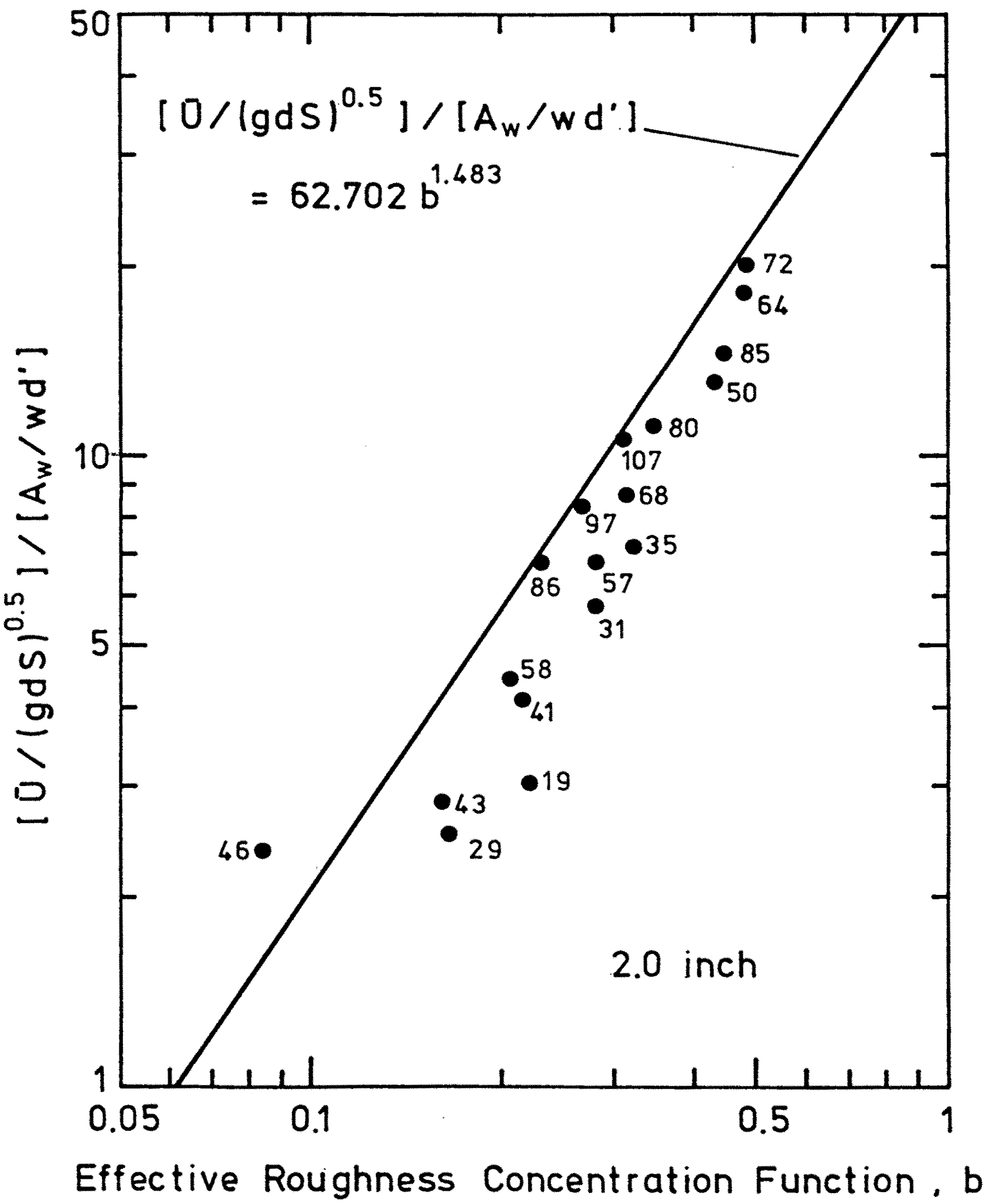

Figure 23. Variation of $[\bar{U}/(gdS)^{0.5}]/[A_w/wd']$ with the effective roughness concentration function for the flows over the 2.0 inch fixed roughness bed. Corresponding Froude numbers, multiplied by 100, are given by each data point.

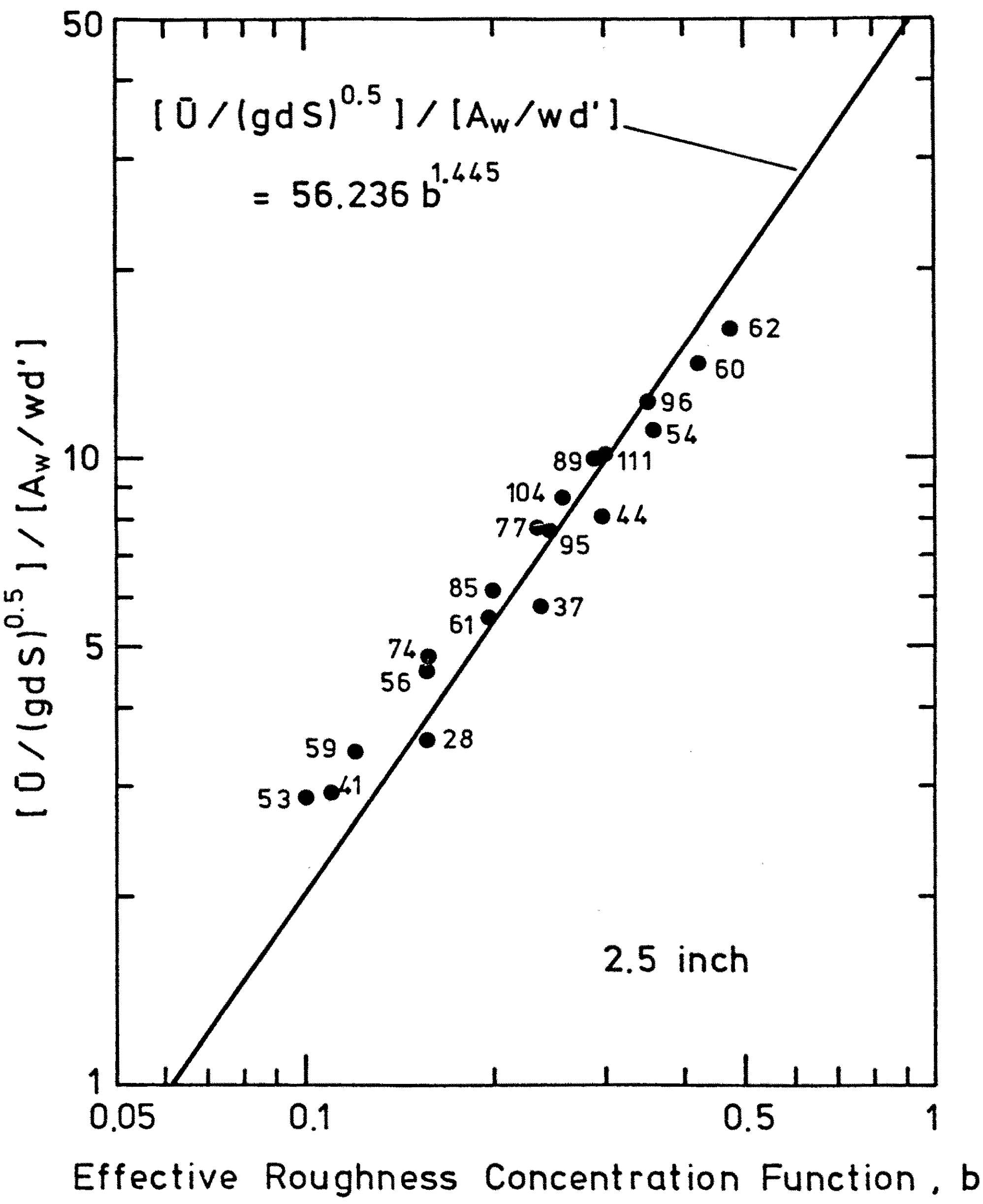

Figure 24. Variation of $[\bar{U}/(gdS)^{0.5}]/[A_w/wd']$ with the effective roughness concentration function for the flows over the 2.5 inch fixed roughness bed. Corresponding Froude numbers, multiplied by 100, are given by each data point.

points.) Consequently the maximum size (for a log-normal distribution) is given by:

$$\log S_{100} = \log S_{50} + 3\ \sigma \tag{27}$$

Values are given in Appendix C.

Data points were then chosen according to the following criteria:

Data points with Froude number > 1.5

Data points with values of $d/S_{100} \gtrsim 1.5$ and Froude number > 1.3

Data points with values of $d/S_{100} \gtrsim 2.5$ and Froude number > 1.1

Data points with values of $d/S_{100} \gtrsim 3.0$ and Froude number > 1.0

Data points with values of $d/S_{100} \gtrsim 3.5$ and Froude number > 0.9

This segregation reduced the number of available data points to eight for the 0.5 inch material, six for the 0.75 inch material, one for the 1.5 inch material and none for the 2.0 and 2.5 inch materials. Using these limited data the general function of b for the three smaller bed materials was found to be:

$$\left[\frac{\bar{U}}{(gdS)^{0.5}}\right] \Big/ \left[\frac{A_w}{wd'}\right] = e\ b^m \tag{28}$$

where e and m are constants dependent on roughness geometry.

Since only one theoretically acceptable data point was available for the 1.5 inch material, an approximate value for the gradient, m, of the relationship for that material was obtained using a few other points. Generally these were characterized by Froude numbers and values of d/S_{100} both greater than unity, so the free surface drag, while present, should not have had a great effect. Values of e and m derived from the data for the three chip beds and the accuracies of fit of Equation (28) are given in Table 4. The plots of Equation (28) appear in Figures 20 to 22.

TABLE 4.--Parameters of Equation (28) for the Flume Data

Bed material size in inches (1)	Constant e (2)	Constant m (3)	Accuracy of fit of Equation (28) in percent+ (4)
0.5	127.794	1.698	6.81
0.75	116.565	1.817	5.28
1.5	69.261	1.496	1.75
2.0	62.702*	1.483*	---
2.5	56.236*	1.445*	---

+The smaller the percentage, the greater the accuracy of fit

*Calculated with Equations (29) and (30)

With data available for only three bed materials, the functions defining e and m could not be derived with great certainty. The physical meaning of the constants is not clear but on an empirical basis they seem to vary with w/Y_{50}, the function representing the number of elements at a section (Figures 25 and 26). This makes some sense for the constant e since that constant determines the magnitude of the roughness geometry function and might therefore depend on the number of elements. However, it is also possible that roughness shape might have a significant effect. As for the constant, m, although it can apparently be related to w/Y_{50} over the limited range of data, it might

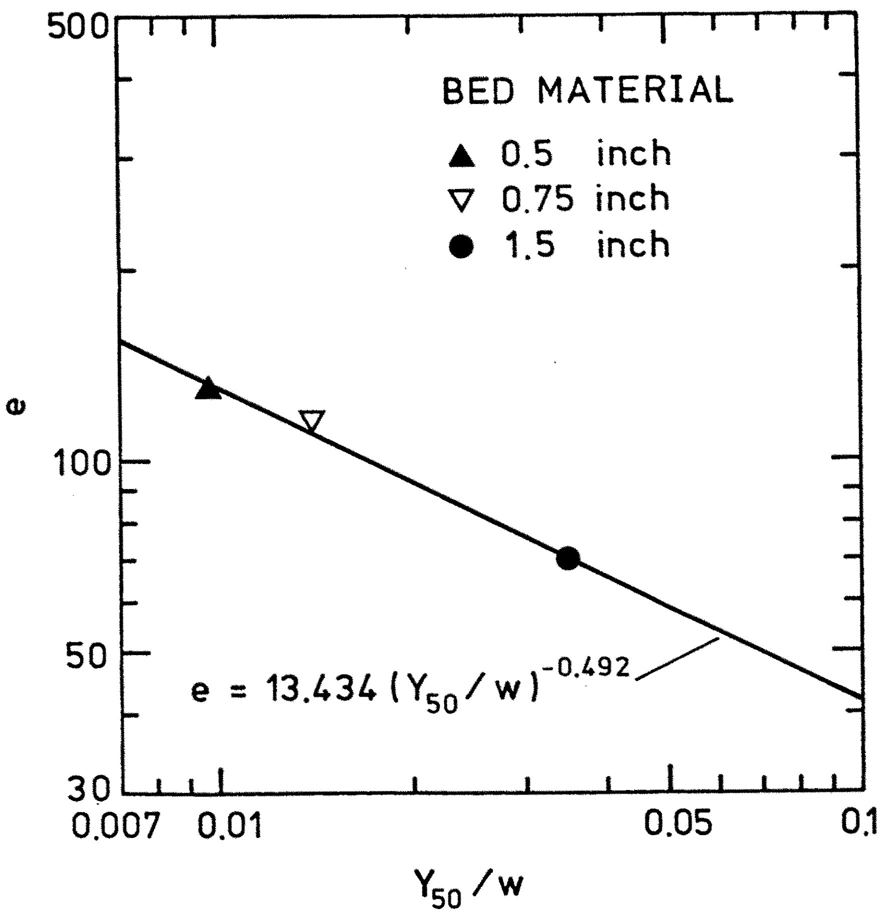

Figure 25. Variation of the parameter, e, with the parameter, Y_{50}/w, for the 0.5, 0.75 and 1.5 inch fixed roughness beds.

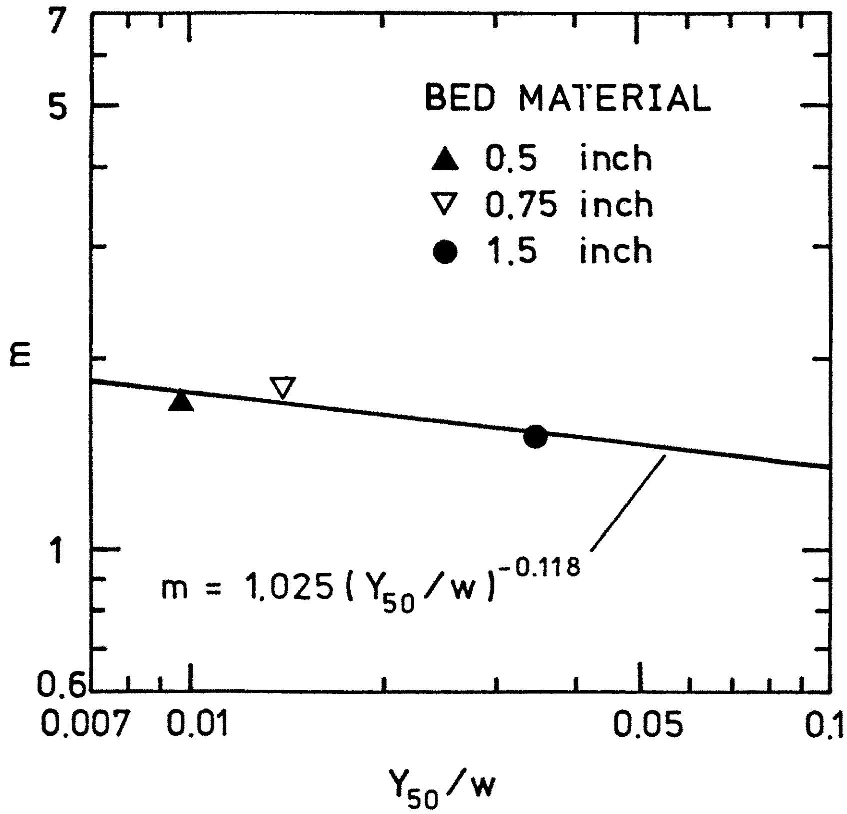

Figure 26. Variation of the parameter, m, with the parameter, Y_{50}/w, for the 0.5, 0.75 and 1.5 inch fixed roughness beds.

also vary with roughness shape or even, given the restricted range of its values, be an absolute constant.

The equations fitted to the data are:

$$e = 13.434 \left(\frac{w}{Y_{50}}\right)^{0.492} \tag{29}$$

(accuracy of fit, 2.33 percent)

$$m = 1.025 \left(\frac{w}{Y_{50}}\right)^{0.118} \tag{30}$$

(accuracy of fit, 2.74 percent).

Equation (29) seems a reasonable representation of the available data. Equation (30) is less certain because of the small range in the values of m. However, that small range also suggests that, if Equation (30) is wrong, the errors involved may not be large.

Values of e and m for the 2.0 and 2.5 inch materials were calculated with Equations (29) and (30) and are given in Table 4. The resultant plots of Equation (28) appear in Figures 23 and 24.

Based on the analysis of this section, the resistance equation for the roughness beds, neglecting Froude and Reynolds numbers effects, is:

$$\frac{\bar{U}}{(gdS)^{0.5}} = \left(\frac{8}{f}\right)^{0.5}$$

$$= \left[13.434 \left(\frac{w}{Y_{50}}\right)^{0.492}\right] \times \left[b^{1.025(w/Y_{50})^{0.118}}\right] \times \left[\frac{A_w}{wd'}\right] \tag{31}$$

where the relative roughness area is given by Equations (22) and (26). Equation (31) is directly comparable with Equations (5) and (8) for given roughness beds.

10.3 FREE SURFACE DRAG

The disposition of the data points in Figures 20 to 24 suggests that free surface drag is significant at flows with low relative submergences, essentially in the region of large-scale roughness. The data also indicate that, for a given relative submergence, the free surface drag of the bed as a whole decreases as Froude number increases. This pattern is different from the pattern for individual elements where the drag first increases then decreases as Froude number increases (Flammer, Tullis and Mason, 1970).

Since Reynolds number effects are assumed to be absent from the flume flows, the variations in the resistance coefficient which are not accounted for by the parameters of roughness geometry and relative roughness area should be a function of free surface drag only. The resistance coefficient is a direct function of the element drag coefficient, so the complete resistance equation for the flume flows (assuming a power law relationship) should be:

$$\left(\frac{8}{f}\right)^{0.5} = \text{fn}\left(\frac{1}{C_{DF}}\right) \text{x RHS} \qquad (32)$$

where C_{DF} = the component of the drag coefficient accounting for free surface drag; fn () = a function; and RHS = the right side of Equation (31). The function of the drag coefficient can therefore be calculated as the ratio of $(8/f)^{0.5}$ to the right side of Equation (31) and should be unity for those data points representing flows unaffected by free surface drag. Calculated values of the function are presented in Appendix D. (The values for the 2.0 and 2.5 inch materials depend on the calculated values of the constants e and m in Equation (28).)

As the resistance, and the drag coefficient, vary inversely with Froude number, the function of the drag coefficient should vary directly with Froude number at any given relative submergence or, more generally, at any given effective roughness concentration. Consequently the calculated values of the function are plotted against Froude number in Figure 27. Separate plots are prepared for different ranges of the effective roughness concentration function, the ranges being defined by a margin of 0.05 above and below values of b equal to 0.1, 0.2, 0.3, 0.4, 0.5, 0.6 and 0.7. The range of the actual data and the mean value of b for each range are noted in Figure 27.

There is a certain amount of scatter in the diagrams. This is to be expected since the results of this stage of the analysis depend on the derived results of the stages concerned with roughness geometry and relative roughness area and, as the analysis has proceeded from stage to stage, uncertainties have build up. However, the trends in Figure 27 are obvious, indicating that the function of the drag coefficient related to free surface drag does indeed vary directly with Froude number, Fr. The relationship takes the form:

$$\mathrm{fn}\left(\frac{1}{C_{DF}}\right) = i\ \mathrm{Fr}^{j} \qquad (33)$$

where i and j are constants which depend on the function of effective roughness concentration, b. The values of i and j and the accuracies of fit of Equation (33) are given in Table 5.

It should be expected that as the relative submergence, or the function of effective roughness concentration, increases, the free surface drag effect should decrease. Constants i and j should

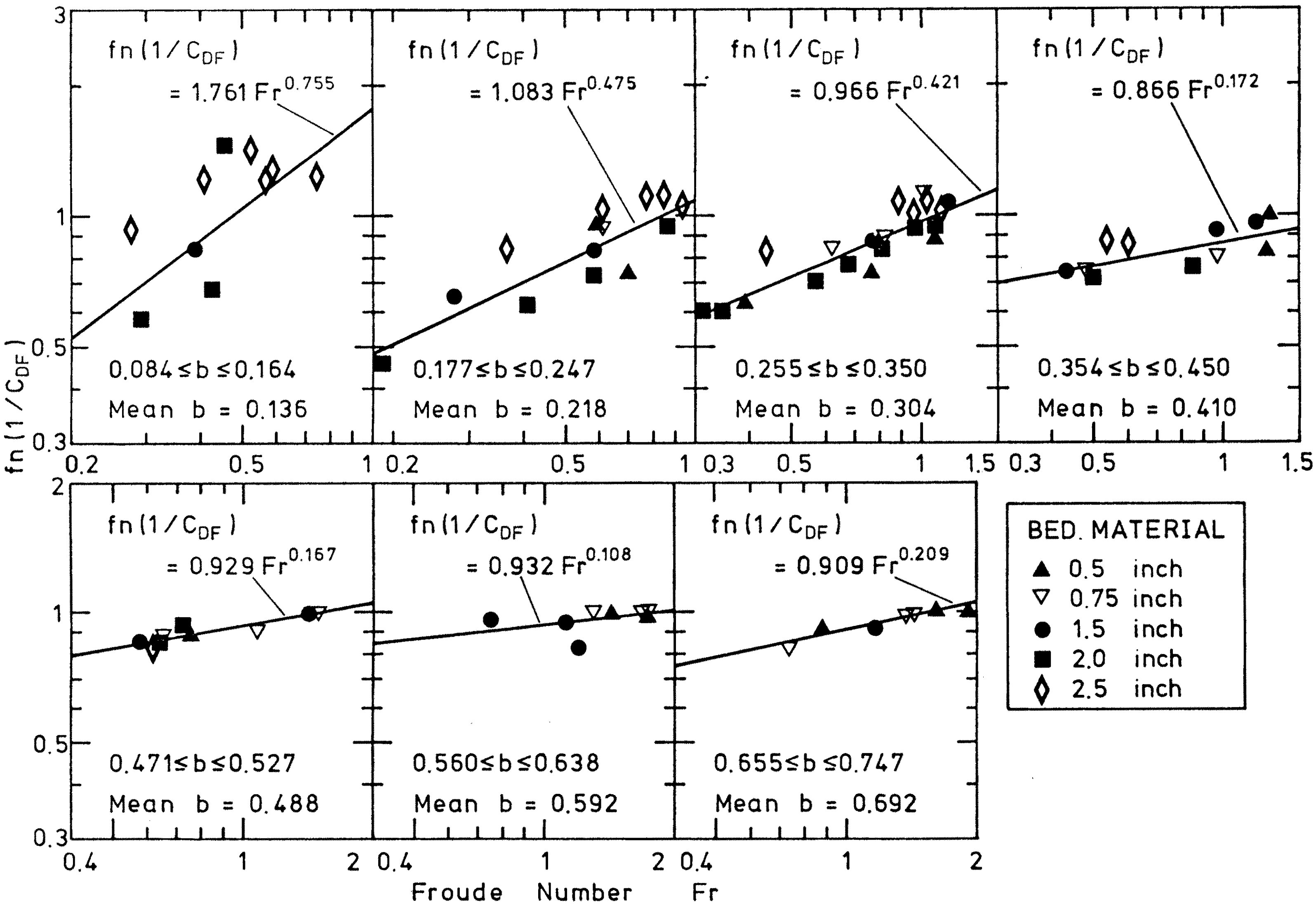

Figure 27. Variation of the function of the drag coefficient accounting for free surface drag with Froude number and the effective roughness concentration function for all the flows over the fixed roughness bed.

TABLE 5.--Parameters of Equation (33) for the Flume Data

Mean effective roughness concentration (1)	Constant j (2)	Constant i (3)	Constant $i^{1/j}$ (4)	Accuracy of fit of Equation (33) in percent* (5)
0.136	0.755	1.761	2.116	7.20
0.218	0.475	1.083	1.183	3.49
0.304	0.421	0.966	0.921	2.01
0.410	0.172	0.866	0.433	2.32
0.488	0.167	0.929	0.643	0.91
0.592	0.108	0.932	0.521	2.19
0.692	0.209	0.909	0.633	1.02

*The smaller the percentage, the greater the accuracy of fit

therefore be inverse functions of b. Figures 28 and 29 support this argument, indicating the relationships to be:

$$j = \log\left(\frac{0.755}{b}\right) \tag{34}$$

(accuracy of fit, 14.30 percent)

$$i^{1/j} = \frac{0.28}{b} \tag{35}$$

(accuracy of fit, 8.24 percent).

Thus:

$$\text{fn}\left(\frac{1}{C_{DF}}\right) = \left[\frac{0.28}{b}\,\text{Fr}\right]^{\log\,(0.755/b)} \tag{36}$$

Once b rises to a value of 0.755, the constant j becomes zero and the function of the drag coefficient equals unity, in other words the free surface drag is negligible. For greater values of b the

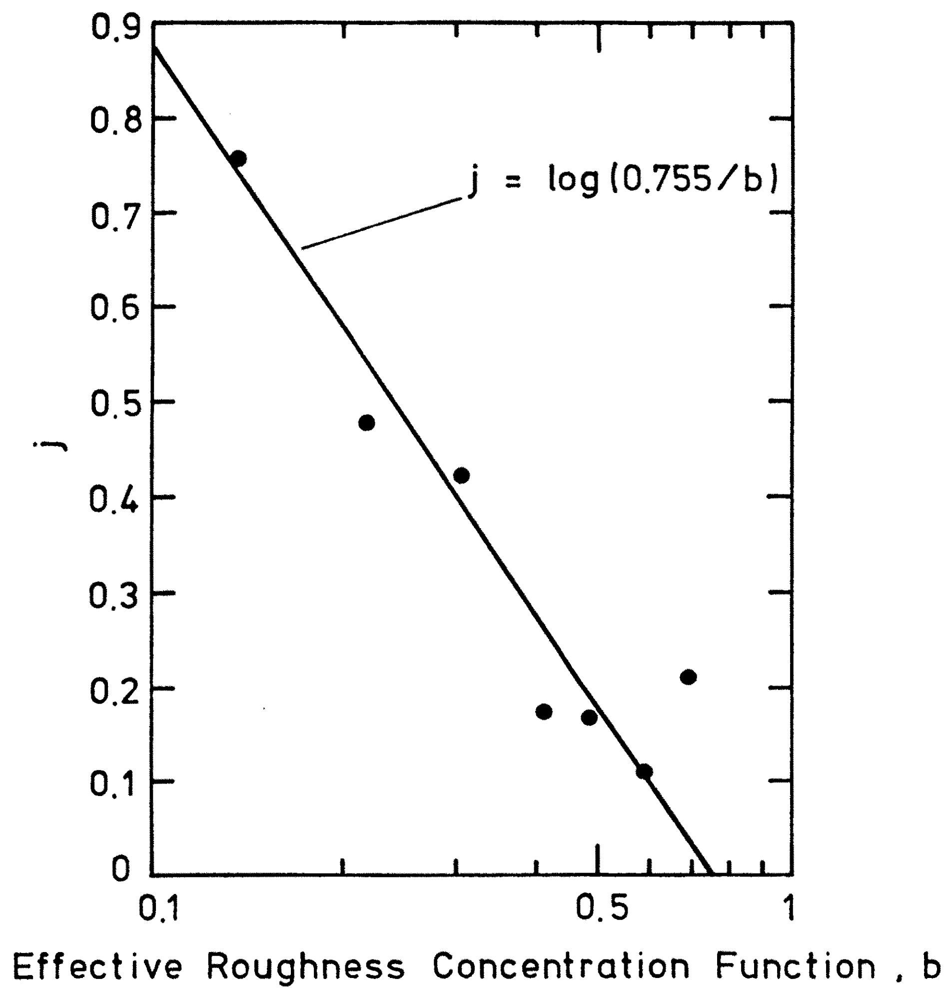

Figure 28. Variation of the parameter, j, with the effective roughness concentration function for the fixed roughness beds.

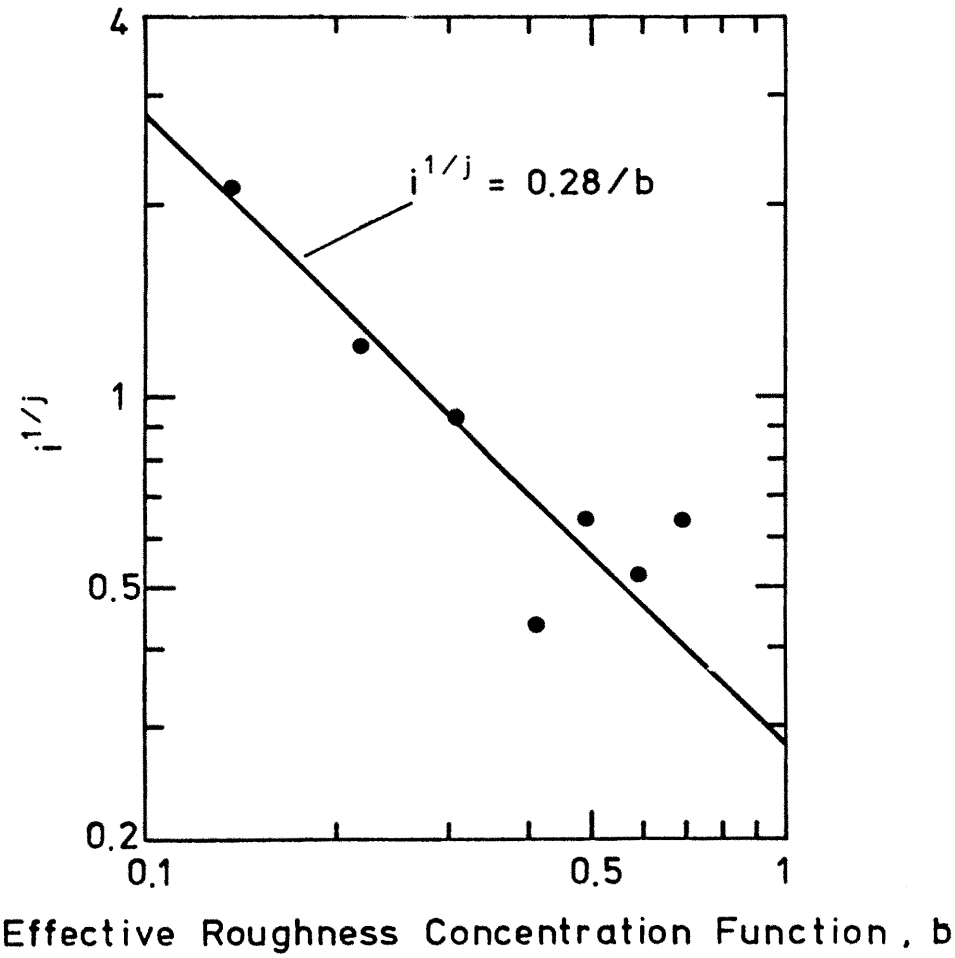

Figure 29. Variation of the parameter, $i^{1/j}$, with the effective roughness concentration function for the fixed roughness beds.

function of the drag coefficient should be set equal to unity rather than remain defined by Equation (36), since the free surface drag of the elements should continue to be negligible.

10.4 FLOW RESISTANCE EQUATION FOR THE FIXED BEDS

Combination of Equations (31), (32), and (36) results in the resistance equation for the fixed beds:

$$\frac{\bar{U}}{(gdS)^{0.5}} = \left(\frac{8}{f}\right)^{0.5}$$

$$= \Bigg[\underbrace{\frac{0.28}{b}\,Fr}_{(1)}\Bigg]^{\log\,(0.755/b)}$$

$$\times \underbrace{\left[13.434\left(\frac{w}{Y_{50}}\right)^{0.492} b^{1.025\,(w/Y_{50})^{0.118}}\right]}_{(2)}$$

$$\times \underbrace{\left[\frac{A_w}{wd'}\right]}_{3} \tag{37}$$

where

$$b = \left[1.175\left(\frac{Y_{50}}{w}\right)^{0.557}\left(\frac{d}{S_{50}}\right)\right]^{0.648\,\sigma^{-0.134}} \tag{26}$$

Term (1) accounts for the free surface drag of the elements and is equal to unity once b exceeds a value of 0.755. Term (2) accounts for the roughness geometry and term (3) accounts for the relative roughness area. For channel flows or flows with lateral boundaries the relative roughness area is given by:

$$\frac{A_w}{wd'} = \left(\frac{w}{d}\right)^{-b} \tag{22}$$

Equation (37) applies to steady, uniform flows over closely packed roughness beds with nonuniform size distributions, under the following restrictions:

$0.1 < b < 1$

$0.41 < d/S_{50} < 12.10$

$13 < w/d < 153$

$0.19 < \bar{U}/(gd)^{0.5} < 1.93$

$10^3 < \bar{U}\ D_{50}/\ \nu < 4.4 \times 10^4$

The standard deviations, σ, of the size distributions of the bed materials varied from 0.047 to 0.187.

Because the relative roughness area, the effective roughness concentration and the variable function of free surface drag all apply to submerged or protruding roughness elements, Equation (37) can be used with both large-scale and intermediate-scale roughnesses, at least for the given range of flume flows. In this respect it is superior to Bathurst's (1978) equation (Equation (8)) which applies only to large-scale roughness.

Using all the flume data, values of the resistance function $(8/f)^{0.5}$ were calculated with Equations (22), (26) and (37) and are plotted against the measured values in Figure 30. Since the data are those on which the equations are based, agreement is naturally reasonable. It is encouraging, though, that the calculated values are generally within 10 percent of the measured values and do not exhibit any obvious trends away from the line of perfect agreement.

10.5 FLOW RESISTANCE OF LOOSE BEDS

Using the data collected from the experiments with loose beds, a few details of the effect of sediment transport on flow resistance can be outlined.

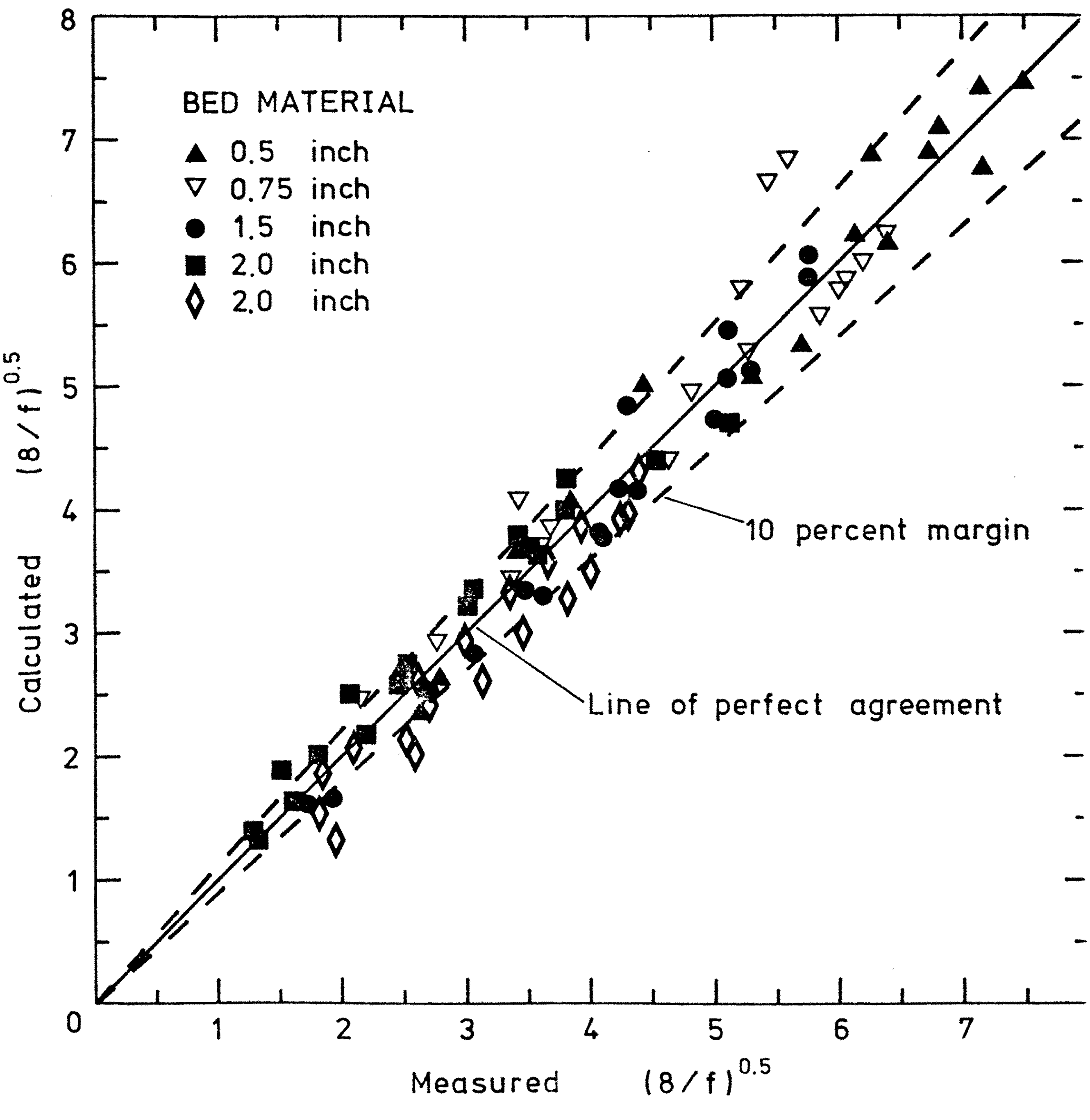

Figure 30. Comparison of values of the resistance function calculated using Equation (37) with measured values for all the flows over the fixed roughness beds.

Figure 31 shows the variation of sediment discharge with water discharge for the four sets of data. The straight lines are fitted by eye. Once sediment movement begins, sediment discharge increases with water discharge. For a given material, the steeper the channel slope, the lower is the critical water discharge at which sediment movement begins because of the increasing aid that gravitational forces provide.

The relationship between the resistance function, $(8/f)^{0.5}$, and relative submergence for the loose beds and for the equivalent fixed beds is shown in Figure 32. As expected, there is a difference in pattern between the fixed and loose beds, the flow resistance of the loose beds without sediment movement generally being greater at a given relative submergence. It also appears that for a given bed material, the greater the channel slope, the greater is the flow resistance of a loose bed at a given relative submergence. This is the reverse of the pattern observed with the fixed beds where a steeper slope results in a higher Froude number and therefore a lower flow resistance. The reason for the reverse may be related to a variation with slope of the proportion of the total water discharge which occurs through, rather than over, the loose bed.

In general the flow resistance of the fixed beds decreases at a uniform rate as relative submergence increases. In the case of the loose beds, once sediment movement has begun, there is an initial sharp decrease in flow resistance followed by an equally sharp increase in resistance. At the intervening peak value of the resistance function the resistance of the loose beds (with sediment movement) is less than the resistance of the fixed beds, bearing in mind the different datum levels for the resistances of fixed and loose beds. Also the peak

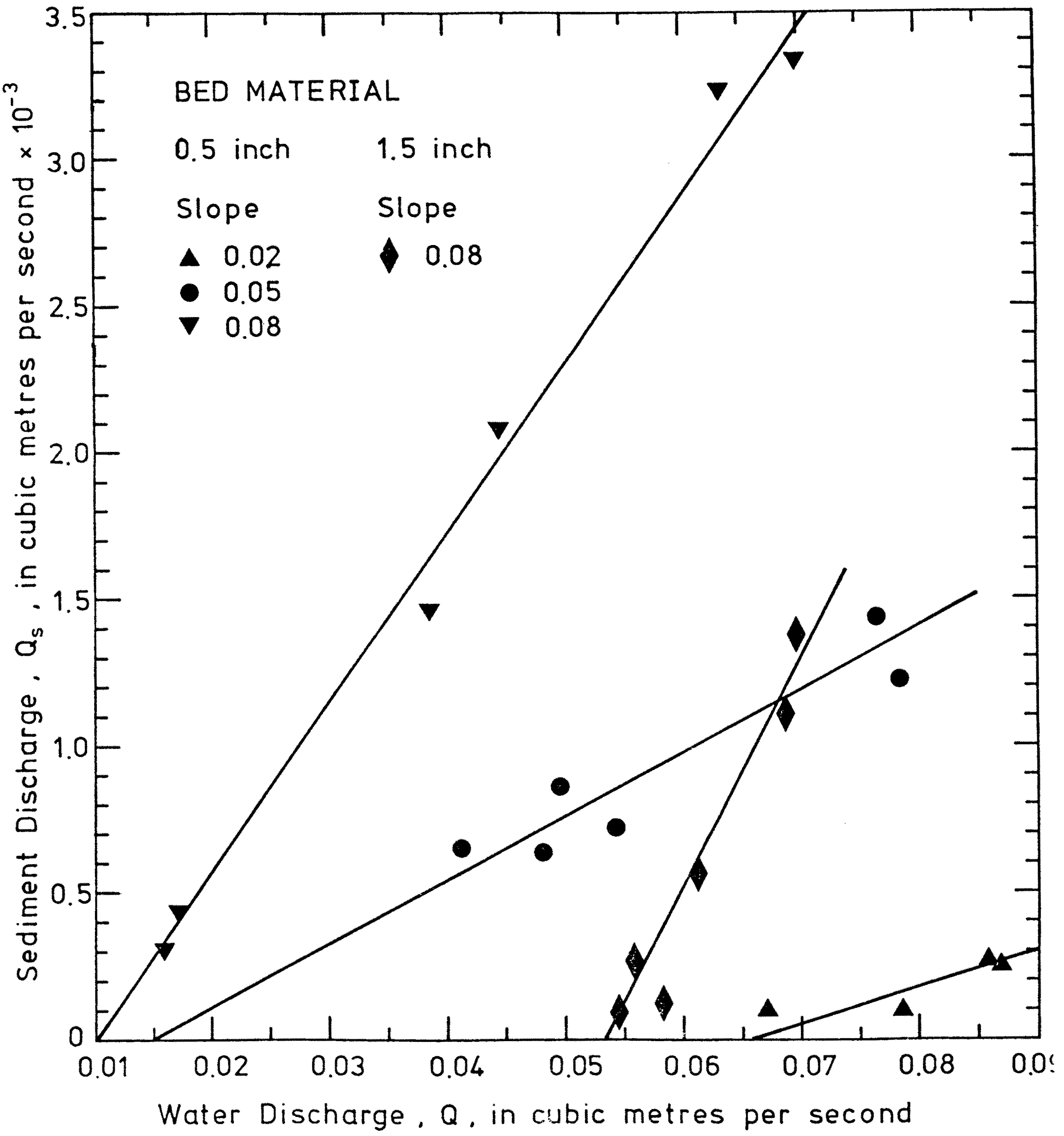

Figure 31. Variation of sediment discharge with water discharge for the flows over the loose roughness beds.

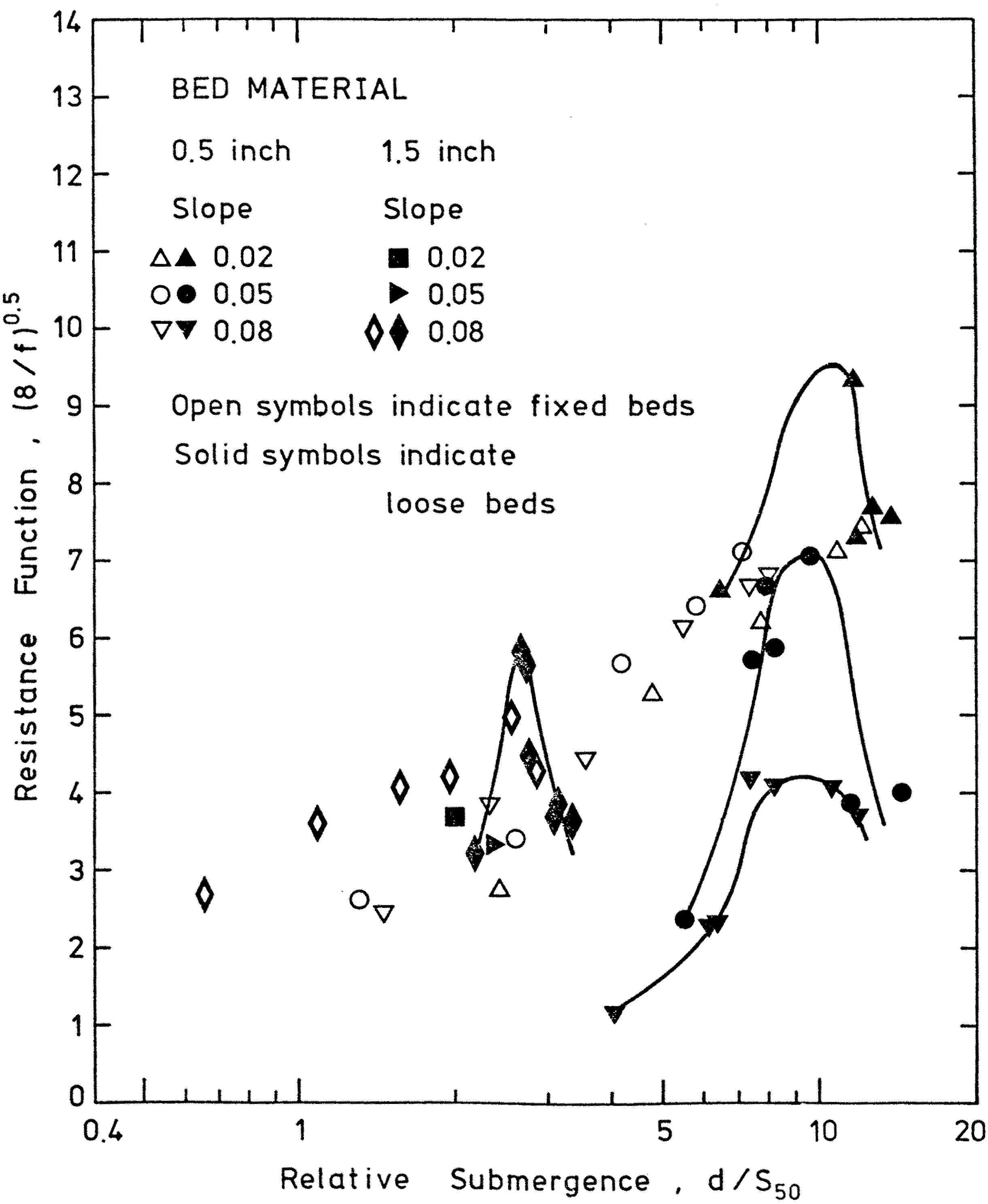

Figure 32. Variation of the resistance function with relative submergence for all the flows over the loose roughness beds. For each slope the data point with the lowest relative submergence corresponds to a flow without sediment movement. Data points for flows over the corresponding fixed roughness beds are provided for purposes of comparison.

appears to occur at approximately the same relative roughness for a given bed material, whatever the channel slope. There are insufficient data to show whether the increase in resistance continues as relative submergence increases or whether some other trend is adopted.

The data are presented a little differently in Figure 33 where the measured values of the resistance function are compared with those predicted by the resistance equation for fixed beds. Since the calculated values are direct functions of relative submergence, Figure 33 shows the same trends as does Figure 32. It also indicates that, once sediment transport begins, the resistance equation for fixed beds does not account for the observed trends of the resistance function.

Because of the paucity of data it is not possible to give a definitive reason for the observed variation in resistance. It may be, though, that over the region where the resistance decreases as relative submergence increases, the bed material is only rolling. This could result in a smoothing of the bed by comparison with the loose bed without sediment movement. Also the moving material might act in effect as a lubricant, thereby reducing the drag on the flow.

At the higher discharges the material might be induced to leave the bed for short periods and bounce or saltate. It is unlikely that such movement would be as vigorous as with a sand-bed but even small jumps would propel the material into the flow. The elements, being supported by the fluid, would then extract momentum from the flow as they fell to the bed. The result would be a much greater drag on the flow than could be generated by rolling elements, which are supported by the bed. Such a process could therefore be responsible for the observed increase in resistance at the higher relative submergences.

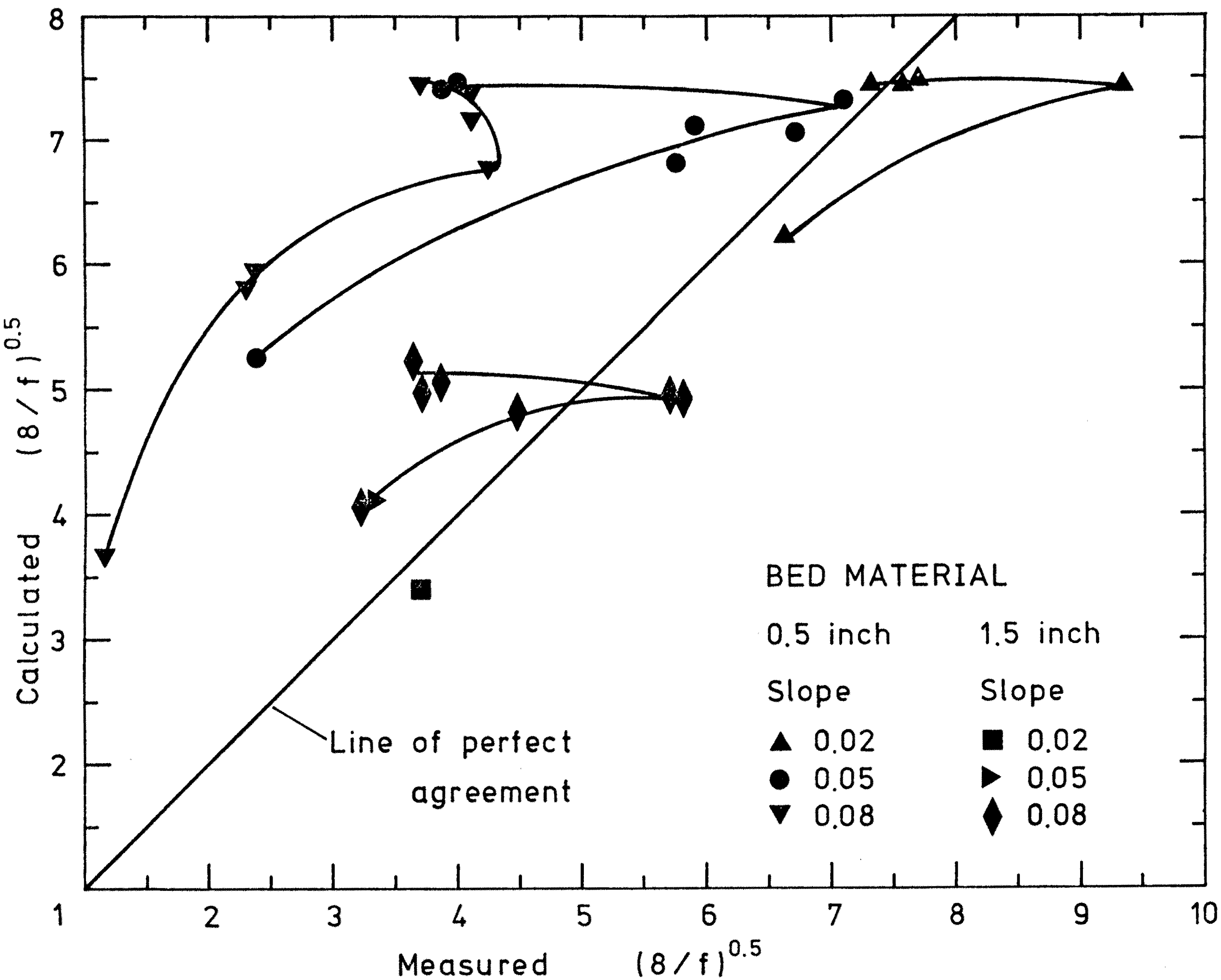

Figure 33. Comparison of values of the resistance function calculated using Equation (37) with measured values for all the flows over the loose roughness beds.

It should be noted that the experimental results are based on flows in which the entire upper layer of the bed moved. In mountain rivers this is not always the case and high rates of sediment movement generally occur only at relatively high discharges. Consequently the pattern of resistance in rivers with sediment movement may not be as observed in the flume.

SECTION 11 COMPARISON OF RESULTS WITH INDEPENDENT DATA

Equation (37) was tested against the river data of Barnes (1967), Judd and Peterson (1969), Emmett (1972), Virmani (1973) and Bathurst (1978) (Appendix F). The only alteration that was made to the equation was the substitution of hydraulic radius for mean depth in the relative submergence and in the calculation of the resistance function from Equations (1) and (3). This did not apply to Virmani's data in which hydraulic radius is not included. In fact, because mountain rivers have relatively high ratios of width to depth, the difference between mean depth and hydraulic radius is not often large.

Both Reynolds number and the standard deviation of sediment size distribution extend to higher values in the river data than in the flume data, so the comparison with the river data should enable deficiencies in Equation (37) related to those parameters to be identified. None of the data include details of the shapes of the roughness elements and generally only the size distribution of the median axis is given. Consequently the standard deviations of the size distributions are based on the median and not the short axis. Also it was assumed that the median size of the short axis, S_{50}, equals 0.57 D_{50} and that the median size of the long axis, L_{50}, equals $D_{50}/0.57$. These ratios were suggested by measurements of Limerinos (1970) and Bathurst (1977) at various river sites with blocklike bed material typical of mountain rivers. An exception was made for some of Virmani's data for which it was known that S_{50} equals 0.47 D_{50}. Another assumption was that the long axis of the material corresponds to the cross-stream axis.

Kinematic viscosity of the water, unless otherwise given, was assumed to be 1.140×10^{-6} m^2 s^{-1} (12.27×10^{-6} ft^2 s^{-1}), corresponding to a temperature of 15°C (59°F).

Measured and calculated values of the resistance function, $(8/f)^{0.5}$, given in Appendix F, are compared in Figures 34, 35, and 36. In all cases the relative submergence is less than 15, the probable limit to the region of intermediate-scale roughness. Data points representing flows with theoretically insignificant free surface drag ($b > 0.755$) are indicated separately.

The only data which are known to have been compiled by the same method as were the flume data (regarding sampling of the bed material, delineation of channel cross-sectional shape and so on), and which are therefore directly comparable with the flume results, are those of Bathurst (1978) (Figure 34). The calculated values of the resistance function for those data vary with a consistent trend not far removed from that of the measured values, an agreement which tends to support the basic form of Equation (37). In fact the calculated values of the function appear to be about 12 percent too low, a difference which may be attributable to the difference in Reynolds number between the flume and river flows. Although the relative submergences of the river flows are such that Reynolds number has an insignificant effect on the variation of flow resistance compared with that of free surface drag, the range of Reynolds numbers is such that the individual elements should have had turbulent boundary layers. In contrast the elements on the flume beds had laminar boundary layers and would therefore have had higher drag coefficients. Since Equation (37) is based on the flume data, it may overpredict the resistance coefficients for river flows.

The calculated values of the resistance function for the other data show a much wider scatter, over the range of +66 percent to -33 percent of the measured values for data points with values of b less than

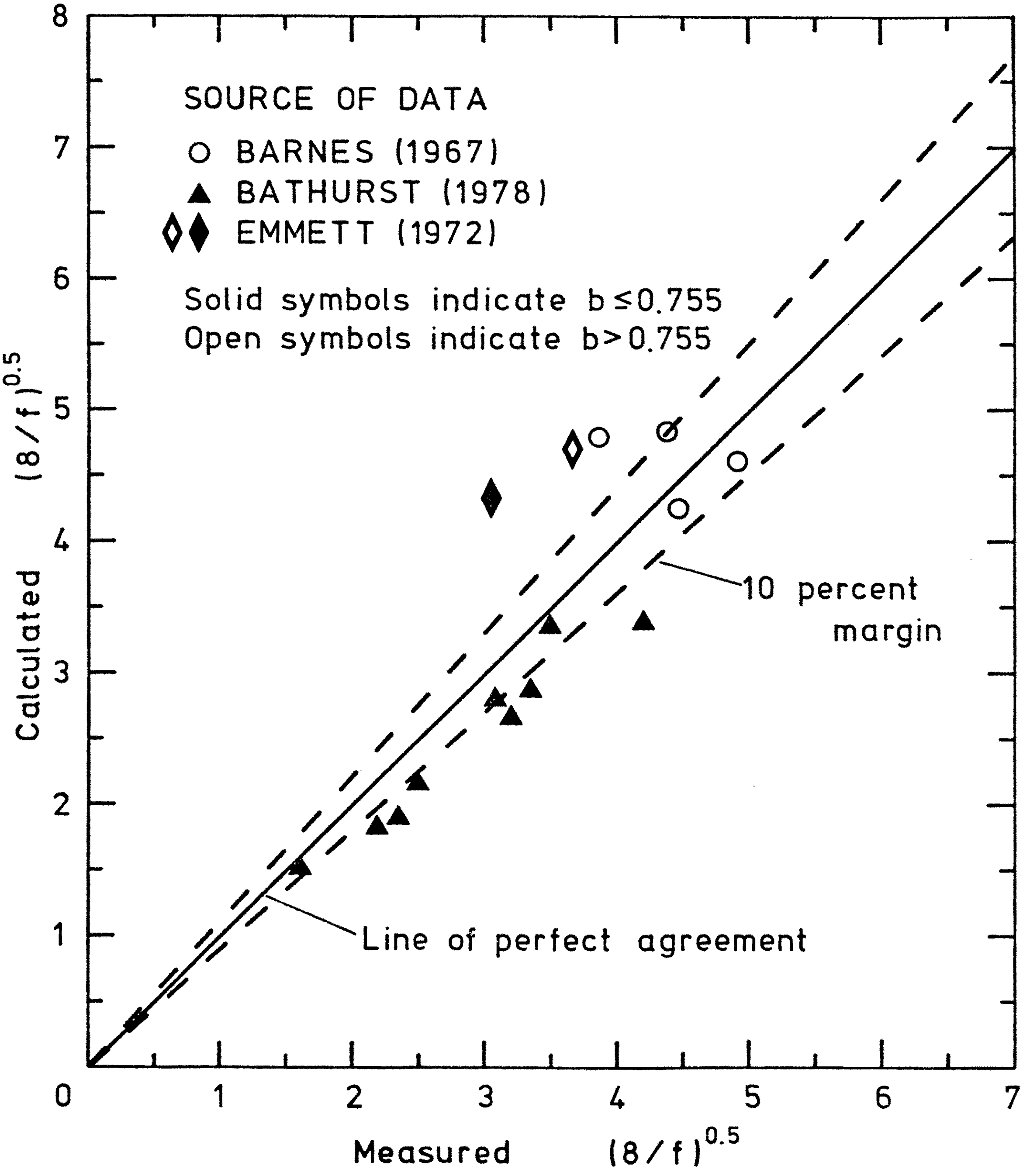

Figure 34. Comparison of values of the resistance function calculated using Equation (37) with measured values for flows at selected river sites.

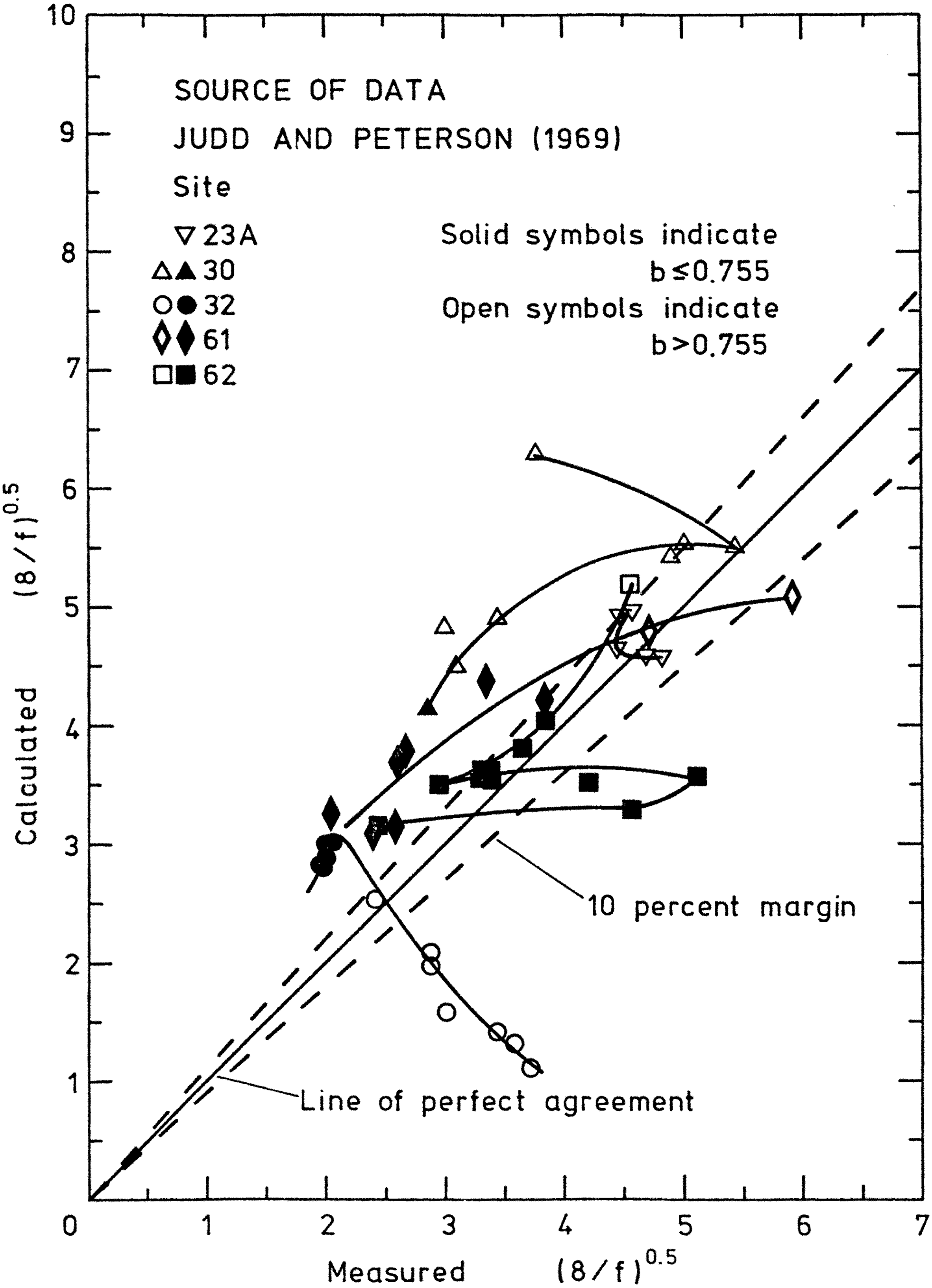

Figure 35. Comparison of values of the resistance function calculated using Equation (37) with measured values for flows at selected river sites.

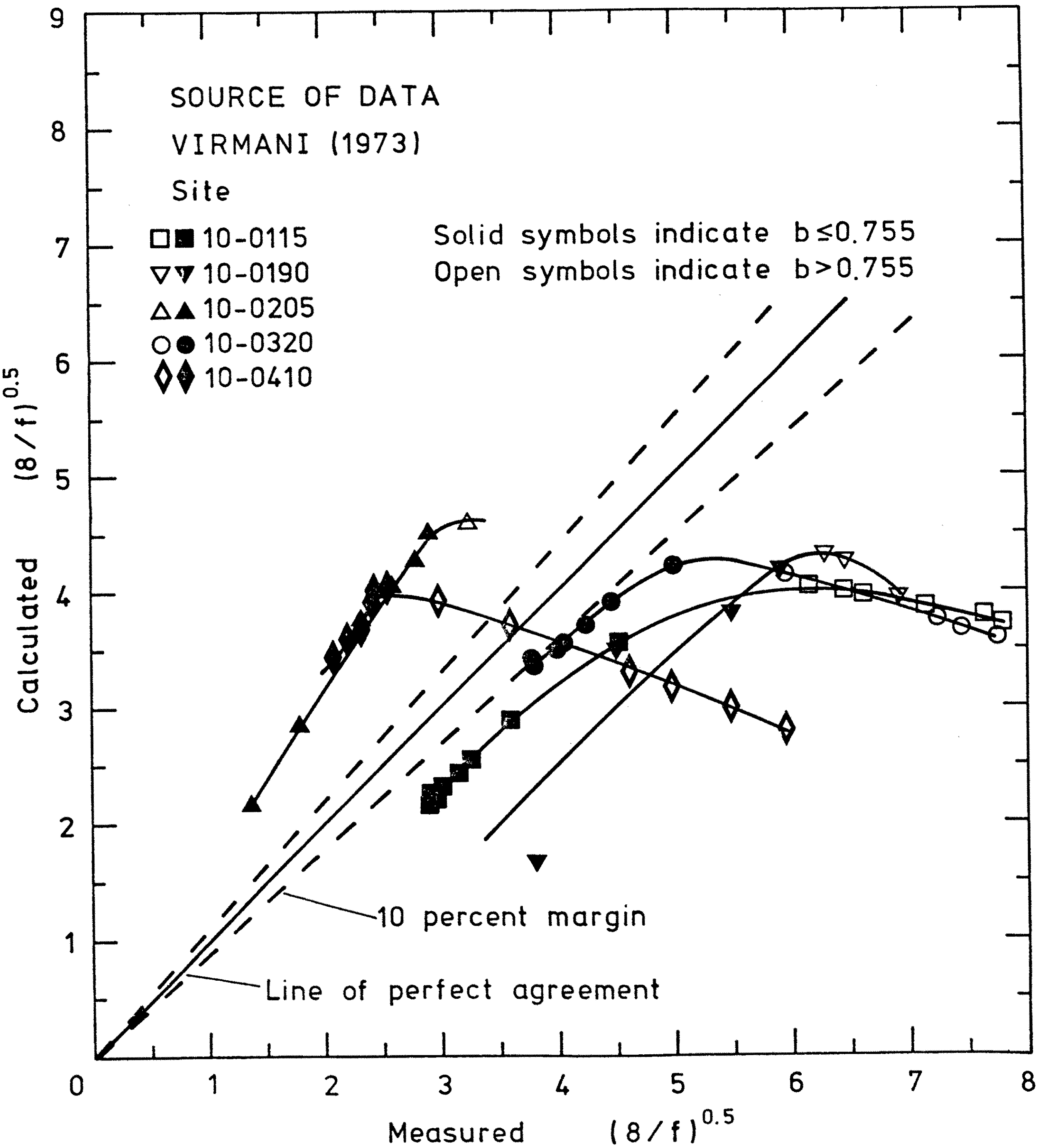

Figure 36. Comparison of values of the resistance function calculated using Equation (37) with measured values for flows at selected river sites.

0.755. Some of this scatter is probably due to differences between the experimental techniques of the various studies and to the assumptions concerning roughness shape. For example, tests made with different ratios of long axis to median axis showed that the resistance function could be significantly affected. However, it appears that there are definite trends for each site and this suggests that the scatter is not random but derives from some deficiency in the equation.

Some of that deficiency can be attributed to the term describing the free surface -ag. For example, during the calculations it was noted that, for some c the sites, the values of the resistance function predicted with and without that term straddle the measured values. The free surface drag may not therefore be represented as accurately as it should be.

Another deficiency may be related to sediment movement. In two cases the patterns resemble the patterns for the loose beds of the flume (Figure 33), suggesting again that Equation (37) does not apply in such cases.

Generally, in the region where free surface drag should be significant ($b < 0.755$) the calculated values of resistance function vary in the same way as do the measured values. This suggests that Equation (37), if suitably calibrated for roughness shape and free surface drag, accounts for the major resistive effects of a fixed bed in that region and that its form is basically correct. However, once b exceeds 0.755 in value, serious differences occur. In most cases the calculated values of the resistance function then vary inversely with the measured values, indicating that Equation (37) overpredicts the resistance coefficient to a greater and greater extent.

The change of pattern is abrupt and corresponds very obviously to the value of b equal to 0.755. It is uncertain, though, whether the change is related to a mathematical deficiency in Equation (37) connected with the representation of the limit to the region of free surface drag or to a theoretical deficiency connected with some resistance process which comes into play once free surface drag is negligible. Certainly some of the mathematical representations require refinement and it is also possible that in the region of intermediate-scale roughness the resistance function should vary with the logarithm of relative submergence rather than with a power as in Equation (37). Equally, though, once the elements become submerged and free surface drag disappears, the effects of Reynolds number and standing waves, unaccounted for in Equation (37), could become important.

In order to investigate the possible importance of these effects, the square root of the ratio of the predicted to the measured resistance coefficients for the river data, given in Appendix F, is plotted against Reynolds number, $\bar{U}\ D_{50}/\nu$, in Figure 37. In order that the effects of roughness geometry and flow depth should not cause spurious patterns, separate plots are provided for different ranges of effective roughness concentration function. The limits to each range lie at a value of 0.05 either side of the given values of b equal to 0.7, 0.8, 0.9, 1.0, 1.1 and 1.2.

Figure 37 shows that over the range of Reynolds numbers of about 5×10^4 to 2×10^5 there is an increase in the ratio of the resistance coefficients, indicating that there is a relative decrease in the flow resistance which is not accounted for by Equation (37). The range of Reynolds numbers corresponds extremely well to the range for an element

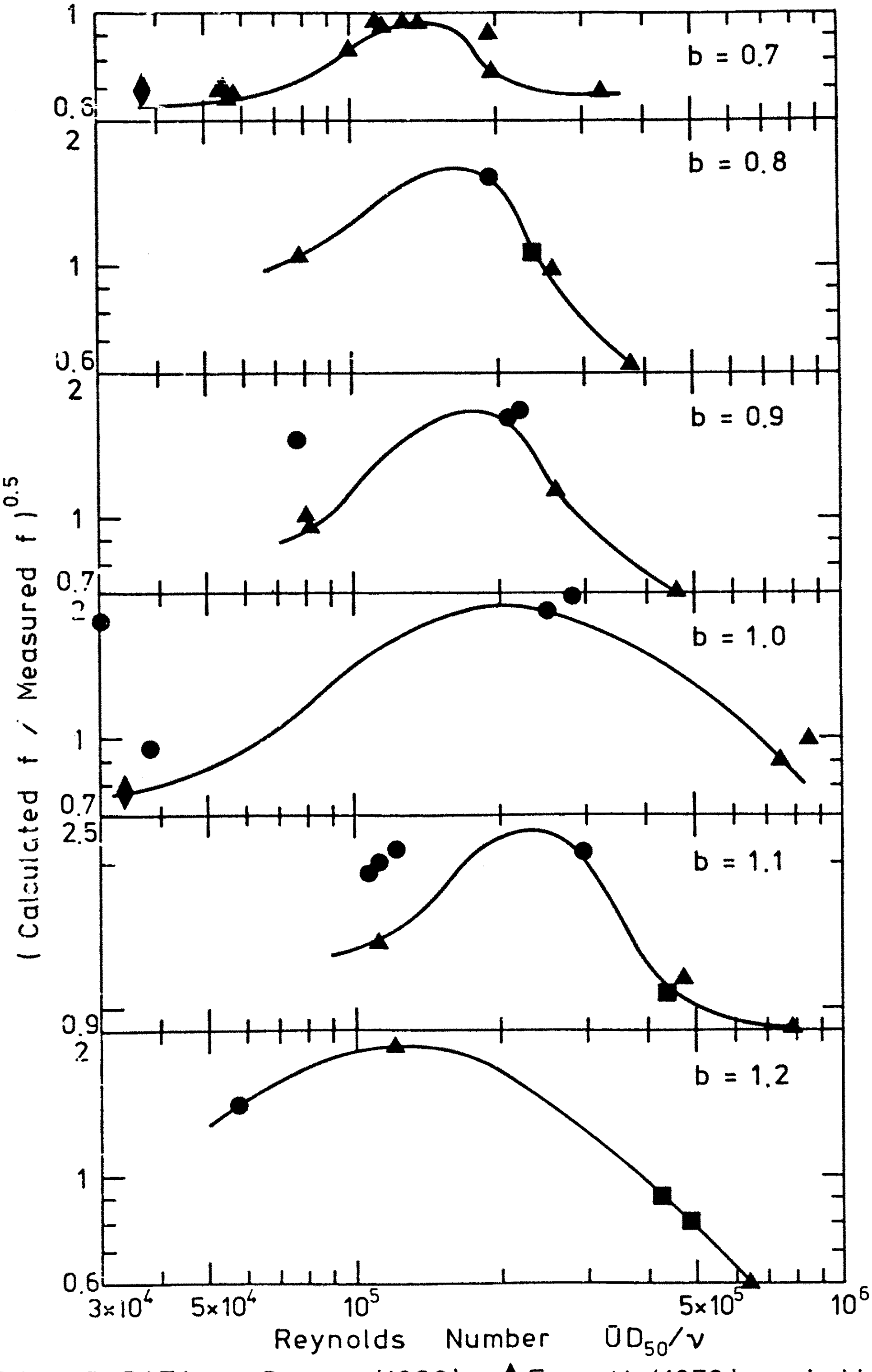

SOURCE OF DATA : ■ Barnes (1969) ; ♦ Emmett (1972); ▲ Judd and Peterson (1969); ● Virmani (1973)

Figure 37. Variation with Reynolds number and the effective roughness concentration function of the square root of the ratio of the calculated to the measured resistance coefficient for flows at selected river sites. Lines are provided as guides. Values of b for the data points lie within 0.05 of the given values.

lying on a surface in which transition from a laminar to a turbulent boundary layer occurs (Flammer, Tullis and Mason, 1970). In this transitional range the drag coefficient, and therefore the resistance coefficient, decrease as Reynolds number increases. It is possible therefore that the Reynolds number effect is responsible for the observed variation of resistance over the given range.

The variation is present for values of b equal to 0.7, when free surface drag effects should be present. However, the variation is then relatively small which suggests that while free surface drag effects, varying with Froude number, are present, Reynolds number has a relatively small effect on the flow resistance.

At Reynolds numbers greater than about 2×10^5 the ratio of the resistance coefficients falls, indicating that there is a relative increase in the flow resistance which is not accounted for by Equation (37). This might be partly due to a Reynolds number effect since, once a turbulent boundary layer is established on an element, the drag coefficient can increase slightly as Reynolds number increases (Schlichting, 1968, p. 622). However, the extent of the increase suggests that other processes might be at work. One possibility is that a system of standing waves could develop over the submerged elements, causing energy to be lost in the free surface distortions. Observations in the flume (Plates 12b, 15a, 16b and 16d) and the field (Plate 3) and the photographs of Barnes (1967) and Judd and Peterson (1969) certainly indicate that standing waves appear in flows over intermediate-scale roughness and kayaking acquaintances of one of the authors (J.C.B) have mentioned that in mountain rivers such waves can be up to two metres (about six feet) high. Presumably, for a given relative roughness or effective roughness concentration, the energy loss in the waves intensifies as Froude number increases, rather as antidunes do in sand-bed rivers. As increases of Froude number in river flows are usually accompanied by increases of Reynolds number, it seems possible that standing waves could be responsible for the observed increase in flow resistance with Reynolds number.

Representation of the effect of standing waves in a resistance equation is likely to depend on a parameter involving Froude number. Consequently in the region where free surface drag becomes small and standing wave drag begins to appear, there could be some overlap of the respective terms involving Froude number. Since standing waves were not considered when analyzing the flume flows, that overlap could be repsonsible for the greater inaccuracy apparent in Equations (34) and (35) (Figures 28 and 29) at the higher values of b.

Other processes which might be responsible for the observed variations in resistance could be linked to bed material movement or overbank flow. Neither of these possibilities is catered for by Equation (37).

SECTION 12 APPLICATION OF THE RESISTANCE EQUATION

The comparison with the independent data suggests that Equation (37) can probably be applied to mountain rivers with large-scale roughness and fixed beds as long as the function of effective roughness concentration is less than 0.755 in value. However, it is important that the relevant axes of the bed material be correctly determined, that the term describing free surface drag be refined and that allowance be made for the likelihood that the boundary layers on the elements are turbulent and not, as in the flume flows, laminar. It may also be necessary to take account of differences in the shapes of the roughness elements. Generally, though, roughness elements in mountain rivers seem to be blocklike and may not vary significantly in shape from river to river.

For larger values of the function of effective roughness concentration, Equation (37) can not be applied with certainty because it does not account for the effects of Reynolds number, bed material movement and standing waves which may be important once the roughness elements are submerged.

Equation (37) is inevitably complex since the processes which it describes are themselves complex. Simpler equations, such as Equation (8), can be devised but these need to be calibrated for individual sites whereas Equation (37) is more general. However, use of Equation (37) can be simplified if the relationship between width and depth at a given site is expressed as:

$$w = \alpha\, d^{\beta} \qquad (38)$$

where α and β are constants specific to the site. This equation can be determined from surveying data for natural rivers and from design specifications for artificial channels. With channel slope and the various roughness parameters also specified, Equation (37) can be reduced to a relationship between mean velocity, or discharge, and depth. Its solution, by an iterative technique, enables calculation of depth for a given discharge (for example, for prediction of flood levels), or calculation of mean velocity, discharge or resistance coefficient for a given depth (for example, for flood routing). An example of the technique is presented in Appendix B.

It has so far been assumed that Equation (37) can most usefully be applied to a channel reach if the various parameters in the equation are average parameters for the reach and if the relative roughness area can be given by the semiempirical Equation (22). This should be true as long as the channel properties are similar to those of the flume. In particular the boundary material should be homogeneous and there should not be significant bank effects or variations in depth across the channel. However, these conditions can not always be met and, especially, the boundary material may not be homogeneous. For example there could be boulders on one part of the bed, sand on another and vegetation on the banks and in such circumstances Equation (37) could not be applied to the whole section. It could be applied, though, to any part of the channel where there is large-scale roughness.

Because the flume flows on which Equation (37) is based were essentially one-dimensional, the equation, too, is one-dimensional. Consequently it can be applied at any vertical to give an average velocity or depth at a vertical. (This assumes, of course, that the roughness parameters can be derived from measurements over a width of channel around the vertical equal to a few element diameters.) It should therefore be possible to apply Equation (37) at intervals across that part of the channel which is relevant, thereby giving point values of the required parameter. Other resistance equations would have to be used to give similar values over the regions of different boundary material and all the point values could then be integrated across the channel to give the average value. Equation (37) could also be applied in the same way to overland flow.

SECTION 13 BED MATERIAL MOVEMENT

As mentioned earlier, a sediment transport equation for mountain rivers has to account not only for the relevant hydraulic factors but also for geomorphic factors, such as watershed characteristics, which restrict the supply of sediment to the river. Thus the data obtained from the flume experiments with loose beds, in which sediment supply was unlimited, can not be used to develop a practical sediment transport equation. In any case the data are not numerous enough to permit sound theoretical development of such an equation. They are therefore presented here more to complete the catalogue of results and with the aim of identifying some of the hydraulic processes which are important.

13.1 INITIATION OF MOTION

Values of the critical water discharge, Q_c, at which movement of the bed material began, were obtained from Figure 31 by back-extrapolation. The critical discharge for the 1.5 inch material at the 5 percent slope is assumed to be just greater than the maximum discharge measured at that slope, since at that discharge the elements were seen to be on the point of movement. Knowing the relationship between discharge and depth for each slope and bed material, the values of the critical shear stress, τ_c, were calculated using Equations (2) and (3). Values of the various parameters are given in Table 6.

It can be seen that, for a given bed material, as channel slope increases, the critical water discharge decreases but the critical shear stress increases. The critical shear stresses are not in fact directly comparable with each other because of the variation in channel slope and therefore also in the degree to which the weight component affects the shear stress at which the material moves. If the shear stresses were

TABLE 6.--Critical Values of Parameters Related to the Initiation of Movement of the Loose Beds

Bed material size in inches	Channel slope	Critical water discharge in cubic metres per second	Critical depth in metres	Critical shear stress in newtons per square metre	Critical Shields parameter	Critical relative submergence d/S_{50}	Critical Reynolds number $u_* D_{50}/\nu$
(1)	(2)	(3)	(4)	(5)	(6)	(7)	(8)
0.5	0.02	0.0660	0.0675	13.24	0.092	11.64	881
0.5	0.05	0.0150	0.0330	16.19	0.113	5.69	974
0.5	0.08	0.0100	0.0310	24.33	0.170	5.34	1194
1.5	0.05	0.0700*	---	---	---	---	---
1.5	0.08	0.0535	0.0560	43.95	0.079	2.95	6198

*Estimated value

corrected to equivalent values corresponding to a channel of zero slope, the increase in critical shear stress with slope would be even greater.

Also shown in Table 6 are values of the critical Shields parameter, S_c, calculated using Equation (9) with $D_n = D_{50}$ and $(\gamma_s - \gamma) = 1.629 \times 10^2$ N m^{-3}. The results agree with those of Ashida and Bayazit (1973) and Bayazit (1978) which show that, for a given bed material, the lower the relative submergence, the higher is the critical Shields parameter. Since the critical discharge, and therefore depth, vary with channel slope, the critical Shields parameter could also be related to channel slope.

Because of the variation in the Shields parameter and because the Reynolds numbers, $u_* D_{50}/\nu$, are higher than those at which the Shields criterion is commonly applied (Simons and Şentürk, 1977, p. 409), the conditions determining the initiation of motion need to be represented in a fashion different from that for sand-bed rivers, for which the Shields criterion is designed. Using the data of this study, a short, empirical analysis is therefore carried out to indicate some of the features which should be considered. Because of the paucity of data, firm conclusions can not be drawn.

Channel slope has an obvious effect since for a given discharge, bed material and channel it determines the depth and the shear stress. Critical water discharge is therefore plotted against channel slope in Figure 38. The two appear to be related by an equation of the form:

$$Q_c = - 0.0903 \log S + p \qquad (39)$$

where p is a constant which seems to vary with the bed material. It has the values of -0.0886 for the 0.5 inch material and -0.0466 for the 1.5 inch material. (Equation (39) was fitted to the data by eye.)

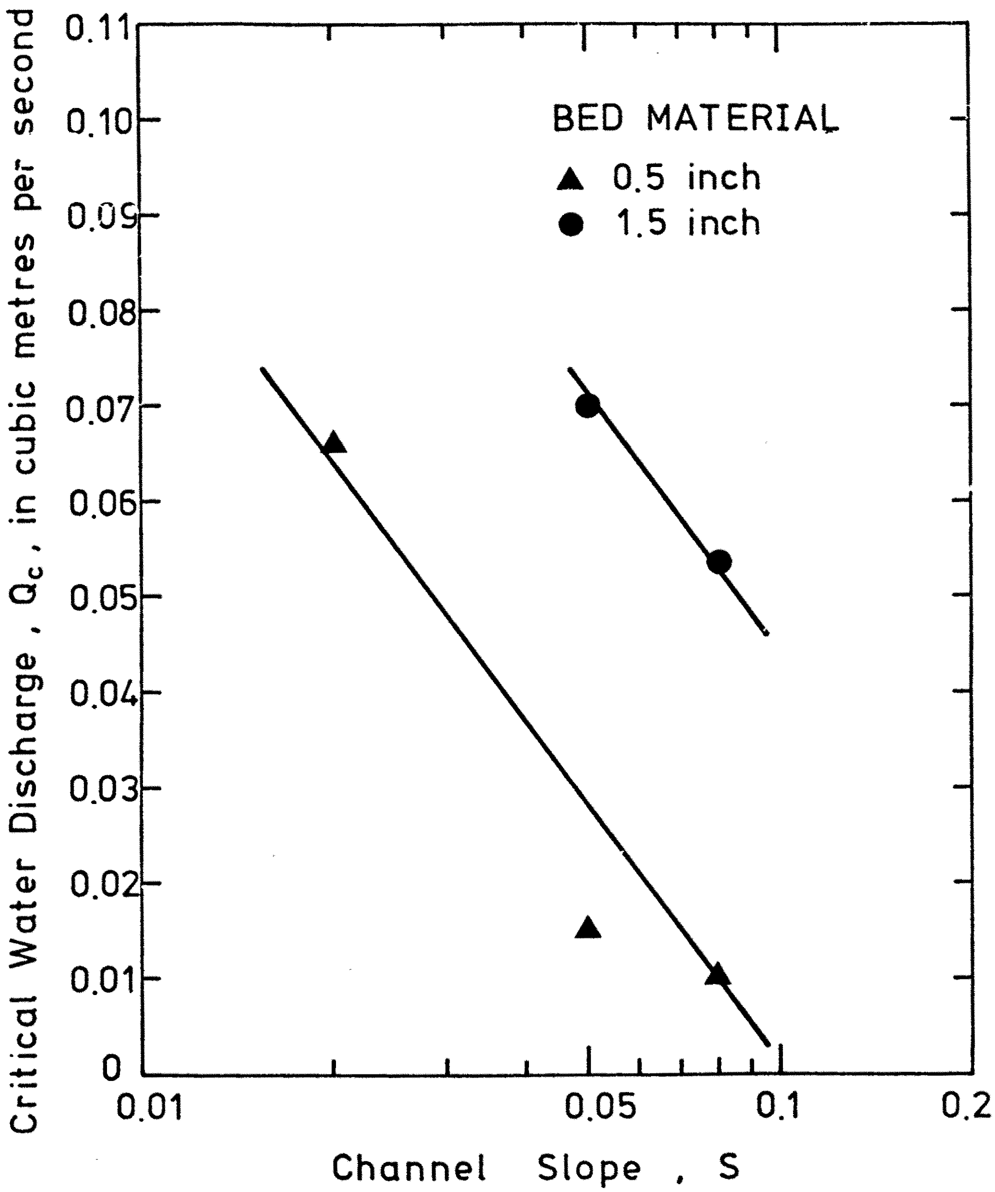

Figure 38. Variation of the critical water discharge with channel slope for the loose roughness beds.

Without further data the dependence of p on the bed material can not be described with certainty. Probably, though, roughness size is the most important parameter, so using the rather few data, a power law relating p to sediment size is constructed in Figure 39. The relationship takes the form:

$$p = - 0.0102\ L_{50}^{-0.5} \tag{40}$$

The long axis is chosen to represent size since, for a loose bed, it should equal the cross-stream axis, which is of hydraulic significance for bed material movement. Thus:

$$Q_c = - 0.0903 \log S - 0.0102\ L_{50}^{-0.5} \tag{41}$$

The width of the flume is 1.168 m (3.832 ft) so Equation (41) can be converted to give the critical discharge per unit width of channel, q_c:

$$q_c = - 0.0773 \log S - 0.00873\ L_{50}^{-0.5} \tag{42}$$

Equation (42) is tested against the independent data of Ashida and Bayazit (1973) in Figure 40. The equation is empirical, the constants are dimensional and the bed material used by Ashida and Bayazit was more uniform than that of this study. It is not expected therefore that the agreement between the measured and calculated values of critical water discharge should be perfect and in fact the data do seem to exhibit a trend different from that predicted. However, it is encouraging to note that the order of magnitude of the prediction is correct.

It seems, then, that in steep channels, the initiation of movement of the sediment depends in part on channel slope and the properties of the bed material.

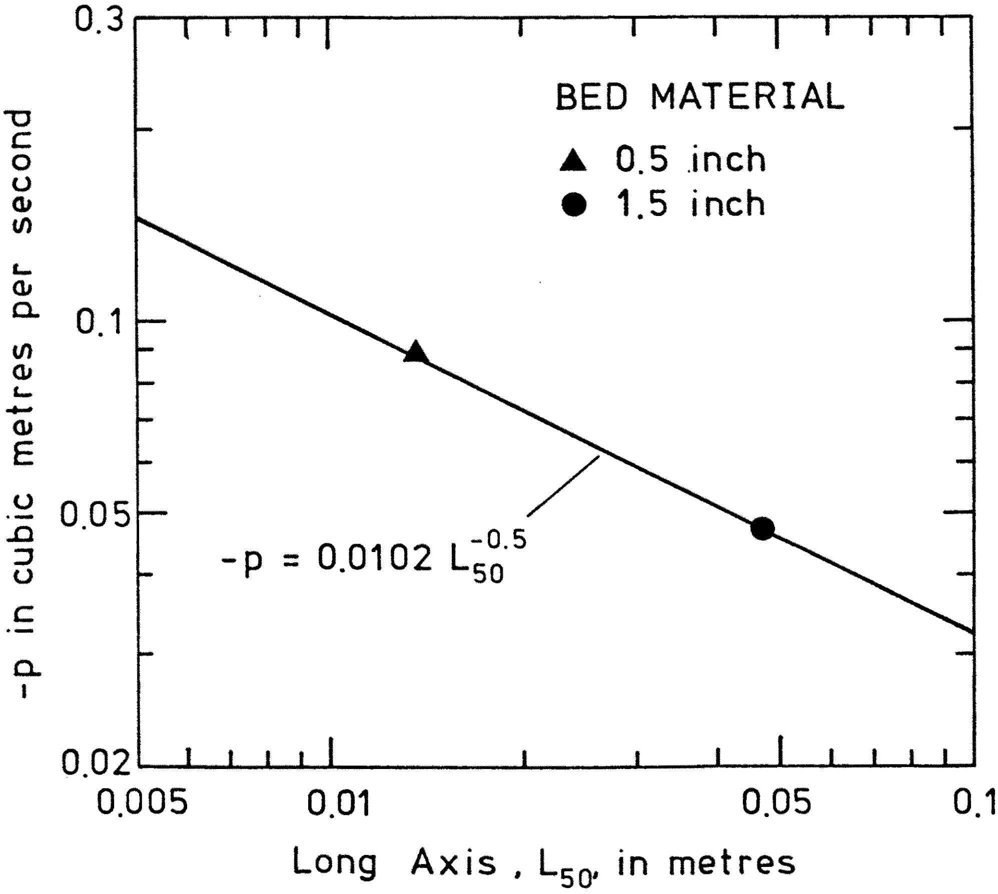

Figure 39. Variation of the parameter, p, with the median size of the long axis of the bed material for the loose roughness beds.

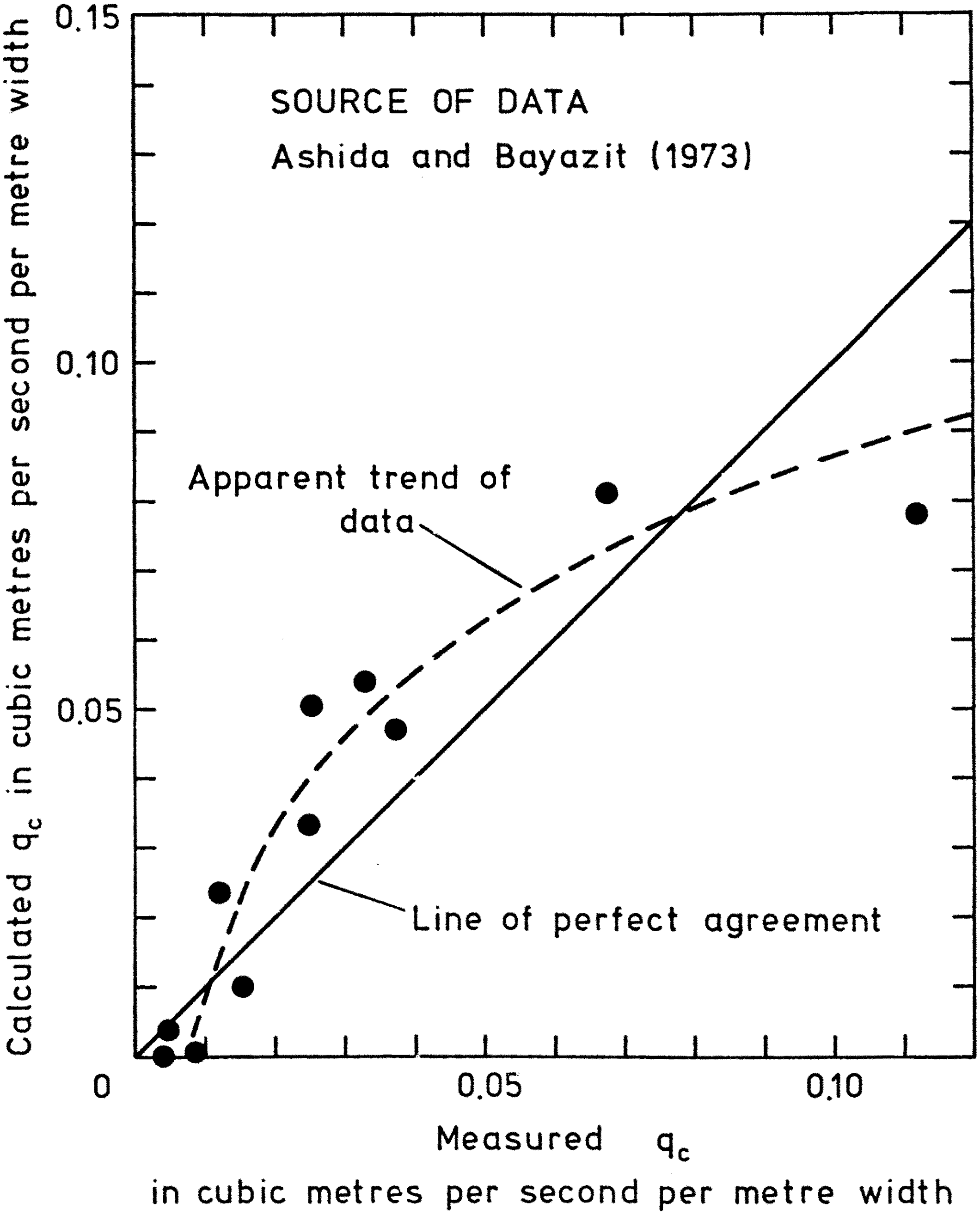

Figure 40. Comparison of values of critical water discharge per unit width of channel calculated using Equation (42) with measured values for the roughness beds of Ashida and Bayazit (1973).

13.2 BED MATERIAL MOVEMENT

Movement of the material in the flume experiments was entirely in the form of bed load, either rolling or saltating. No obvious bed forms appeared during the short period of each experiment, although channelization occurred. These conditions are typical of mountain rivers (Gole, Chitale and Galgali, 1973).

The approach used in analyzing the data is based on the relationship which exists between the sediment discharge, Q_s, and the difference between the water discharge, Q, and the critical water discharge, Q_c, at which movement begins (Simons and Şentürk, 1977, p. 514). This relationship is shown in Figure 41. Also included in that diagram are the data of Li et al., (1977) collected in the same flume and by the same technique used in this study. The bed material of the earlier study was a sand-gravel mixture for which the critical discharge, at the slopes involved, is effectively zero. Relevant details are given in Table 7.

The relationship takes the form:

$$Q_s = \Delta\ (Q - Q_c) \tag{43}$$

where Δ is constant which seems to vary mainly with channel slope (Table 7). (The lines in Figure 41 were fitted by eye.) The data points for the 0.5 and 1.5 inch materials at the 8 percent slope coincide approximately but the data points for the 0.5 inch and sand-gravel materials at the 5 percent slope do not. This may be because the sand of the mixture could have moved as suspended load, in which case the sediment discharge would have been higher at a given value of $(Q - Q_c)$ than if it moved, like the 0.5 inch material, as bed load only.

TABLE 7.--Data for the Analysis of the Bed Material Movement of the Loose Beds

Bed material size in inches (1)	Channel slope (2)	Sediment discharge in cubic metres per second (x 10^3) (3)	$(Q - Q_c)$ in cubic metres per second (4)	Constant Δ (5)
0.5	0.02	0.097	0.0011	0.0125
		0.098	0.0125	
		0.265	0.0197	
		0.250	0.0210	
0.5	0.05	0.649	0.0261	0.0213
		0.636	0.0330	
		0.866	0.0347	
		0.717	0.0393	
		1.443	0.0615	
		1.226	0.0633	
0.5	0.08	0.308	0.0058	0.0640
		0.433	0.0069	
		1.463	0.0284	
		2.079	0.0346	
		3.230	0.0534	
		3.319	0.0598	
1.5	0.08	0.096	0.0008	0.0640
		0.260	0.0022	
		0.118	0.0048	
		0.569	0.0078	
		1.103	0.0152	
		1.375	0.0160	
0.0266*	0.05	0.535	0.0114	0.0448
		0.797	0.0178	
		0.933	0.0234	
		1.133	0.0299	
		2.238	0.0428	
0.0266*	0.15	1.500	0.0039	0.4530
		5.380	0.0099	
		7.420	0.0160	
		11.380	0.0232	
		15.880	0.0403	

Cont'd...

TABLE 7.--Continued

(1)	(2)	(3)	(4)	(5)
0.0266*	0.25	5.810	0.0050	0.8700
		9.740	0.0127	
		17.810	0.0207	
		20.750	0.0232	
		36.420	0.0374	

*Sand-gravel mixture of Li et al., (1977).
D_{50} = 0.676 mm (0.0266 inch or 0.00222 ft) and σ = 0.617

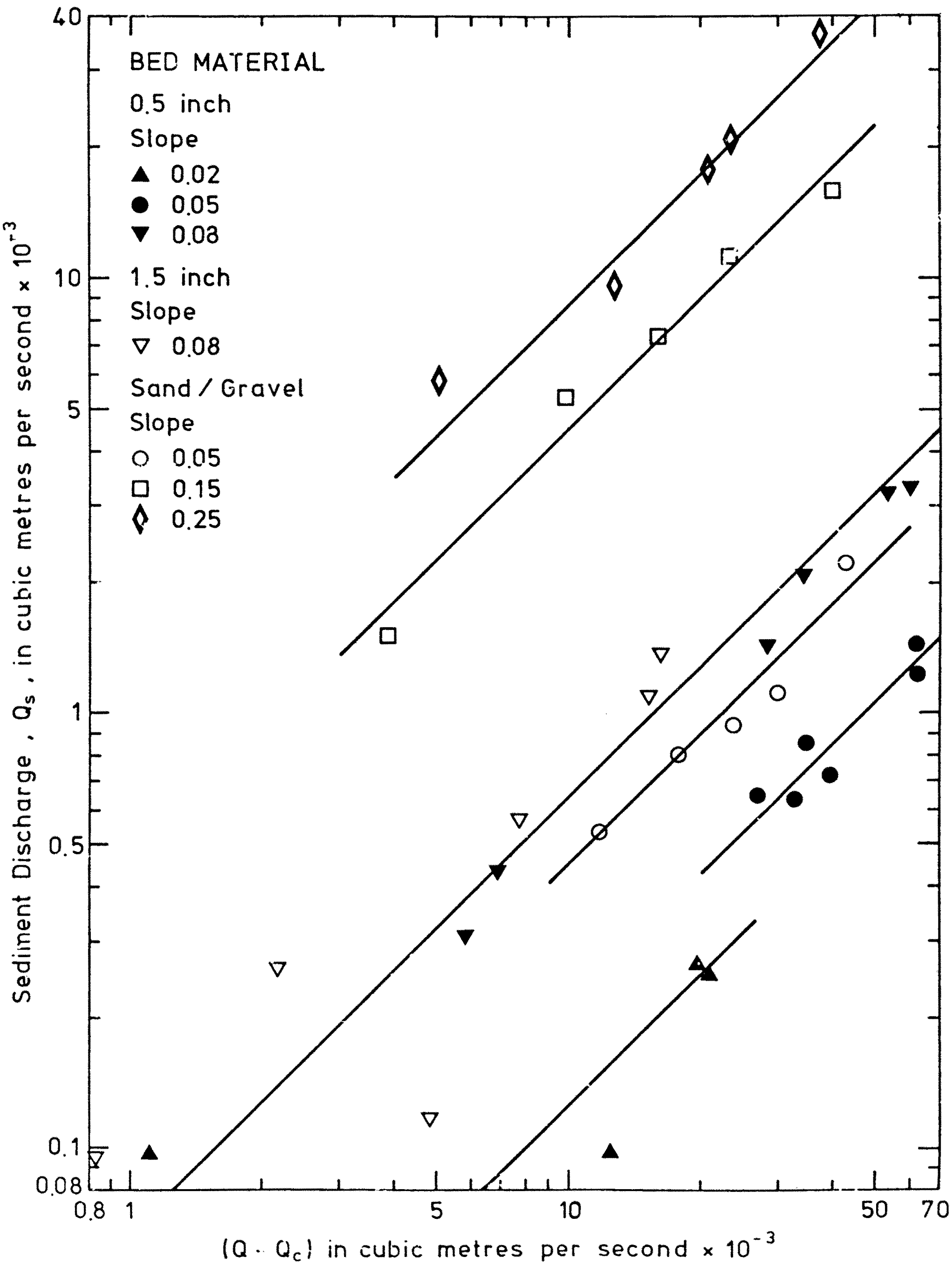

Figure 41. Variation of sediment discharge with the water discharge parameter ($Q-Q_c$) for the loose roughness beds. The data of Li et al., (1977) for sand/gravel roughness beds are also included.

Figure 42 shows that Δ can be given as:

$$\Delta = 13.7\ S^2 \tag{44}$$

the line being fitted by eye. Thus:

$$Q_s = 13.7\ S^2\ (Q - Q_c) \tag{45}$$

or in terms of discharge per unit width of channel, q:

$$q_s = 13.7\ S^2\ (q - q_c) \tag{46}$$

where q_c is given by Equation (42).

This brief analysis suggests that, in mountain rivers, channel slope and the critical water discharge can be important factors in determining the sediment discharge. However, the analysis is restricted in scope and range of data and is based on flows with unlimited supplies of bed material. Consequently the derived equations are unlikely to apply to natural rivers.

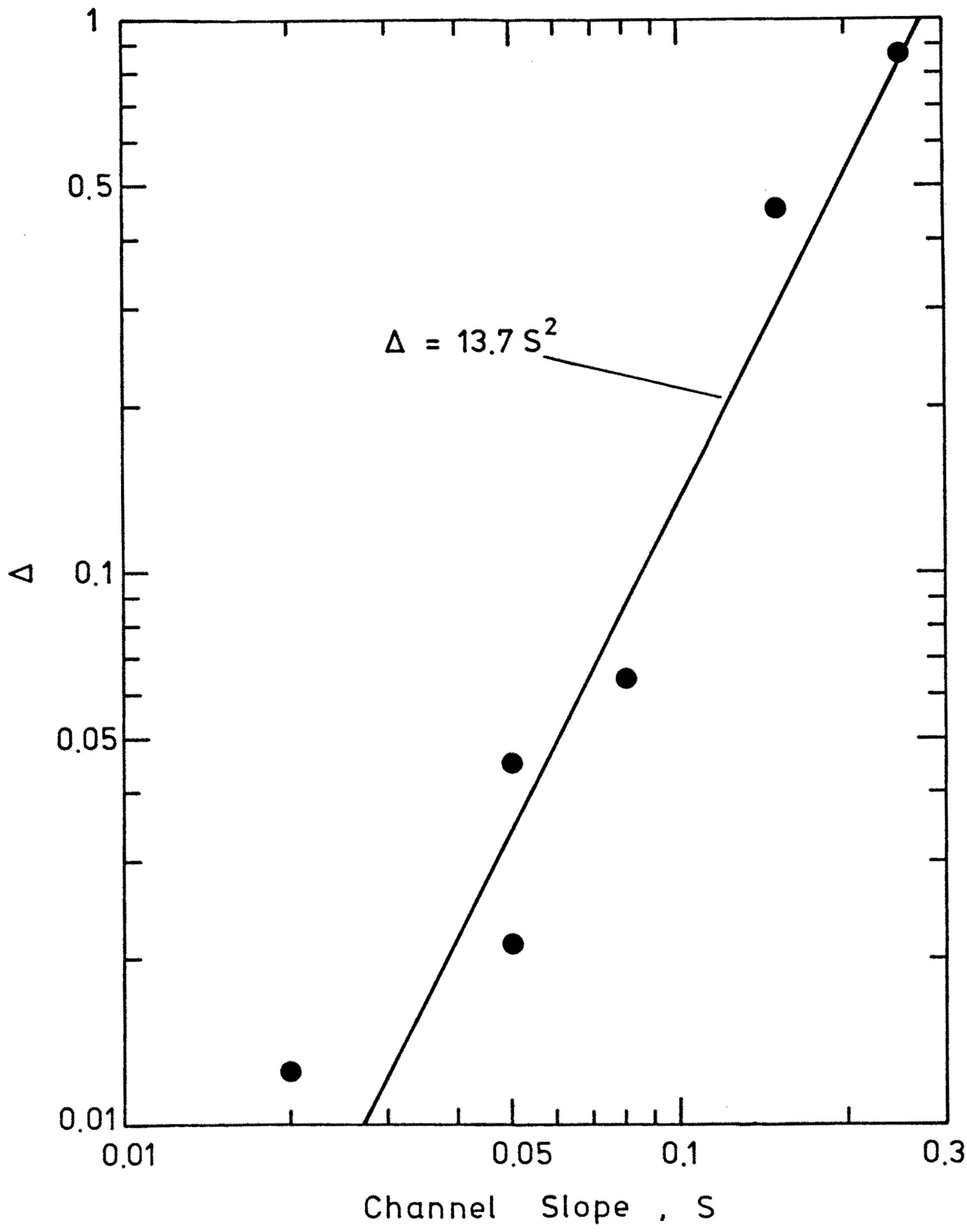

Figure 42. Variation of the parameter, Δ, with channel slope for loose roughness beds. Data points are derived from Figure 41.

SECTION 14 CONCLUSIONS AND RECOMMENDATIONS

An attempt has been made to describe the hydraulics of flow in mountain rivers and to produce a process-based equation accounting for the flow resistance.

Mountain rivers are one form of cobble-bed rivers and are characterized by channel slopes of approximately 0.4 to 10 percent and by relative submergences of less than about 15, corresponding to the regions of large-scale and intermediate-scale roughness. The processes of flow resistance are not the same as those in cobble-bed rivers of lesser gradients and small-scale roughness so the flow resistance equations for those rivers can not be used. Most of the flow resistance is derived from the form drag of the roughness elements and the distortions to the flow around the elements. Consequently a flow resistance equation for mountain rivers has to account both for the processes of fluid mechanics by which the form drag is generated and for the processes of wall geometry by which the combined drag of the elements affects the flow resistance. More specifically the resistance varies with Reynolds number, Froude number, roughness geometry, channel geometry and, where relevant, sediment movement.

Theoretical analysis, supported by the results of the flume study, suggests that, for the range of Reynolds numbers given by $4 \times 10^4 < \bar{U} D_{50}/\nu < 2 \times 10^5$, resistance is likely to fall significantly as Reynolds number increases. However, if there are roughness elements protruding through the free surface, the effect is small by comparison with Froude number effects related to the appearance of hydraulic jumps and the generation of free surface drag. For the bed as a whole, free surface drag decreases as Froude number and relative submergence increase. Once the elements are submerged, Froude number effects related to free surface drag are small but Froude number effects related to standing waves may be important.

The effect of roughness geometry can largely be described by a single parameter, b, the function of effective roughness concentration. This accounts for the variation of the roughness geometry both with depth and with bed material, although it does not make allowance for differing element shapes.

$$b = \left[1.175\left(\frac{Y_{50}}{w}\right)^{0.557}\left(\frac{d}{S_{50}}\right)\right]^{0.648\ \sigma^{-0.134}} \tag{26}$$

Similarly the effect of channel geometry is accounted for by the relative roughness area, A_w/wd', which indicates the proportion of a channel cross section occupied by roughness and thence the degree of funnelling of the flow. For river channels of homogeneous boundary material:

$$\frac{A_w}{wd'} = \left(\frac{w}{d}\right)^{-b} \tag{22}$$

Based on the analysis of the flume data, the resistance equation for large-scale roughness (b < 0.755) is:

$$\begin{aligned}\frac{\bar{U}}{(gdS)^{0.5}} &= \left(\frac{8}{f}\right)^{0.5} \\ &= \left[\frac{0.28}{b}\ Fr\right]^{\log\ (0.755/b)} \\ &\times \left[13.434\left(\frac{w}{Y_{50}}\right)^{0.492} b^{\ 1.025\ (w/Y_{50})^{0.118}}\right] \\ &\times \left[\frac{A_w}{wd'}\right]\end{aligned} \tag{37}$$

This equation does not apply where Reynolds number effects are significant, where there is bed material movement or where there is a system of standing waves. However, within its range of application the equation seems to work well as long as the various parameters, particularly the roughness sizes and the channel wetted perimeter, are derived or measured as in this study.

In spite of its complex form, Equation (37) contains relatively few parameters and can be applied using a simple iteration procedure (Appendix B). Comparison with independent river data shows that, when based on mean parameters of flow and with semiempirical equations describing relative roughness area and channel width, it can be used to calculate a mean resistance coefficient for a channel reach. Alternatively, in its more general form related to a single vertical through the flow, the equation can be applied to overland flow and to regions of large-scale roughness in channels where there are significant changes in boundary material and depth across a section.

Derivation of Equation (37) proceeded on a semiempirical basis and some of the terms need to be refined. This is particularly true of the parameter describing the free surface drag of elements protruding through the flow. The possible significance of roughness element shape, neglected here, needs to be studied, too. Future research should also be directed towards extending the usefulness of the equation to the region of intermediate-scale roughness which is important in flood studies. This requires that the effects of Reynolds number, sediment movement and standing waves be quantified. In addition it is necessary to find whether the relationship between the resistance function and relative submergence is better represented by a semilogarithmic or a power law.

The brief investigation of bed material movement shows that sediment transport equations developed for sand-bed rivers do not apply to mountain rivers. The flume data suggest that two of the hydraulic factors determining sediment movement are channel slope and bed material characteristics. Other studies, though, show that geomorphic factors, which determine the supply of sediment to the channel, are at least as important and future research should be directed towards identifying these factors.

REFERENCES

Aguirre Pe, J., "Incipient Erosion in High Gradient Open Channel Flow with Artificial Roughness Elements," Proceedings of the Sixteenth Congress of the International Association for Hydraulic Research, Sao Paulo, Brazil, Vol. 2, July-Aug., 1975, pp. 173-180.

American Society of Civil Engineers, "Friction Factors in Open Channels," Progress Report of the Task Force on Friction Factors in Open Channels of the Committee of Hydromechanics of the Hydraulics Division," E. Silberman, Chmn., Journal of the Hydraulics Division, ASCE, Vol. 89, No. HY2, Proc. Paper 3464, Mar., 1963, pp. 97-143.

Ashida, K., and Bayazit, M., "Initiation of Motion and Roughness of Flows in Steep Channels," Proceedings of the Fifteenth Congress of the International Association for Hydraulic Research, Istanbul, Turkey, Vol. 1, 1973, pp. 475-484.

Barnes, H. H., "Roughness Characteristics of Natural Channels," Water Supply Paper 1849, United States Geological Survey, Department of the Interior, United States Government Printing Office, Washington, D. C., 1967.

Bathurst, J. C., "Resistance to Flow in Rivers with Stony Beds," thesis presented to the University of East Anglia, Norwich, England, in 1977, in fulfillment of the requirements for the degree of Doctor of Philosophy.

Bathurst, J. C., "Flow Resistance of Large-Scale Roughness," Journal of the Hydraulics Division, ASCE, Vol. 104, No. HY12, Proc. Paper 14239, Dec., 1978, pp. 1587-1603.

Bayazit, M., "Free Surface Flow in a Channel of Large Relative Roughness," Journal of Hydraulic Research, International Association for Hydraulic Research, Vol. 14, No. 2, Delft, Netherlands, 1976, pp. 115-126.

Bayazit, M., "Scour of Bed Material in Very Rough Channels," Journal of the Hydraulics Division, ASCE, Vol. 104, No. HY9, Proc. Paper 13984, Sept., 1978, pp. 1345-1349.

Bray, D. I., "Estimation of Average Velocity in Gravel-Bed Rivers," paper submitted to Journal of the Hydraulics Division, ASCE, in 1979.

Briggs, D., Sediments, 1st ed., Butterworth and Co. (Publishers) Ltd., London, England, 1977.

Calhoun, R. G., "A Statistical Roughness Model for Computation of Large Bed-Element Stream Resistance," thesis presented to Washington State University, at Pullman, Wash., in 1975, in partial fulfillment of the requirements for the degree of Master of Science.

Cheng, E. D. H., and Clyde, C. G., "Instantaneous Hydrodynamic Lift and Drag Forces on Large Roughness Elements in Turbulent Open Channel Flow," Sedimentation: Symposium to Honor Prof. H. A. Einstein, H. W. Shen, ed., 1st ed., H. W. Shen, Fort Collins, Colo., 1972, pp. 3.1-3.20.

Duncan, W. J., Thom, A. S., and Young, A. D., Mechanics of Fluids, 2nd ed. , Edward Arnold Ltd., London, England, 1970.

Emmett, W. W., "The Hydraulic Geometry of Some Alaskan Streams South of the Yukon River," Open-File Report, Water Resources Division, Alaska District, United States Geological Survey, Department of the Interior, July, 1972.

Flammer, G. H., Tullis, J. P., and Mason, E. S., "Free Surface, Velocity Gradient Flow Past Hemisphere," Journal of the Hydraulics Division, ASCE, Vol. 96, No. HY7, Proc. Paper 7418, July, 1970, pp. 1485-1502.

Galay, V. J., "Observed Forms of Bed Roughness in an Unstable Gravel River," Proceedings of the Twelfth Congress of the International Association for Hydraulic Research, Fort Collins, Colo., Vol.1, Sept., 1967, pp. 85-94.

Gole, C. V., Chitale, S. V., and Galgali, V. G., "Sediment Problems of Canal Offtakes in Mountain Streams," Proceedings of the Fifteenth Congress of the International Association for Hydraulic Research, Istanbul, Turkey, Vol. 1, 1973, pp. 545-551.

Golubtsov, V. V., "Hydraulic Resistance and Formula for Computing the Average Flow Velocity of Mountain Rivers," Soviet Hydrology: Selected Papers, American Geophysical Union, No. 5, 1969, pp. 500-511.

Haddock, D. R., "Modeling Bedload Transport in Mountain Streams of the Colorado Front Range," thesis presented to Colorado State University, at Fort Collins, Colo., in 1978, in partial fulfillment of the requirements for the degree of Master of Science.

Hartung, F., and Scheuerlein, H., "Macroturbulent Flow in Steep Open Channels with High Natural Roughness," Proceedings of the Twelfth Congress of the International Association for Hydraulic Research, Fort Collins, Colo., Vol. 1, Sept., 1967, pp. 1-8.

Henderson, F. M., Open Channel Flow, 1st ed., The Macmillan Co., New York, N. Y., 1966.

Herbich, J. B., and Shulits, S., "Large-Scale Roughness in Open Channel Flow," Journal of the Hydraulics Division, ASCE, Vol. 90, No. HY6, Proc. Paper 4145, Nov., 1964, pp. 203-230.

Hsieh, T., "Resistance of Cylindrical Piers in Open-Channel Flow," Journal of the Hydraulics Division, ASCE, Vol. 90, No. HY1, Proc. Paper 3770, Jan., 1964, pp. 161-173.

Johansson, C. E., "Orientation of Pebbles in Running Water," Geografiska Annaler, Vol. 45, Stockholm, Sweden, 1963, pp. 85-112.

Judd, H. E., and Peterson, D. F., "Hydraulics of Large Bed Element Channels," Report No. PRWG 17-6, Utah Water Research Laboratory, Utah State University, Logan, Utah, 1969.

Kellerhals, R., "Stable Channels with Gravel-Paved Beds," Journal of the Waterways and Harbors Division, ASCE, Vol. 93, No. WW1, Proc. Paper 5091, Feb., 1967, pp. 63-84.

Kellerhals, R., and Bray, D. I., "Sampling Procedures for Coarse Fluvial Sediments," Journal of the Hydraulics Division, ASCE, Vol. 97, No. HY8, Proc. Paper 8279, Aug., 1971, pp. 1165-1180.

Koloseus, H. J., and Davidian, J., "Roughness-Concentration Effects on Flow over Hydrodynamically Rough Surfaces," Water Supply Paper 1592-D, United States Geological Survey, Department of the Interior, United States Government Printing Office, Washington, D.C., 1966.

Krumbein, W. C., "Measurement and Geological Significance of Shape and Roundness of Sedimentary Particles," Journal of Sedimentary Petrology, Vol. 11, No. 2, Aug., 1941, pp. 64-72.

Leopold, L. B., "An Improved Method for Size Distribution of Stream Bed Gravel," Water Resources Research, Vol. 6, No. 5, Oct., 1970, pp. 1357-1366.

Leopold, L. B., Bagnold, R. A., Wolman, M. G., and Brush, L. M., "Flow Resistance in Sinuous or Irregular Channels," Professional Paper 282-D, United States Geological Survey, Department of the Interior, United States Government Printing Office, Washington, D. C., 1960.

Li, R. M., Simons, D. B., Ward, T. J., and Steele, K. S., "Phase 1 Report: Hydraulic Model Study of Flow Control Structures," Report No. CER77-78RML-DBS-TJW-KSS15, Department of Civil Engineering, Colorado State University, Fort Collins, Colo., Nov., 1977.

Liggett, J. A., "Stability," Unsteady Flow in Open Channels, K. Mahmood and V. Yevjevich, ed., Vol. 1, Water Resources Publications, Fort Collins, Colo., 1975, pp. 259-311.

Limerinos, J. T., "Determination of the Manning Coefficient from Measured Bed Roughness in Natural Channels," Water Supply Paper 1898-B, United States Geological Survey, Department of the Interior, United States Government Printing Office, Washington, D.C., 1970.

Mahmood, K., "Lognormal Size Distribution of Particulate Matter," Journal of Sedimentary Petrology, Vol. 43, No. 4, Dec., 1973, pp. 1161-1166.

Milhous, R. T., and Klingeman, P. C., "Sediment Transport System in a Gravel-Bottomed Stream," Hydraulic Engineering and the Environment, ASCE, 1973, pp. 293-303.

Miller, J. P., "High Mountain Streams: Effects of Geology on Channel Characteristics and Bed Material," Memoir No. 4, State Bureau of Mines and Mineral Resources, New Mexico Institute of Mining and Technology, Socorro, N. Mex., 1958.

Monro, J. C., "Direct Search Optimization in Mathematical Modeling and a Watershed Model Application," Technical Memorandum NWS HYDRO-12, United States National Oceanic and Atmospheric Administration, Department of Commerce, Office of Hydrology, Silver Spring, Md., Apr., 1971.

Morris, H. M., "Design Methods for Flow in Rough Conduits," Journal of the Hydraulics Division, ASCE, Vol. 85, No. HY7, Proc. Paper 2081, July, 1959, pp. 43-62.

Morris, H. M., "Hydraulics of Energy Dissipation in Steep, Rough Channels," Bulletin No. 19, Research Division, Virginia Polytechnic Insitute, Blacksburg, Va., Nov., 1968.

Nanson, G. C., "Bedload and Suspended Load Transport in a Small, Steep, Mountain Stream," American Journal of Science, Vol. 274, No. 5, 1974, pp. 471-486.

Overton, D. E., Judd, H. E., and Johnson, C. W., "Optimizing Resistance Coefficients for Large Bed Element Streams," Report No. PRWG 59a-1, Utah Water Research Laboratory, Utah State University, Logan, Utah, June, 1972.

Peterson, D. F., and Mohanty, P. K., "Flume Studies of Flow in Steep, Rough Channels," Journal of the Hydraulics Division, ASCE, Vol. 86, No. HY9, Proc. Paper 2653, Nov., 1960, pp. 55-76.

Richter, A., and Naudascher, E., "Fluctuating Forces on a Rigid Circular Cylinder in Confined Flow," Journal of Fluid Mechanics, Vol. 78, Part 3, Cambridge, England, Dec. 7, 1976, pp. 561-576.

Rouse, H., "Critical Analysis of Open-Channel Resistance," Journal of the Hydraulics Division, ASCE, Vol. 91, No. HY4, Proc. Paper 4387, July, 1965, pp. 1-25.

Scheuerlein, H., "The Mechanics of Flow in Steep, Rough, Open Channels," Proceedings of the Fifteenth Congress of the International Association for Hydraulic Research, Istanbul, Turkey, Vol. 1, 1973, pp. 457-465.

Schlichting, H., Boundary-Layer Theory, 6th ed., McGraw-Hill Book Co., Inc., New York, N. Y., 1968.

Schumm, S. A., The Fluvial System, 1st ed., John Wiley and Sons, Inc., New York, N. Y., 1977.

Shen, H. W., "Flow Resistance over Short Simulated Vegetation and Various Tall Simulated Vegetation Groupings on Flow Resistance and Sediment Yield," Environmental Impact on Rivers (River Mechanics III), H. W. Shen, ed., 1st ed., H. W. Shen, Fort Collins, Colo., 1973, pp. 3.1-3.51.

Simons, D. B., Al-Shaikh Ali, K. S., and Li, R. M., "Flow Resistance in Cobble and Boulder Riverbeds," Journal of the Hydraulics Division, ASCE, Vol. 105, No. HY5, Proc. Paper 14576, May, 1979, pp. 477-488.

Simons, D. B., and Şentürk, F., Sediment Transport Technology, 1st ed., Water Resources Publications, Fort Collins, Colo., 1977.

Simpson, D. H., "Modeling of Bedload Transport and Hydraulic Roughness in Mountain Streams," thesis presented to Colorado State University, at Fort Collins, Colo., in 1978, in partial fulfillment of the requirements for the degree of Master of Science.

Virmani, J. K., "The Relationship between Channel Forming Flows and the Cross-Section Shape, Slope, and Bed Materials in Large Bed Element Streams," thesis presented to Utah State University, at Logan, Utah, in 1973, in partial fulfillment of the requirements for the degree of Doctor of Philosophy.

Wolman, M. G., "A Method of Sampling Coarse River-Bed Material," Transactions, American Geophysical Union, Vol. 35, No. 6, Part 1, Dec., 1954, pp. 951-956.

APPENDIX A

CALCULATION OF A THEORETICAL ROUGHNESS CONCENTRATION

A method of calculating the concentration of roughness elements on the bed is demonstrated. Only those elements which protrude through the free surface at a given depth are considered. It is assumed that each protruding element should be accounted for in the concentration, although in practice a certain number of elements are likely to lie in the wake of other elements and should not strictly be considered since they have little effect on the flow.

If n_i is the number of elements in the size class interval i lying on an area of bed, A_{bed}, and the basal plan area of those elements is A_{Bi}, then it is approximately true that:

$$\sum_{i=1}^{I} n_i A_{Bi} = A_{bed} \tag{47}$$

where I is the number of size class intervals covering the total size distribution of the elements.

Further, on the area of bed, A_{bed}, x_i percent of the elements by count lie in the size class interval i and have basal plan areas A_{Bi}. It can therefore be stated that if a hundred elements occupy an area of bed, A_{bed}, then A_{bed} is equal to $\sum_{i=1}^{I} x_i A_{Bi}$. More generally if the total number of elements of all sizes lying on the area of bed, A_{bed}, is n, then:

$$A_{bed} = \sum_{i=1}^{I} \frac{n}{100} x_i A_{Bi} \tag{48}$$

and therefore

$$n = \frac{A_{bed}}{\sum_{i=1}^{I} \frac{x_i}{100} A_{Bi}} \tag{49}$$

Since n_i is the number of elements of the size class interval i on the area of bed, A_{bed}, it is related to n by

$$n_i = \frac{x_i}{100} n \tag{50}$$

Substituting for n from Equation (49):

$$n_i = \frac{x_i A_{bed}}{\sum_{i=1}^{I} x_i A_{Bi}} \tag{51}$$

Knowing the number of elements of each size in the specified area of bed, it is possible to calculate roughness concentration directly using Equation (51).

Frontal concentration, λ_1, is given by the ratio of the average frontal cross-sectional area, A_F, of the elements to the area of bed per element (Equation (14)). Basal concentration, λ_2, is given by the ratio of the average basal plan area, A_B, of the elements to the area of bed per element (Equation (15)). Consequently for a given size class interval, frontal concentration is:

$$\begin{aligned} \lambda_{1i} &= n_i \frac{A_{Fi}}{A_{bed}} \\ &= \frac{x_i A_{Fi}}{\sum_{i=1}^{I} x_i A_{Bi}} \end{aligned} \tag{52}$$

(using the substitution of Equation (51)).

Basal concentration is:

$$\lambda_{2i} = \frac{n_i A_{Bi}}{A_{bed}}$$

$$= \frac{x_i A_{Bi}}{\sum_{i=1}^{I} x_i A_{Bi}} \tag{53}$$

Total concentrations for the bed are then:

$$\lambda_1 = \sum_{i=1}^{I} \lambda_{1i} \tag{54}$$

and

$$\lambda_2 = \sum_{i=1}^{I} \lambda_{2i} \tag{55}$$

In calculating a roughness concentration for the protruding elements, only those size class intervals containing elements of height greater than the depth of flow should be included. Denoting these intervals by the range $i = j$ to I, Equations (54) and (55) can be written in more detail by substituting from Equations (52) and (53):

$$\lambda_1 = \sum_{i=j}^{I} \frac{x_i A_{Fi}}{\sum_{i=1}^{I} x_i A_{Bi}} \tag{56}$$

and

$$\lambda_2 = \sum_{i=j}^{I} \frac{x_i A_{Bi}}{\sum_{i=1}^{I} x_i A_{Bi}} \tag{57}$$

If the size distribution of the elements is specified, the roughness concentration for any depth can be determined using these equations.

The technique is applied to the five bed materials used in this study. It is assumed that the elements were semielliptical in frontal cross section and elliptical in basal plan section. The wetted frontal cross-sectional area of a given element is therefore:

$$A_{Fi} = \frac{Y_i}{2}\left\{d'\left[1 - \left(\frac{d'}{k_i}\right)^2\right]^{0.5} + k_i \sin^{-1}\left(\frac{d'}{k_i}\right)\right\} \qquad (58)$$

where Y_i = the cross-stream axis of the element; d' = the depth of flow at the element; k_i = the height of the element; and d'/k_i is less than or equal to unity. The basal plan area is:

$$A_{Bi} = \pi \frac{X_i}{2}\frac{Y_i}{2} \qquad (59)$$

where X_i = the longstream axis of the element.

For this analysis it is assumed that the height of an element equals its short axis, its cross-stream axis equals its long axis and its longstream axis equals its median axis. Also, both the long and median axes are calculated as fixed ratios to the short axis, the values of the ratios depending in this instance on the 84 percentile values of the relevant size distributions. The data used to illustrate the calculation of roughness concentration are those describing the roughness materials of this study. Details of these materials and the size distributions are presented in Appendix C.

In order to improve the accuracy of the calculations, the upper limit of the uppermost size class interval of the short axis is given, not by the size noted in Appendix C, but by the maximum size of the short axis, S_{100}. The means by which this is calculated is described by Equation (27) in the main text.

Roughness concentration is then calculated by the following procedure. Depth, d', is set equal to the lower limit of a size class interval, that interval corresponding to j in the range of intervals $i = j$ to I which contain protruding elements. For each of the intervals in that range, A_{Fi} and A_{Bi} are calculated using Equations (58) and (59), with height, k_i, equal to the maximum size of the short axis of each interval. The roughness concentrations for each interval are calculated using Equations (52) and (53) and the total concentrations for the bed are given by Equations (56) and (57). The procedure is repeated by setting depth, d', equal to each size interval boundary in turn so that roughness concentration is calculated for a variety of depths.

The results for the data of this study are given in Table A1 and the variation of frontal roughness concentration with relative submergence d'/S_{50} is shown in Figure 5 in the main text. Over the upper range of relative submergences, concentration falls as relative submergence increases. This agrees with the results of Bathurst (1978). However, because of the assumptions behind the method outlined, particularly that every protruding element can affect the flow whereas in fact those elements which lie in the wakes of other elements should be neglected, the calculated values of concentration are likely to be higher than equivalent measured values.

TABLE A1.--Calculated Roughness Concentration for the Flume Bed Materials

Bed material size in inches (1)	Relative submergence d'/S_{50} (2)	Frontal concentration (3)	Basal concentration (4)
0.5	0.430	0.171	0.980
	0.863	0.273	0.881
	1.293	0.159	0.434
	1.724	0.042	0.113
	2.431	0.000	0.000
0.75	0.313	0.104	1.000
	0.625	0.190	0.975
	0.938	0.215	0.853
	1.250	0.202	0.698
	1.875	0.065	0.238
	3.638	0.000	0.000
1.5	0.264	0.114	1.000
	0.396	0.168	0.999
	0.525	0.219	0.996
	0.789	0.277	0.922
	1.053	0.233	0.680
	1.317	0.157	0.432
	1.578	0.113	0.293
	1.842	0.036	0.102
	2.868	0.000	0.000
2.0	0.336	0.180	1.000
	0.504	0.261	0.996
	0.672	0.319	0.960
	0.840	0.348	0.892
	1.009	0.270	0.633
	1.176	0.064	0.147
	1.345	0.009	0.020
	1.492	0.000	0.000
2.5	0.380	0.220	1.000
	0.506	0.285	0.995
	0.633	0.338	0.980
	0.759	0.344	0.887
	0.886	0.352	0.820
	1.013	0.267	0.587
	1.139	0.089	0.194
	1.266	0.034	0.072
	1.382	0.000	0.000

APPENDIX B

ITERATIVE TECHNIQUE FOR SOLUTION OF THE RESISTANCE EQUATION

The derived resistance equation is:

$$\frac{\bar{U}}{(gdS)^{0.5}} = \left[\frac{0.28}{b}\,Fr\right]^{\log(0.755/b)} \times \left[13.434\left(\frac{w}{Y_{50}}\right)^{0.492} b^{1.025(w/Y_{50})^{0.118}}\right] \times \left[\frac{A_w}{wd'}\right] \qquad (37)$$

where

$$b = \left[1.175\left(\frac{Y_{50}}{w}\right)^{0.557}\left(\frac{d}{S_{50}}\right)\right]^{0.648}\sigma^{-0.134} \qquad (26)$$

and for rivers of homogeneous boundary material

$$\frac{A_w}{wd'} = \left(\frac{w}{d}\right)^{-b} \qquad (22)$$

An iterative technique by which Equation (37) can be solved is demonstrated using the data of Virmani (1973).

A relationship between channel width, w, and mean depth, d, such as Equation (26), should first be delineated. Taking Virmani's site 10-0115 as an example, the data show that:

$$w = 64.05\ d^{0.1858} \qquad (60)$$

Thus the mean velocity, $\bar{U}$, is related to discharge, Q, by:

$$\bar{U} = \frac{Q}{64.05\ d^{1.1858}} \qquad (61)$$

Substituting for w and $\bar{U}$ in Equation (37) and using Equation (22) to describe relative roughness area, depth is related to just discharge and the parameters of roughness geometry:

$$\frac{Q}{200.6\ d^{1.6858} S^{0.5}} = \left[\frac{0.001396\ Q}{b\ d^{1.6858}}\right]^{\log(0.755/b)}$$

$$\times \left[104 \left(\frac{d^{0.1858}}{Y_{50}}\right)^{0.492} b^{1.675(d^{0.1858}/Y_{50})^{0.118}}\right]$$

$$\times \left[64.05\ d^{-0.8142}\right]^{-b} \qquad (62)$$

where

$$b = \left[0.1158\ Y_{50}^{0.557} \frac{d}{S_{50}}^{0.8965}\right]^{0.648} \sigma^{-0.134} \qquad (63)$$

Virmani's data show that:

$$D_{50} = 0.144 \text{ m}$$

$$\sigma = 0.313$$

$$S = 0.0117$$

Assuming that $S_{50} = 0.57\ D_{50}$ and that the cross-stream axis, Y_{50}, is equal to L_{50} and $L_{50} = D_{50}/0.57$, then:

$$S_{50} = 0.0821 \text{ m}$$

$$Y_{50} = 0.253 \text{ m}$$

The calculated value of the function of effective roughness concentration, b, is therefore $0.7268\ d^{0.6787}$ (Equation (63)). Substituting into Equation (62):

$$\frac{Q}{21.7\ d^{1.6858}} = \left[\frac{0.00192\ Q}{d^{2.3645}}\right]^{\log(1.039/d^{0.6787})}$$

$$\times \left[204.5\ d^{0.0914}\left(0.7268\ d^{0.6787}\right)^{1.969\ d^{0.02192}}\right]$$

$$\times \left[\frac{64.05}{d^{0.8142}}\right]^{-0.7267\ d^{0.6787}} \qquad (64)$$

The only two unknowns in this equation are discharge and depth, so specifying one allows the other to be calculated. Virmani's data show that at a discharge of 0.906 m^3s^{-1} the depth is 0.146 m. If, however, the depth were unknown it could have been calculated by the following iterative technique.

The known value of discharge and a guessed value of depth are substituted into the right side of Equation (64). With depth set at, say, 1 m, the value of the right side is 4.775. Equating this with the left side of the equation, and including the known value of discharge, a calculated value of depth equal to 0.0601 m is obtained.

Using this derived value as the new guessed value of depth for the right side of the equation, the next iteration gives a depth equal to 0.1134 m. Subsequent iterations give depths of 0.1546 m, 0.1623 m and 0.1625 m. As the difference between the last two values is insignificant, the final value can be assumed to be the required value. Five iterations therefore seem to be sufficient for the calculation of depth and the result is about 10 percent in error relative to the measured value.

APPENDIX C

ROUGHNESS CHARACTERISTICS OF THE FLUME BED MATERIALS

This appendix contains data describing the size distribution, shape and specific gravity of the materials used for the roughness beds in the flume experiments.

ROUGHNESS CHARACTERISTICS OF 0.5 INCH MATERIAL

TABLE C1.--Size Distribution of the Long, Median and Short Axes

Size class interval in millimetres (1)	CUMULATIVE PERCENTAGE OF SAMPLE LESS THAN OR EQUAL TO UPPER SIZE OF CLASS INTERVAL OF Long axis (2)	Median axis (3)	Short axis (4)
0 - 2.5			17
2.5 - 5		6	38
5 - 7.5	8	32	80
7.5 - 10	18	66	97
10 - 15	64	100	100
15 - 20	97		
20 - 25	100		

Percentile n of size distribution (5)	SIZE (IN MILLIMETRES) CORRESPONDING TO PERCENTILE n OF Long axis (6)	Median axis (7)	Short axis (8)
84	17.0	11.5	7.8
50	13.6	8.8	5.8
16	9.6	6.4	2.3

Standard Deviation of Size Distribution for:

Long axis : 0.097

Median axis: 0.116

Short Axis : 0.129

Maximum Size of Short Axis, S_{100} = 14.1 mm

TABLE C2.--Parameters of Shape

Percentile n of size distribution (1)	Krumbein intercept sphericity ψ (2)	Ratio $\frac{L_n + S_n}{2D_n}$ (3)	Ratio $\frac{L_n S_n}{D_n^2}$ (4)	Ratio $\frac{S_n}{D_n}$ (5)	Ratio $\frac{S_n}{L_n}$ (6)
84	0.677	1.078	1.003	0.678	0.459
50	0.651	1.102	1.019	0.659	0.426
16	0.543	0.930	0.539	0.359	0.240

Specific Gravity of Packed Sediment (Voids plus Material) = 1.556

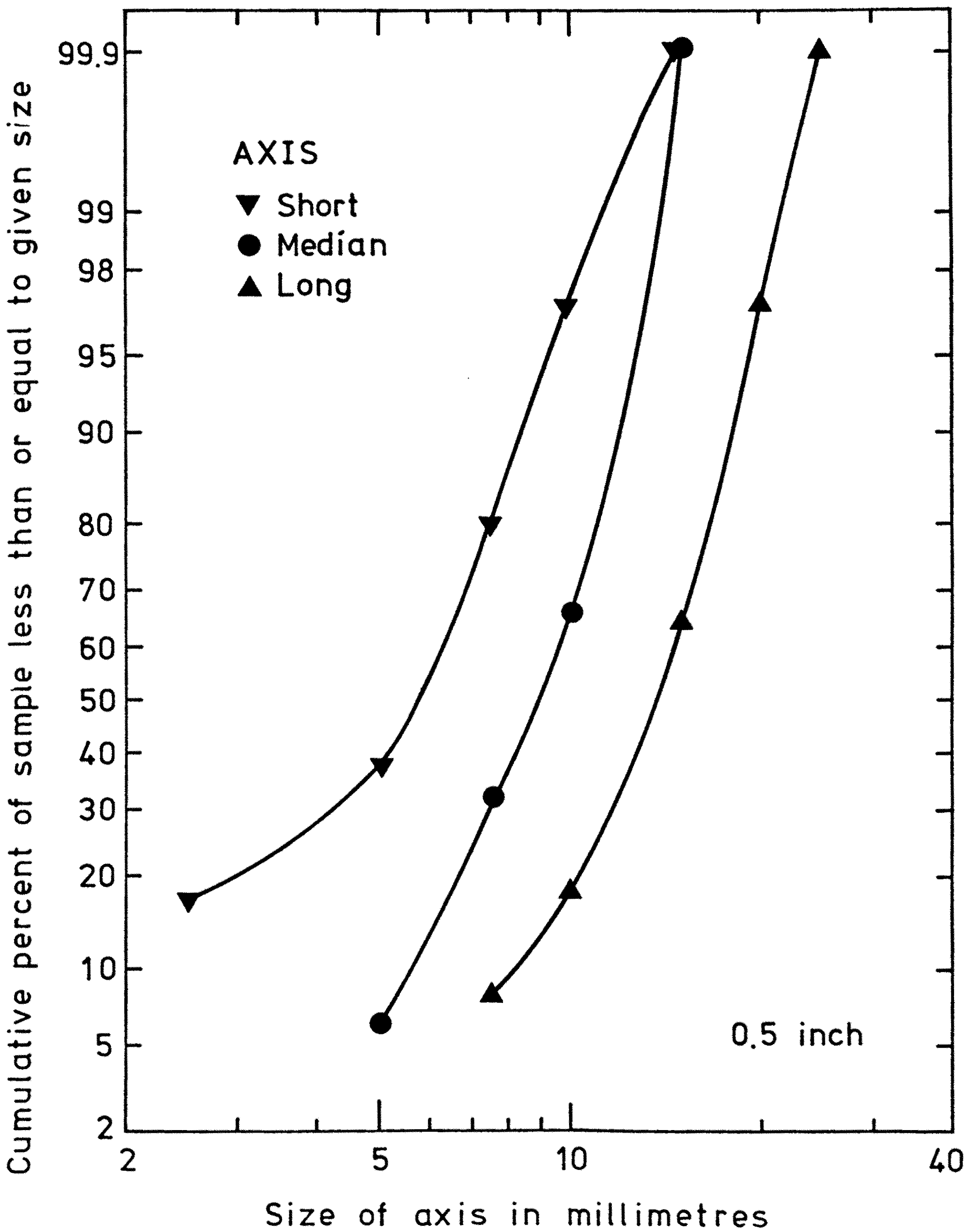

Figure C1. Cumulative percentage frequency curves for the long, median and short axes of the 0.5 inch roughness material, plotted on a log-probability graph.

ROUGHNESS CHARACTERISTICS OF 0.75 INCH MATERIAL

TABLE C3.--Size Distribution of the Long, Median and Short Axes

Size class interval in millimetres (1)	CUMULATIVE PERCENTAGE OF SAMPLE LESS THAN OR EQUAL TO UPPER SIZE OF CLASS INTERVAL OF Long axis (2)	Median axis (3)	Short axis (4)
2.5 - 5			14
5 - 7.5		9	45
7.5 - 10	8	30	67
10 - 15	27	62	96
15 - 20	51	87	100
20 - 25	72	100	
25 - 30	92		
30 - 35	99		
35 - 40	100		

Percentile n of size distribution (5)	SIZE (IN MILLIMETRES) CORRESPONDING TO PERCENTILE n OF Long axis (6)	Median axis (7)	Short axis (8)
84	28.0	19.3	12.3
50	19.75	13.0	8.0
16	12.4	8.5	5.2

Standard Deviation of Size Distribution for:

Long axis : 0.152

Median axis: 0.172

Short axis : 0.187

Maximum Size of Short Axis, S_{100} = 29.1 mm

TABLE C4.--Parameters of Shape

Percentile n of size distribution (1)	Krumbein intercept sphericity ψ (2)	Ratio $\frac{L_n + S_n}{2D_n}$ (3)	Ratio $\frac{L_n S_n}{D_n^2}$ (4)	Ratio $\frac{S_n}{D_n}$ (5)	Ratio $\frac{S_n}{L_n}$ (6)
84	0.672	1.044	0.925	0.637	0.439
50	0.644	1.067	0.935	0.615	0.405
16	0.660	1.035	0.892	0.612	0.419

Specific Gravity of Packed Sediment (Voids plus Material) = 1.649

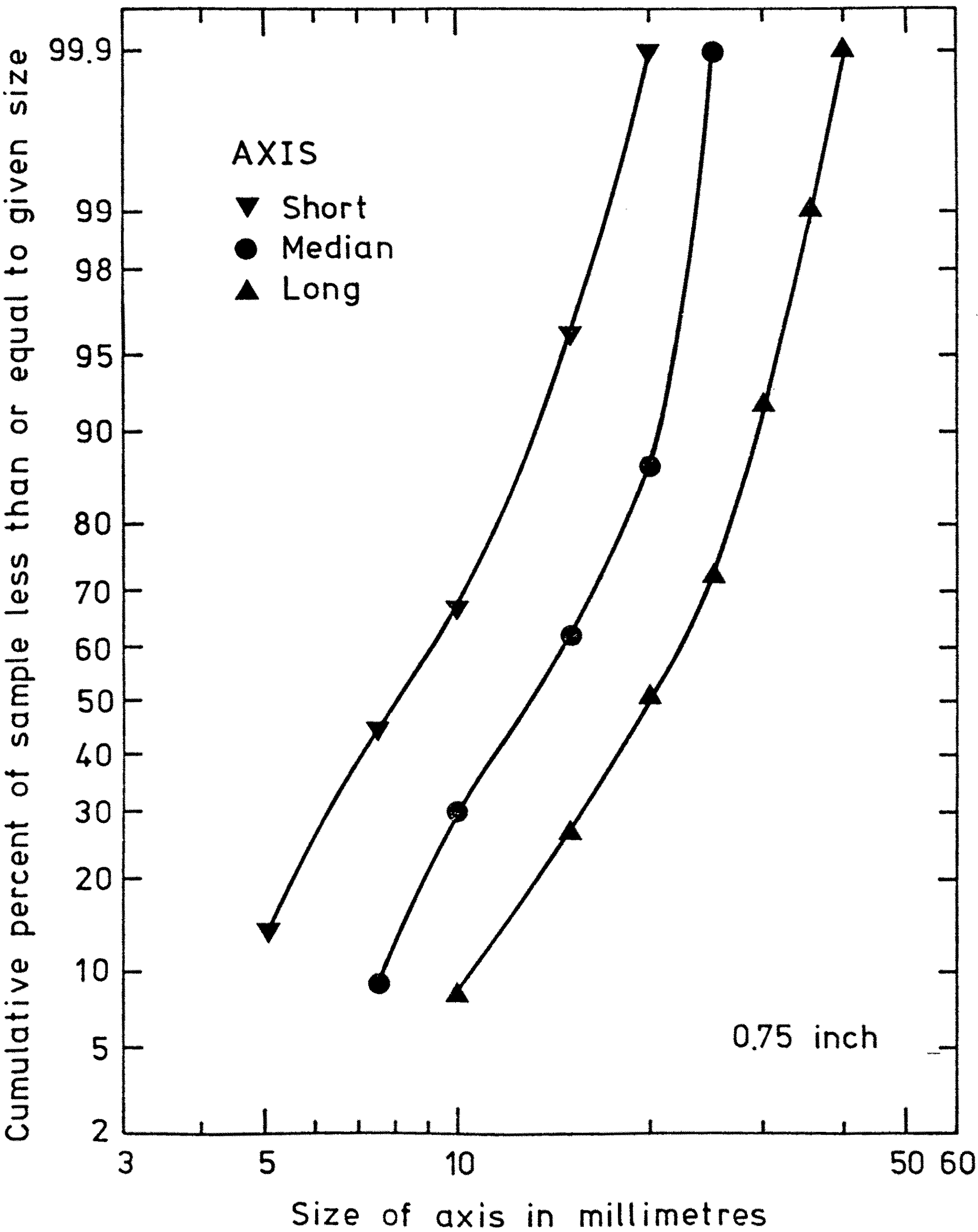

Figure C2. Cumulative percentage frequency curves for the long, median and short axes of the 0.75 inch roughness material, plotted on a log-probability graph.

ROUGHNESS CHARACTERISTICS OF 1.5 INCH MATERIAL

TABLE C5.--Size Distribution of the Long, Median and Short Axes

Size class interval in millimetres (1)	CUMULATIVE PERCENTAGE OF SAMPLE LESS THAN OR EQUAL TO UPPER SIZE OF CLASS INTERVAL OF Long axis (2)	Median axis (3)	Short axis (4)
5 - 7.5			1
7.5 - 10			3
10 - 15			22
15 - 20		3	57
20 - 25		22	80
25 - 30	5	39	89
30 - 35	18	54	98
35 - 40	34	74	100
40 - 45	44	90	
45 - 50	60	97	
50 - 60	87	100	
60 - 70	97		
70 - 80	99		
80 - 90	99		
90 -100	100		

Percentile n of size distribution (5)	SIZE (IN MILLEMETRES) CORRESPONDING TO PERCENTILE n OF Long axis (6)	Median axis (7)	Short axis (8)
84	59.0	43.0	27.0
50	47.0	34.0	19.0
16	34.0	23.5	13.8

Standard Deviation of Size Distribution for:

Long axis : 0.099

Median axis: 0.102

Short axis : 0.153

Maximum Size of Short Axis, S_{100} = 54.5 mm

TABLE C6.--Parameters of Shape

Percentile n of size distribution (1)	Krumbein intercept sphericity ψ (2)	Ratio $\frac{L_n + S_n}{2D_n}$ (3)	Ratio $\frac{L_n S_n}{D_n^2}$ (4)	Ratio $\frac{S_n}{D_n}$ (5)	Ratio $\frac{S_n}{L_n}$ (6)
84	0.693	1.000	0.862	0.628	0.458
50	0.664	0.971	0.772	0.559	0.404
16	0.655	1.017	0.850	0.587	0.406

Specific Gravity of Packed Sediment (Voids plus Material) = 1.601

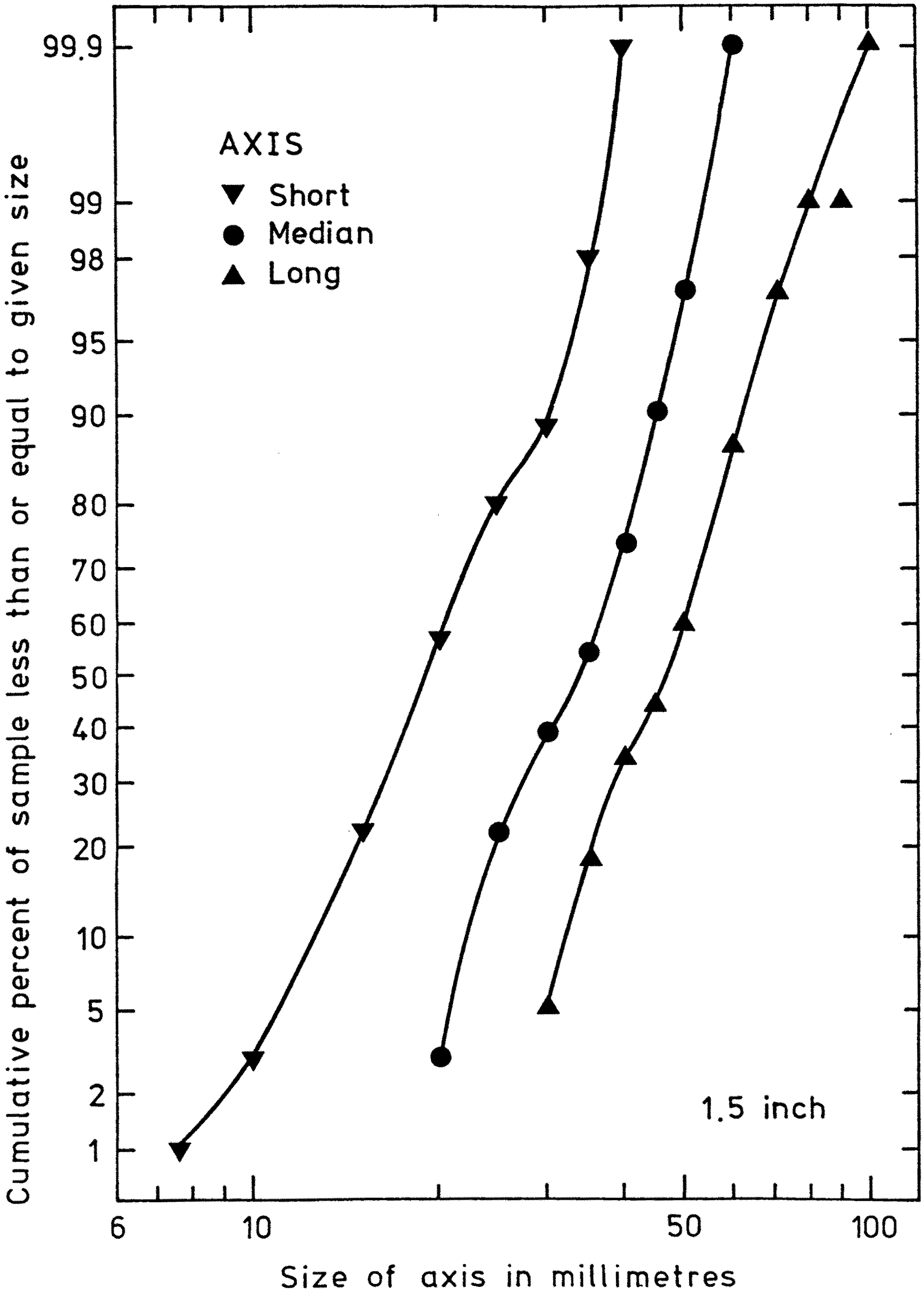

Figure C3. Cumulative percentage frequency curves for the long, median and short axes of the 1.5 inch roughness material, plotted on a log-probability graph.

ROUGHNESS CHARACTERISTICS OF 2.0 INCH MATERIAL

TABLE C7.--Size Distribution of the Long, Median and Short Axes

Size class interval in millimetres (1)	CUMULATIVE PERCENTAGE OF SAMPLE LESS THAN OR EQUAL TO UPPER SIZE OF CLASS INTERVAL OF		
	Long axis (2)	Median axis (3)	Short axis (4)
10 - 15			2
15 - 20			11
20 - 25			22
25 - 30			51
30 - 35		5	91
35 - 40	1	25	99
40 - 45	6	64	100
45 - 50	18	98	
50 - 60	53	100	
60 - 70	78		
70 - 80	93		
80 - 90	98		
90 -100	100		

Percentile n of size distribution (5)	SIZE (IN MILLIMETRES) CORRESPONDING TO PERCENTILE n OF		
	Long axis (6)	Median axis (7)	Short axis (8)
84	73.0	47.0	34.0
50	59.0	43.0	29.75
16	49.0	38.5	22.5

Standard Deviation of Size Distribution for:

Long axis : 0.0925

Median axis: 0.0386

Short axis : 0.0580

Maximum Size of Short Axis, S_{100} = 44.4 mm

TABLE C8.--Parameters of Shape

Percentile n of size distribution	Krumbein intercept sphericity ψ	Ratio $\frac{L_n + S_n}{2D_n}$	Ratio $\frac{L_n S_n}{D_n^2}$	Ratio $\frac{S_n}{D_n}$	Ratio $\frac{S_n}{L_n}$
(1)	(2)	(3)	(4)	(5)	(6)
84	0.669	1.138	1.124	0.723	0.466
50	0.716	1.032	0.949	0.692	0.504
16	0.712	0.929	0.744	0.584	0.459

Specific Gravity of Packed Sediment (Voids plus Material) = 1.703

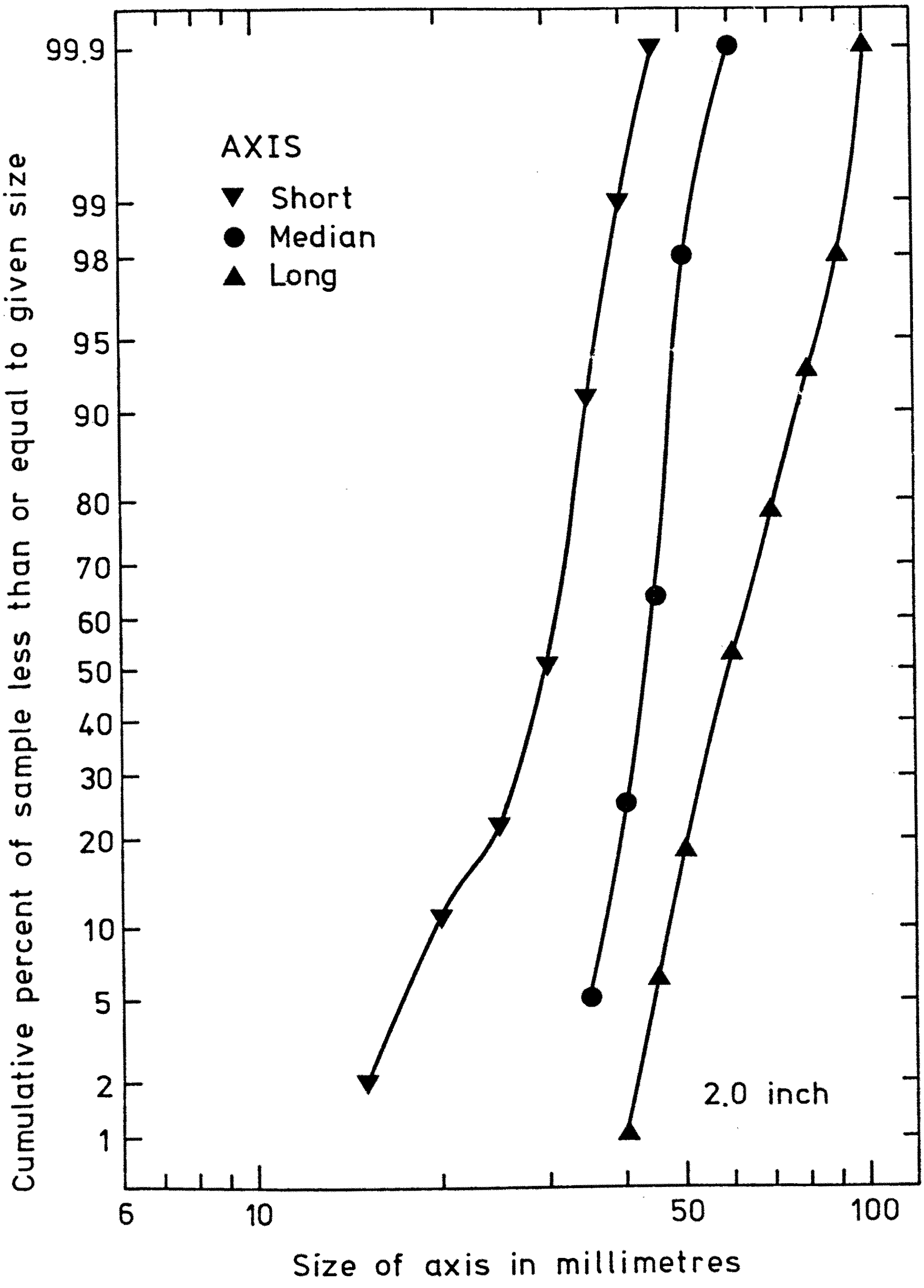

Figure C4. Cumulative percentage frequency curves for the long, median and short axes of the 2.0 inch roughness material, plotted on a log-probability graph.

ROUGHNESS CHARACTERISTICS OF 2.5 INCH MATERIAL

TABLE C9.--Size Distribution of the Long, Median and Short Axes

Size class interval in millimetres (1)	CUMULATIVE PERCENTAGE OF SAMPLE LESS THAN OR EQUAL TO UPPER SIZE OF CLASS INTERVAL OF Long axis (2)	Median axis (3)	Short axis (4)
15 - 20			2
20 - 25			6
25 - 30			23
30 - 35			32
35 - 40			56
40 - 45			88
45 - 50		16	96
50 - 55	3	56	100
55 - 60	7	95	
60 - 70	40	100	
70 - 80	66		
80 - 90	84		
90 -100	96		
100 -120	98		
120 -140	100		
Percentile n of size distribution (5)	**SIZE (IN MILLIMETRES) CORRESPONDING TO PERCENTILE n OF Long axis (6)**	**Median axis (7)**	**Short axis (8)**
84	90.0	58.0	44.0
50	73.0	54.25	39.5
16	62.5	50.0	28.5

Standard Deviation of Size Distribution for:

Long axis : 0.0909

Median axis: 0.0290

Short Axis : 0.0469

Maximum Size of Short Axis, S_{100} = 54.6 mm

TABLE C10.--Parameters of Shape

Percentile n of size distribution (1)	Krumbein intercept sphericity ψ (2)	Ratio $\frac{L_n + S_n}{2D_n}$ (3)	Ratio $\frac{L_n S_n}{D_n^2}$ (4)	Ratio $\frac{S_n}{D_n}$ (5)	Ratio $\frac{S_n}{L_n}$ (6)
84	0.680	1.155	1.177	0.759	0.489
50	0.738	1.037	0.980	0.728	0.541
16	0.715	0.910	0.713	0.570	0.456

Specific Gravity of Packed Sediment (Voids plus Material) = 1.673

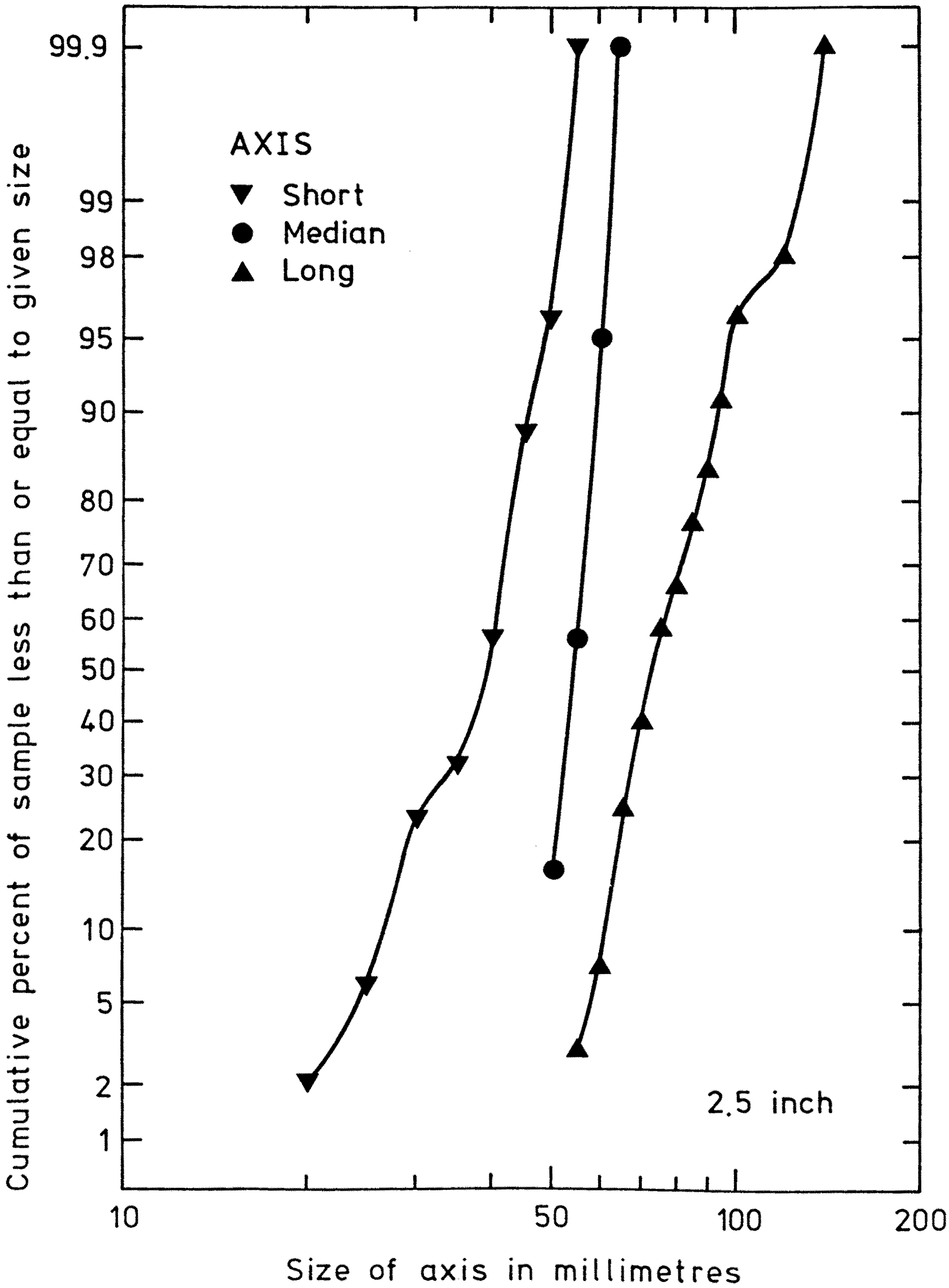

Figure C5. Cumulative percentage frequency curves for the long, median and short axes of the 2.5 inch roughness material, plotted on a log-probability graph.

APPENDIX D

PARAMETERS OF THE FLOWS OVER THE FIXED BEDS

This appendix contains basic and derived data for the flows over the fixed beds. For each bed material one table gives the basic flow parameters, another gives the derived flow parameters and a third gives the resistance parameters derived during development of the flow resistance equation.

PARAMETERS OF FLOW OVER 0.5 INCH FIXED BED

TABLE D1.--Basic Parameters of Flow for 0.5 Inch Bed

Experiment number (1)	Channel slope (2)	Discharge in cubic metres per second (3)	Mean velocity in metres per second (4)	Cross-sectional area in square metres (5)	Mean depth in metres (6)	Water temperature in degrees centigrade (7)	Kinematic viscosity of water in square metres per second (x 10^6) (8)
1	0.02	0.00241	0.146	0.0165	0.0141	14	1.173
2	0.02	0.01274	0.391	0.0326	0.0279	14	1.173
3	0.02	0.03046	0.584	0.0521	0.0446	14	1.173
4	0.02	0.05746	0.785	0.0732	0.0627	14	1.173
5	0.02	0.07197	0.877	0.0821	0.0702	14	1.173
6	0.05	0.00143	0.161	0.0089	0.0076	16	1.110
7	0.05	0.00522	0.296	0.0177	0.0151	16	1.110
8	0.05	0.01737	0.619	0.0281	0.0240	16.5	1.095
9	0.05	0.03249	0.823	0.0395	0.0338	16	1.110
10	0.05	0.04896	1.017	0.0481	0.0412	15.5	1.125
11	0.08	0.00196	0.201	0.0098	0.0084	9	1.345
12	0.08	0.00610	0.392	0.0156	0.0133	13	1.205
13	0.08	0.01355	0.563	0.0241	0.0206	13	1.205
14	0.08	0.03576	0.965	0.0370	0.0317	12.5	1.222
15	0.08	0.06061	1.225	0.0495	0.0424	12.5	1.222
16	0.08	0.07065	1.301	0.0543	0.0465	12.5	1.222

TABLE D2.--Derived Parameters of Flow for 0.5 Inch Bed

Experiment number (1)	Shear velocity $(gdS)^{0.5}$ in metres per second (2)	Relative submergence d/S_{50} (3)	Resistance function $(8/f)^{0.5} = \overline{U}/(gdS)^{0.5}$ (4)	Darcy-Weisbach resistance coefficient (5)	Ratio of width to depth (6)	Reynolds number $\overline{U}D_{50}/\nu$ $(\times 10^{-3})$ (7)	Froude number $\overline{U}/(gd)^{0.5}$ (8)
1	0.0526	2.436	2.769	1.044	82.7	1.095	0.392
2	0.0740	4.806	5.289	0.286	41.9	2.933	0.748
3	0.0936	7.695	6.242	0.205	26.2	4.381	0.883
4	0.1109	10.804	7.079	0.160	18.7	5.889	1.001
5	0.1174	12.111	7.469	0.143	16.6	6.579	1.056
6	0.0611	1.312	2.636	1.151	153.5	1.276	0.590
7	0.0861	2.606	3.433	0.679	77.3	2.347	0.768
8	0.1085	4.141	5.702	0.246	48.7	4.975	1.275
9	0.1288	5.827	6.390	0.196	34.6	6.525	1.429
10	0.1422	7.103	7.156	0.156	28.4	7.955	1.600
11	0.0810	1.441	2.478	1.303	139.8	1.315	0.701
12	0.1023	2.299	3.830	0.545	87.6	2.863	1.083
13	0.1272	3.552	4.427	0.408	56.7	4.112	1.252
14	0.1577	5.466	6.121	0.214	36.9	6.949	1.731
15	0.1823	7.303	6.717	0.177	27.6	8.822	1.900
16	0.1910	8.013	6.813	0.172	25.1	9.369	1.927

TABLE D3.--Parameters of the Resistance Equation for 0.5 Inch Bed

Experiment number (1)	Function of effective roughness concentration b (2)	Depth d' of bed datum in metres (3)	Relative roughness area A_w/wd' (4)	Ratio of $\bar{U}/(gdS)^{0.5}$ to A_w/wd' (5)	Free surface drag function fn$(1/C_{DF})$ (6)	Resistance function $(8/f)^{0.5}$ calculated with Equation (37) (7)
1	0.300	0.0192	0.2659	10.41	0.629	2.628
2	0.527	0.0324	0.1398	37.83	0.879	5.086
3	0.747	0.0489	0.0874	71.43	0.918	6.882
4	0.942	0.0669	0.0635	111.51	0.965	7.411
5	1.038	0.0743	0.0540	138.20	1.015	7.458
6	0.177	0.0129	0.4104	6.43	0.952	2.334
7	0.336	0.0197	0.2318	14.81	0.738	3.668
8	0.450	0.0291	0.1739	32.79	0.994	5.324
9	0.592	0.0385	0.1227	52.07	0.992	6.206
10	0.669	0.0461	0.1068	67.02	1.038	6.761
11	0.227	0.0124	0.3262	7.60	0.738	2.711
12	0.307	0.0179	0.2532	15.13	0.879	4.064
13	0.439	0.0248	0.1701	26.03	0.825	5.003
14	0.600	0.0358	0.1149	53.28	0.993	6.230
15	0.725	0.0466	0.0903	74.42	1.005	6.880
16	0.772	0.0507	0.0829	82.18	0.997	7.089

PARAMETERS OF FLOW OVER 0.75 INCH FIXED BED

TABLE D4.--Basic Parameters of Flow for 0.75 Inch Bed

Experiment number (1)	Channel slope (2)	Discharge in cubic metres per second (3)	Mean velocity in metres per second (4)	Cross-sectional area in square metres (5)	Mean depth in metres (6)	Water temperature in degrees centigrade (7)	Kinematic viscosity of water in square metres per second ($\times 10^6$) (8)
17	0.02	0.00580	0.222	0.0261	0.0223	20	1.000
18	0.02	0.01181	0.348	0.0339	0.0290	20.5	0.989
19	0.02	0.02482	0.484	0.0512	0.0439	20	1.000
20	0.02	0.04047	0.586	0.0690	0.0591	20.5	0.989
21	0.02	0.05348	0.656	0.0816	0.0698	20.5	0.989
22	0.05	0.00381	0.230	0.0165	0.0141	20.5	0.989
23	0.05	0.00843	0.363	0.0232	0.0199	20.5	0.989
24	0.05	0.02037	0.583	0.0349	0.0299	20.5	0.989
25	0.05	0.03333	0.782	0.0426	0.0365	21.0	0.978
26	0.05	0.04586	0.904	0.0507	0.0434	20.5	0.989
27	0.05	0.05460	0.979	0.0558	0.0477	19.5	1.014
28	0.08	0.00207	0.186	0.0111	0.0095	19.5	1.014
29	0.08	0.00631	0.380	0.0166	0.0142	20	1.000
30	0.08	0.01007	0.430	0.0234	0.0200	20	1.000
31	0.08	0.02825	0.807	0.0350	0.0299	20	1.000
32	0.08	0.04518	1.032	0.0438	0.0375	20	1.000
33	0.08	0.04879	1.064	0.0459	0.0392	20	1.000

TABLE D5.--Derived Parameters of Flow for 0.75 Inch Bed

Experiment number (1)	Shear velocity $(gdS)^{0.5}$ in metres per second (2)	Relative submergence d/S_{50} (3)	Resistance function $(8/f)^{0.5} = \overline{U}/(gdS)^{0.5}$ (4)	Darcy-Weisbach resistance coefficient (5)	Ratio of width to depth (6)	Reynolds number $\overline{U}D_{50}/\nu$ $(\times 10^{-3})$ (7)	Froude number $\overline{U}/(gd)^{0.5}$ (8)
17	0.0662	2.790	3.361	0.708	52.4	2.886	0.475
18	0.0754	3.626	4.617	0.375	40.3	4.574	0.653
19	0.0928	5.482	5.221	0.294	26.6	6.292	0.738
20	0.1076	7.383	5.447	0.270	19.8	7.703	0.770
21	0.1170	8.728	5.601	0.255	16.7	8.623	0.792
22	0.0833	1.768	2.766	1.046	82.6	3.023	0.619
23	0.0987	2.484	3.678	0.591	58.8	4.771	0.822
24	0.1211	3.736	4.817	0.345	39.1	7.663	1.077
25	0.1337	4.557	5.851	0.234	32.1	10.395	1.308
26	0.1459	5.428	6.193	0.209	26.9	11.883	1.385
27	0.1530	5.965	6.402	0.195	24.5	12.551	1.432
28	0.0864	1.190	2.150	1.731	122.8	2.385	0.608
29	0.1056	1.776	3.601	0.617	82.3	4.940	1.018
30	0.1254	2.505	3.430	0.680	58.3	5.590	0.970
31	0.1533	3.743	5.266	0.289	39.0	10.491	1.489
32	0.1714	4.682	6.022	0.221	31.2	13.416	1.703
33	0.1755	4.905	6.063	0.218	29.8	13.442	1.715

TABLE D6.--Parameters of the Resistance Equation for 0.75 Inch Bed

Experiment number (1)	Function of effective roughness concentration b (2)	Depth d' of bed datum in metres (3)	Relative roughness area A_w/wd' (4)	Ratio of $\bar{U}/(gdS)^{0.5}$ to A_w/wd' (5)	Free surface drag function $fn(1/C_{DF})$ (6)	Resistance function $(8/f)^{0.5}$ calculated with Equation (37) (7)
17	0.397	0.0282	0.2081	16.15	0.744	3.456
18	0.480	0.0349	0.1696	27.23	0.886	4.419
19	0.660	0.0495	0.1146	45.56	0.832	5.803
20	0.846	0.0642	0.0801	67.98	0.791	6.657
21	0.975	0.0746	0.0641	87.35	0.785	6.839
22	0.269	0.0204	0.3052	9.06	0.846	2.945
23	0.349	0.0262	0.2411	15.26	0.886	3.857
24	0.482	0.0360	0.1709	28.19	0.911	4.959
25	0.560	0.0426	0.1433	40.83	1.003	5.555
26	0.655	0.0491	0.1156	53.56	0.991	5.999
27	0.693	0.0536	0.1090	58.75	0.981	6.251
28	0.189	0.0159	0.4031	5.33	0.945	2.465
29	0.255	0.0211	0.3253	11.07	1.140	3.705
30	0.370	0.0258	0.2222	15.44	0.807	4.092
31	0.477	0.0363	0.1742	30.23	0.996	5.285
32	0.575	0.0435	0.1382	43.56	1.021	5.789
33	0.605	0.0450	0.1285	47.20	1.010	5.880

PARAMETERS OF FLOW OVER 1.5 INCH FIXED BED

TABLE D7.--Basic Parameters of Flow for 1.5 Inch Bed

Experiment number (1)	Channel slope (2)	Discharge in cubic metres per second (3)	Mean velocity in metres per second (4)	Cross-sectional area in square metres (5)	Mean depth in metres (6)	Water temperature in degrees centigrade (7)	Kinematic viscosity of water in square metres per second (x 10^6) (8)
34	0.02	0.00250	0.116	0.0215	0.0184	16	1.110
35	0.02	0.00868	0.239	0.0364	0.0311	17	1.081
36	0.02	0.01893	0.375	0.0505	0.0432	18	1.053
37	0.02	0.04352	0.587	0.0741	0.0634	17.5	1.067
38	0.02	0.06763	0.721	0.0938	0.0803	17.5	1.067
39	0.02	0.08020	0.764	0.1050	0.0899	15	1.140
40	0.05	0.00181	0.132	0.0137	0.0117	16	1.110
41	0.05	0.00636	0.264	0.0241	0.0206	17	1.081
42	0.05	0.01456	0.419	0.0348	0.0298	18	1.053
43	0.05	0.03073	0.625	0.0491	0.0420	18.5	1.038
44	0.05	0.06061	0.869	0.0697	0.0597	17	1.081
45	0.05	0.07421	0.932	0.0796	0.0681	17	1.081
46	0.08	0.00389	0.267	0.0145	0.0124	13	1.205
47	0.08	0.01092	0.457	0.0239	0.0204	13	1.205
48	0.08	0.02100	0.616	0.0341	0.0292	13	1.205
49	0.08	0.03126	0.721	0.0433	0.0371	14	1.173
50	0.08	0.05498	0.971	0.0566	0.0484	14	1.173
51	0.08	0.05574	0.883	0.0631	0.0540	15	1.140

TABLE D8.--Derived Parameters of Flow for 1.5 Inch Bed

Experiment number (1)	Shear velocity $(gdS)^{0.5}$ in metres per second (2)	Relative submergence d/S_{50} (3)	Resistance function $(8/f)^{0.5} = \overline{U}/(gdS)^{0.5}$ (4)	Darcy-Weisbach resistance coefficient (5)	Ratio of width to depth (6)	Reynolds number $\overline{U}D_{50}/\nu$ (x 10^{-3}) (7)	Froude number $\overline{U}/(gd)^{0.5}$ (8)
34	0.0601	0.967	1.936	2.135	63.6	3.553	0.274
35	0.0781	1.638	3.054	0.858	37.5	7.517	0.432
36	0.0921	2.276	4.069	0.483	27.0	12.108	0.575
37	0.1115	3.337	5.267	0.288	18.4	18.705	0.745
38	0.1255	4.225	5.745	0.242	14.6	22.975	0.812
39	0.1328	4.731	5.750	0.242	13.0	22.786	0.813
40	0.0759	0.617	1.738	2.650	99.6	4.043	0.389
41	0.1006	1.087	2.621	1.164	56.6	8.303	0.586
42	0.1208	1.566	3.465	0.666	39.3	13.529	0.775
43	0.1436	2.213	4.355	0.422	27.8	20.472	0.974
44	0.1711	3.141	5.080	0.310	19.6	27.332	1.136
45	0.1828	3.585	5.100	0.308	17.2	29.314	1.140
46	0.0988	0.655	2.706	1.093	93.9	7.534	0.765
47	0.1267	1.076	3.609	0.614	57.2	12.895	1.021
48	0.1513	1.536	4.069	0.483	40.0	17.381	1.151
49	0.1706	1.952	4.228	0.448	31.5	20.899	1.196
50	0.1950	2.550	4.981	0.322	24.1	28.145	1.409
51	0.2059	2.843	4.289	0.435	21.6	26.335	1.213

TABLE D9.--Parameters of the Resistance Equation for 1.5 Inch Bed

Experiment number (1)	Function of effective roughness concentration b (2)	Depth d' of bed datum in metres (3)	Relative roughness area A_w/wd' (4)	Ratio of $\bar{U}/(gdS)^{0.5}$ to A_w/wd' (5)	Free surface drag function $fn(1/C_{DF})$ (6)	Resistance function $(8/f)^{0.5}$ calculated with Equation (37) (7)
34	0.233	0.0297	0.3803	5.09	0.650	1.645
35	0.364	0.0425	0.2677	11.41	0.748	2.832
36	0.471	0.0548	0.2115	19.24	0.856	3.797
37	0.638	0.0751	0.1559	33.78	0.956	5.092
38	0.766	0.0921	0.1285	44.71	0.961	5.876
39	0.864	0.1009	0.1090	52.75	0.948	6.065
40	0.155	0.0230	0.4909	3.54	0.834	1.590
41	0.247	0.0328	0.3696	7.09	0.832	2.545
42	0.343	0.0416	0.2839	12.21	0.873	3.344
43	0.450	0.0542	0.2237	19.47	0.927	4.164
44	0.603	0.0716	0.1663	30.54	0.940	5.060
45	0.692	0.0792	0.1400	36.44	0.913	5.440
46	0.153	0.0249	0.5002	5.41	1.302	2.532
47	0.206	0.0361	0.4340	8.32	1.273	3.292
48	0.300	0.0436	0.3307	12.30	1.077	3.979
49	0.384	0.0505	0.2661	15.89	0.961	4.150
50	0.511	0.0603	0.1964	25.37	0.999	4.731
51	0.562	0.0657	0.1779	24.11	0.825	4.850

PARAMETERS OF FLOW OVER 2.0 INCH FIXED BED

TABLE D10.--Basic Parameters of Flow for 2.0 Inch Bed

Experiment number (1)	Channel slope (2)	Discharge in cubic metres per second (3)	Mean velocity in metres per second (4)	Cross-sectional area in square metres (5)	Mean depth in metres (6)	Water temperature in degrees centigrade (7)	Kinematic viscosity of water in square metres per second (x 10^6) (8)
52	0.02	0.00329	0.100	0.0330	0.0282	22.5	0.946
53	0.02	0.00837	0.189	0.0442	0.0378	23	0.937
54	0.02	0.01158	0.227	0.0509	0.0436	23	0.937
55	0.02	0.02541	0.377	0.0675	0.0578	23	0.937
56	0.02	0.04047	0.519	0.0780	0.0668	23	0.937
57	0.02	0.04949	0.601	0.0824	0.0705	23.5	0.926
58	0.05	0.00329	0.132	0.0249	0.0213	22.5	0.946
59	0.05	0.00713	0.214	0.0333	0.0285	22.5	0.946
60	0.05	0.01413	0.337	0.0420	0.0359	23	0.937
61	0.05	0.02068	0.431	0.0480	0.0411	23	0.937
62	0.05	0.02941	0.542	0.0543	0.0465	23	0.937
63	0.05	0.04368	0.643	0.0680	0.0582	22.5	0.946
64	0.08	0.00247	0.162	0.0152	0.0130	21.5	0.967
65	0.08	0.00565	0.205	0.0276	0.0236	22	0.957
66	0.08	0.01077	0.313	0.0344	0.0295	22	0.957
67	0.08	0.02187	0.515	0.0425	0.0363	22.5	0.946
68	0.08	0.03249	0.637	0.0510	0.0437	22.5	0.946
69	0.08	0.03724	0.712	0.0523	0.0448	22	0.957

TABLE D11.--Derived Parameters of Flow for 2.0 Inch Bed

Experiment number (1)	Shear velocity $(gdS)^{0.5}$ in metres per second (2)	Relative submergence d/S_{50} (3)	Resistance function $(8/f)^{0.5}$ = $\bar{U}/(gdS)^{0.5}$ (4)	Darcy-Weisbach resistance coefficient (5)	Ratio of width to depth (6)	Reynolds number $\bar{U}D_{50}/\nu$ (x 10^{-3}) (7)	Froude number $\bar{U}/(gd)^{0.5}$ (8)
52	0.0744	0.947	1.339	4.463	41.4	4.545	0.189
53	0.0861	1.269	2.199	1.654	30.9	8.673	0.311
54	0.0925	1.463	2.459	1.323	26.8	10.417	0.348
55	0.1064	1.938	3.538	0.639	20.2	17.301	0.500
56	0.1145	2.241	4.530	0.390	17.5	23.818	0.641
57	0.1176	2.367	5.106	0.307	16.6	27.908	0.722
58	0.1022	0.715	1.291	4.796	54.8	6.000	0.289
59	0.1182	0.956	1.812	2.437	41.0	9.727	0.405
60	0.1328	1.206	2.535	1.245	32.5	15.465	0.567
61	0.1420	1.379	3.033	0.870	28.4	19.779	0.678
62	0.1510	1.559	3.589	0.621	25.2	24.873	0.803
63	0.1689	1.952	3.804	0.553	20.1	29.227	0.851
64	0.1010	0.436	1.609	3.092	89.9	7.204	0.455
65	0.1361	0.792	1.507	3.522	49.5	9.211	0.426
66	0.1521	0.989	2.056	1.892	39.6	14.064	0.582
67	0.1689	1.219	3.050	0.860	32.2	23.409	0.863
68	0.1851	1.466	3.439	0.676	26.8	28.955	0.973
69	0.1874	1.502	3.799	0.554	26.1	31.992	1.074

TABLE D12.--Parameters of the Resistance Equation for 2.0 Inch Bed

Experiment number (1)	Function of effective roughness concentration b (2)	Depth d' of bed datum in metres (3)	Relative roughness area A_w/wd' (4)	Ratio of $\overline{U}/(gdS)^{0.5}$ to A_w/wd' (5)	Free surface drag function fn$(1/C_{DF})$ (6)	Resistance function $(8/f)^{0.5}$ calculated with Equation (37) (7)
52	0.220	0.0505	0.4413	3.03	0.458	1.323
53	0.281	0.0611	0.3814	5.77	0.604	2.188
54	0.324	0.0665	0.3443	7.14	0.605	2.586
55	0.431	0.0795	0.2735	12.94	0.718	3.689
56	0.483	0.0892	0.2511	18.04	0.847	4.398
57	0.486	0.0947	0.2553	20.00	0.929	4.696
58	0.164	0.0442	0.5179	2.49	0.579	1.382
59	0.218	0.0513	0.4450	4.07	0.622	2.027
60	0.282	0.0575	0.3750	6.76	0.706	2.755
61	0.313	0.0633	0.3508	8.65	0.772	3.211
62	0.348	0.0688	0.3252	11.04	0.841	3.660
63	0.447	0.0788	0.2617	14.54	0.766	4.250
64	0.084	0.0411	0.6842	2.35	1.468	1.627
65	0.161	0.0505	0.5330	2.83	0.675	1.883
66	0.208	0.0551	0.4646	4.43	0.723	2.514
67	0.231	0.0659	0.4483	6.80	0.952	3.349
68	0.267	0.0747	0.4155	8.28	0.934	3.805
69	0.312	0.0701	0.3615	10.51	0.943	3.989

PARAMETERS OF FLOW OVER 2.5 INCH FIXED BED

TABLE D13.--Basic Parameters of Flow for 2.5 Inch Bed

Experiment number (1)	Channel slope (2)	Discharge in cubic metres per second (3)	Mean velocity in metres per second (4)	Cross-sectional area in square metres (5)	Mean depth in metres (6)	Water temperature in degrees centigrade (7)	Kinematic viscosity of water in square metres per second (x 10^6) (8)
70	0.02	0.00409	0.138	0.0297	0.0254	23	0.937
71	0.02	0.00993	0.223	0.0445	0.0381	22	0.957
72	0.02	0.01671	0.301	0.0555	0.0475	22.5	0.946
73	0.02	0.02799	0.409	0.0685	0.0586	22.5	0.946
74	0.02	0.04110	0.500	0.0821	0.0703	23	0.937
75	0.02	0.04967	0.543	0.0914	0.0782	23	0.937
76	0.05	0.00369	0.173	0.0214	0.0183	23	0.937
77	0.05	0.00855	0.283	0.0302	0.0259	22	0.957
78	0.05	0.01282	0.342	0.0375	0.0321	22.5	0.946
79	0.05	0.02176	0.478	0.0455	0.0390	22.5	0.946
80	0.05	0.03403	0.611	0.0557	0.0477	23	0.937
81	0.05	0.04896	0.725	0.0676	0.0578	22.5	0.946
82	0.08	0.00397	0.210	0.0189	0.0162	22	0.957
83	0.08	0.00605	0.259	0.0233	0.0200	22.5	0.946
84	0.08	0.01128	0.374	0.0302	0.0258	23	0.937
85	0.08	0.01775	0.474	0.0375	0.0321	22	0.957
86	0.08	0.02737	0.592	0.0462	0.0396	22.5	0.946
87	0.08	0.03319	0.669	0.0496	0.0425	23	0.937
88	0.08	0.04485	0.775	0.0579	0.0495	22.5	0.946

TABLE D14.--Derived Parameters of Flow for 2.5 Inch Bed

Experiment number (1)	Shear velocity $(gdS)^{0.5}$ in metres per second (2)	Relative submergence d/S_{50} (3)	Resistance function $(8/f)^{0.5} = \overline{U}/(gdS)^{0.5}$ (4)	Darcy-Weisbach resistance coefficient (5)	Ratio of width to depth (6)	Reynolds number $\overline{U}D_{50}/\nu$ (x 10^{-3}) (7)	Froude number $\overline{U}/(gd)^{0.5}$ (8)
70	0.0706	0.644	1.947	2.111	46.0	7.990	0.275
71	0.0865	0.964	2.581	1.201	30.7	12.641	0.365
72	0.0966	1.203	3.115	0.824	24.6	17.261	0.441
73	0.1073	1.485	3.809	0.551	19.9	23.455	0.539
74	0.1174	1.780	4.260	0.441	16.6	28.949	0.602
75	0.1239	1.980	4.387	0.416	14.9	31.438	0.620
76	0.0947	0.463	1.826	2.399	63.9	10.016	0.408
77	0.1126	0.655	2.512	1.268	45.2	16.043	0.562
78	0.1255	0.813	2.722	1.080	36.4	19.612	0.609
79	0.1382	0.986	3.459	0.669	30.0	27.412	0.773
80	0.1529	1.206	3.998	0.501	24.5	35.375	0.894
81	0.1684	1.464	4.304	0.432	20.2	41.576	0.962
82	0.1127	0.410	1.862	2.309	72.2	11.904	0.527
83	0.1252	0.506	2.072	1.863	58.5	14.853	0.586
84	0.1424	0.654	2.627	1.159	45.3	21.654	0.743
85	0.1586	0.812	2.987	0.896	36.4	26.870	0.845
86	0.1762	1.002	3.358	0.709	29.5	33.949	0.950
87	0.1825	1.075	3.665	0.596	27.5	38.733	1.037
88	0.1972	1.254	3.930	0.518	23.6	44.444	1.112

TABLE D15.--Parameters of the Resistance Equation for 2.5 Inch Bed

Experiment number (1)	Function of effective roughness concentration b (2)	Depth d' of bed datum in metres (3)	Relative roughness area A_w/wd' (4)	Ratio of $\overline{U}/(gdS)^{0.5}$ to A_w/wd' (5)	Free surface drag function $fn(1/C_{DF})$ (6)	Resistance function $(8/f)^{0.5}$ calculated with Equation (37) (7)
70	0.156	0.0567	0.5513	3.53	0.924	1.305
71	0.234	0.0691	0.4489	5.75	0.834	2.022
72	0.296	0.0777	0.3879	8.03	0.830	2.595
73	0.354	0.0898	0.3469	10.98	0.876	3.283
74	0.426	0.1007	0.3021	14.10	0.861	3.917
75	0.476	0.1081	0.2761	15.89	0.826	4.313
76	0.112	0.0489	0.6266	2.91	1.219	1.521
77	0.153	0.0585	0.5575	4.51	1.204	2.137
78	0.196	0.0635	0.4942	5.51	1.031	2.433
79	0.235	0.0707	0.4490	7.70	1.107	2.998
80	0.284	0.0799	0.4034	9.91	1.088	3.495
81	0.350	0.0889	0.3497	12.31	1.000	3.946
82	0.101	0.0463	0.6503	2.86	1.407	1.850
83	0.120	0.0517	0.6141	3.37	1.287	2.072
84	0.156	0.0575	0.5512	4.77	1.239	2.581
85	0.198	0.0630	0.4911	6.08	1.125	2.946
86	0.244	0.0705	0.4383	7.66	1.048	3.342
87	0.257	0.0740	0.4265	8.59	1.088	3.567
88	0.299	0.0810	0.3887	10.11	1.029	3.882

APPENDIX E

PARAMETERS OF THE FLOWS OVER THE LOOSE BEDS AND OF SEDIMENT DISCHARGE

This appendix contains basic and derived data for the flows over the loose beds. For each bed material one table gives the basic flow parameters, another gives the derived flow parameters and a third gives resistance parameters calculated using the equations in the main text. A fourth set of tables gives the details of sediment discharge.

PARAMETERS OF FLOW OVER 0.5 INCH LOOSE BED

TABLE E1.--Basic Parameters of Flow for 0.5 Inch Bed

Experiment number (1)	Channel slope (2)	Water discharge in cubic metres per second (3)	Mean velocity in metres per second (4)	Cross-sectional area in square metres (5)	Mean depth in metres (6)	Water temperature in degrees centigrade (7)	Kinematic viscosity of water in square metres per second (x 10^6) (8)
89*	0.02	0.02447	0.564	0.0434	0.0372	13	1.205
90	0.02	0.06710	0.844	0.0795	0.0681	13	1.205
91	0.02	0.07850	0.921	0.0852	0.0729	13	1.205
92	0.02	0.08574	1.080	0.0794	0.0680	13	1.205
93	0.02	0.08699	0.943	0.0923	0.0790	13	1.205
94*	0.05	0.01106	0.297	0.0373	0.0319	16	1.110
95	0.05	0.04109	0.833	0.0501	0.0429	16	1.110
96	0.05	0.04796	0.670	0.0714	0.0611	16	1.110
97	0.05	0.04969	0.899	0.0553	0.0474	16	1.110
98	0.05	0.05428	1.009	0.0538	0.0461	16	1.110
99	0.05	0.07646	1.173	0.0652	0.0558	16	1.110
100	0.05	0.07827	0.804	0.0960	0.0822	16	1.110
101*	0.08	0.00421	0.155	0.0271	0.0232	15	1.140
102	0.08	0.01585	0.384	0.0412	0.0353	15	1.140
103	0.08	0.01694	0.397	0.0426	0.0365	15	1.140
104	0.08	0.03[illegible]	0.774	0.0496	0.0425	15	1.140
105	0.08	0.0[illegible]	0.795	0.0561	0.0480	[illegible]	1.140
106	0.08	0.0[illegible]	0.894	0.0709	0.0607	[illegible]	1.140
107	0.08	0.06978	0.867	0.0805	0.0689	15	1.140

*No sediment movement during these experiments

TABLE E2.--Derived Parameters of Flow for 0.5 Inch Bed

Experiment number	Shear velocity $(gdS)^{0.5}$ in metres per second	Relative submergence d/S_{50}	Resistance function $(8/f)^{0.5} = \overline{U}/(gdS)^{0.5}$	Darcy-Weisbach resistance coefficient	Ratio of width to depth	Reynolds number $\overline{U}D_{50}/\nu$ $(x\ 10^{-3})$	Froude number $\overline{U}/(gd)^{0.5}$
(1)	(2)	(3)	(4)	(5)	(6)	(7)	(8)
89*	0.0854	6.414	6.599	0.184	31.4	4.119	0.934
90	0.1156	11.741	7.302	0.150	17.2	6.164	1.033
91	0.1196	12.569	7.704	0.135	16.0	6.726	1.089
92	0.1155	11.724	9.348	0.092	17.2	7.887	1.322
93	0.1245	13.621	7.572	0.140	14.8	6.887	1.071
94*	0.1251	5.500	2.371	1.423	36.6	2.355	0.530
95	0.1451	7.397	5.743	0.243	27.2	6.604	1.284
96	0.1731	10.534	3.870	0.534	19.1	5.312	0.865
97	0.1525	8.172	5.893	0.230	24.7	7.127	1.318
98	0.1504	7.948	6.710	0.178	25.4	7.999	1.501
99	0.1654	9.621	7.088	0.159	20.9	9.299	1.585
100	0.2008	14.172	4.004	0.499	14.2	6.374	0.895
101*	0.1349	4.000	1.151	6.041	50.3	1.196	0.325
102	0.1664	6.086	2.308	1.502	33.1	2.964	0.653
103	0.1693	6.293	2.349	1.450	32.0	3.065	0.665
104	0.1826	7.328	4.238	0.446	27.5	5.975	1.199
105	0.1941	8.276	4.098	0.476	24.3	6.137	1.159
106	0.2183	10.466	4.094	0.477	19.2	6.901	1.158
107	0.2325	11.879	3.728	0.576	16.9	6.693	1.054

*No sediment movement during these experiments

TABLE E3.--Calculated Parameters of Flow Resistance for 0.5 Inch Bed

Experiment number (1)	Function of effective roughness concentration b calculated with Equation (26) (2)	Resistance function $(8/f)^{0.5}$ calculated with Equation (37) (3)
89*	0.616	6.203
90	1.031	7.445
91	1.093	7.470
92	1.030	7.446
93	1.170	7.469
94*	0.540	5.256
95	0.695	6.810
96	0.940	7.399
97	0.757	7.126
98	0.739	7.050
99	0.870	7.327
100	1.211	7.465
101*	0.412	3.666
102	0.589	5.798
103	0.606	5.943
104	0.690	6.759
105	0.765	7.154
106	0.935	7.392
107	1.041	7.455

*No sediment movement during these experiments

TABLE E4.--Parameters of Sediment Discharge for 0.5 Inch Bed at 2 Percent Slope

Experiment number	BED ELEVATION (IN METRES) Before flow	After flow	Volume of sediment (in cubic metres) collected in time t	Time of sampling t in seconds	Sediment discharge during time t in cubic metres per second (x 10^3)	Average sediment discharge in cubic metres per second (x 10^3)
(1)	(2)	(3)	(4)	(5)	(6)	(7)
89	-	-	-	-	-	0
90	0.454	0.454	0.0292	300	0.097	0.097
91	0.436	0.455	0.0236	240	0.098	0.098
92	0.455	0.458	0.0449	180	0.250	0.265
			0.0427	150	0.285	
93	0.448	0.450	0.0158	60	0.263	0.250
			0.0297	120	0.248	
			0.0296	120	0.247	

TABLE E5.--Parameters of Sediment Discharge for 0.5 Inch Bed at 5 Percent Slope

Experiment number	BED ELEVATION (IN METRES) Before flow	After flow	Volume of sediment (in cubic metres) collected in time t	Time of sampling t in seconds	Sediment discharge during time t in cubic metres per second ($\times 10^3$)	Average sediment discharge in cubic metres per second ($\times 10^3$)
(1)	(2)	(3)	(4)	(5)	(6)	(7)
94	-	-	-	-	-	0
95	0.438	0.424	0.0183	24.4	0.752	0.649
			0.0154	34.8	0.442	
			0.0200	23.5	0.850	
96	0.421	0.464	0.0290	61.5	0.472	0.636
			0.0222	35.5	0.625	
			0.0228	19.3	1.183	
97	0.438	0.436	0.0162	21.1	0.768	0.866
			0.0214	20.4	1.050	
			0.0218	27.1	0.803	
98	0.447	0.450	0.0244	30.0	0.814	0.717
			0.231	30.0	0.769	
			0.0170	30.0	0.567	
99	0.446	0.454	0.0464	30.0	1.547	1.443
			0.0429	30.0	1.431	
			0.0405	30.0	1.350	
100	0.422	0.458	0.0199	15.4	1.294	1.226
			0.0246	20.4	1.206	
			0.0249	20.8	1.197	

TABLE E6.--Parameters of Sediment Discharge for 0.5 Inch Bed at 8 Percent Slope

Experiment number	BED ELEVATION (IN METRES) Before flow	After flow	Volume of sediment (in cubic metres) collected in time t	Time of sampling t in seconds	Sediment discharge during time t in cubic metres per second ($x 10^3$)	Average sediment discharge in cubic metres per second ($x 10^3$)
(1)	(2)	(3)	(4)	(5)	(6)	(7)
101	-	-	-	-	-	0
102	0.442	0.436	0.00695	15	0.463	0.308
			0.00569	15	0.379	
			0.00617	30	0.206	
			0.00892	30	0.297	
103	-	-	0.0133	30	0.445	0.433
			0.0106	30	0.354	
			0.0150	30	0.499	
104	0.435	0.444	0.0208	15	1.388	1.463
			0.0232	15	1.546	
			0.0218	15	1.455	
105	0.437	0.435	0.0263	15	1.751	2.079
			0.0431	15	2.875	
			0.0242	15	1.612	
106	0.431	0.435	0.0449	15	2.990	3.230
			0.0524	15	3.496	
			0.0481	15	3.204	
107	0.442	0.441	0.0494	15	3.292	3.319
			0.0477	15	3.179	
			0.0523	15	3.487	

PARAMETERS OF FLOW OVER 1.5 INCH LOOSE BED

TABLE E7.--Basic Parameters of Flow for 1.5 Inch Bed

Experiment number (1)	Channel slope (2)	Water discharge in cubic metres per second (3)	Mean velocity in metres per second (4)	Cross-sectional area in square metres (5)	Mean depth in metres (6)	Water temperature in degrees centigrade+ (7)	Kinematic viscosity of water in square metres per second (x 10^6) (8)
108*	0.02	0.01396	0.318	0.0439	0.0376	15	1.140
109*	0.05	0.02613	0.496	0.0527	0.0451	15	1.140
110*	0.08	0.02749	0.575	0.0478	0.0409	15	1.140
111	0.08	0.05433	0.796	0.0683	0.0584	15	1.140
112	0.08	0.05569	0.909	0.0613	0.0524	15	1.140
113	0.08	0.05834	0.836	0.0697	0.0597	15	1.140
114	0.08	0.06127	0.819	0.0748	0.0641	15	1.140
115	0.08	0.06870	1.162	0.0591	0.0506	15	1.140
116	0.08	0.06952	1.151	0.0605	0.0518	15	1.140

+Estimated temperature

*No sediment movement during these experiments

TABLE E8.--Derived Parameters of Flow for 1.5 Inch Bed

Experiment number (1)	Shear velocity $(gdS)^{0.5}$ in metres per second (2)	Relative submergence d/S_{50} (3)	Resistance function $(8/f)^{0.5}$ = $\overline{U}/(gdS)^{0.5}$ (4)	Darcy-Weisbach resistance coefficient (5)	Ratio of width to depth (6)	Reynolds number $\overline{U}D_{50}/\nu$ $(x\ 10^{-3})$ (7)	Froude number $\overline{U}/(gd)^{0.5}$ (8)
108*	0.0859	1.979	3.703	0.583	31.1	9.484	0.524
109*	0.1487	2.374	3.334	0.720	25.9	14.793	0.745
110*	0.1792	2.153	3.210	0.776	28.5	17.149	0.908
111	0.2141	3.074	3.716	0.579	20.0	23.740	1.050
112	0.2028	2.758	4.480	0.399	22.3	27.111	1.266
113	0.2165	3.142	3.866	0.535	19.6	24.933	1.094
114	0.2243	3.374	3.652	0.600	18.2	24.426	1.033
115	0.1993	2.663	5.830	0.235	23.1	34.656	1.649
116	0.2016	2.726	5.704	0.246	22.5	34.328	1.613

*No sediment movement during these experiments

TABLE E9.--Calculated Parameters of Flow Resistance for 1.5 Inch Bed

Experiment number (1)	Function of effective roughness concentration b calculated with Equation (26) (2)	Resistance function $(8/f)^{0.5}$ calculated with Equation (37) (3)
108*	0.424	3.391
109*	0.494	4.099
110*	0.455	4.050
111	0.612	4.972
112	0.559	4.813
113	0.624	5.044
114	0.662	5.226
115	0.543	4.919
116	0.554	4.943

*No sediment movement during these experiments

TABLE E10.--Parameters of Sediment Discharge for 1.5 Inch Bed

Experiment number (1)	Channel slope (2)	BED ELEVATION (IN METRES) Before flow (3)	After flow (4)	Volume of sediment (in cubic metres) collected in time t (5)	Time of sampling t in seconds (6)	Sediment discharge during time t in cubic metres per second (x 10^3) (7)	Average sediment discharge in cubic metres per second (x 10^3) (8)
108	0.02*	-	-	-	-	-	0
109	0.05*	-	-	-	-	-	0
110	0.08	-	-	-	-	-	0
111	0.08	-	-	0.00951	60	0.158	0.096
				0.00530	65	0.082	
				0.00299	60	0.050	
112	0.08	-	-	0.00887	60	0.148	0.260
				0.00132	60	0.022	
				0.03665	60	0.611	
113	0.08	0.439	0.521	0.02373	240	0.099	0.118
				0.01892	120	0.158	
114	0.08	0.423	0.484	0.03166	40	0.792	0.569
				0.01742	45	0.387	
				0.01637	30	0.546	
115	0.08	0.447	0.450	0.03766	45	0.837	1.103
				0.04213	30	1.404	
				0.04706	40	1.176	
116	0.08	0.423	0.423	0.01221	15	0.814	1.375
				0.02430	15	1.620	
				0.04600	30	1.533	

*No sediment movement was observed at these slopes at the maximum water discharge of 0.06554 m^3s^{-1}

APPENDIX F

PARAMETERS OF ROUGHNESS AND FLOW RESISTANCE FOR VARIOUS RIVER SITES

This appendix contains relevant roughness data and derived resistance data for various river sites. The data are used to test the flow resistance equation developed from the flume study and are taken from the following references: Bathurst (1978), Barnes (1967), Emmett (1972), Judd and Peterson (1969), and Virmani (1973). All the data are selected so that relative submergence, R/S_{50}, is less than 15.

TABLE F1.--Roughness Characteristics of River Sites

Site	SIZE OF MEDIAN AXIS (IN MILLIMETRES) AT Percentile 84	SIZE OF MEDIAN AXIS (IN MILLIMETRES) AT Percentile 50	Standard deviation of distribution
BATHURST			
Whiddybank Farm	452.5	227.5	0.299
Cronkley Pasture A	380	206.5	0.265
Cronkley Pasture B	305	185	0.217
BARNES			
12-3455	375	210	0.252
11-2645	550	253	0.337
12-3215	375	210	0.252
12-3450	415	220	0.276
EMMETT			
Bernard Creek	115	66	0.241
Tiekel River	140	64	0.340
JUDD AND PETERSON			
23A	186	101	0.267
30	625	320	0.291
32	305	159	0.284
61	314	226	0.144
62	317	186	0.232
VIRMANI			
10-0115	296	144	0.313
10-0190	110	70	0.196
10-0205	77	55	0.146
10-0320	156	93	0.225
10-0410	115	84	0.136

TABLE F2.--Parameters of Flow and Flow Resistance at Sites of Bathurst (1978)

Site (1)	Discharge in cubic metres per second (2)	Relative submergence R/S_{50} (3)	Resistance function $(8/f)^{0.5} = \bar{U}/(gRS)^{0.5}$ (4)	Froude number $\bar{U}/(gd)^{0.5}$ (5)	Reynolds number $\bar{U}D_{50}/\nu$ (x 10^{-4}) (6)	Function of effective roughness concentration b calculated with Equation (26) (7)	Resistance function $(8/f)^{0.5}$ calculated with Equation (37) (8)	Square root of ratio of calculated f to measured f (9)
Whiddybank Farm	0.90	1.272	2.180	0.285	7.30	0.295	1.830	1.191
	3.90	2.352	3.068	0.400	14.10	0.428	2.811	1.092
	7.2	3.108	3.496	0.448	17.87	0.513	3.342	1.046
Cronkley Pasture A	1.37	1.784	1.599	0.172	4.08	0.276	1.516	1.055
	4.00	2.379	2.506	0.267	8.84	0.323	2.162	1.159
	7.10	2.889	3.189	0.341	12.10	0.368	2.646	1.205
Cronkley Pasture B	1.10	1.916	2.349	0.208	4.41	0.322	1.888	1.244
	4.00	3.139	3.324	0.298	8.90	0.434	2.859	1.163
	7.10	3.803	4.209	0.377	12.99	0.495	3.381	1.245

TABLE F3.--Parameters of Flow and Flow Resistance at Sites of Barnes (1967) and Emmett (1972)

Site (1)	Discharge in cubic metres per second (2)	Relative submergence R/S_{50} (3)	Resistance function $(8/f)^{0.5} = \bar{U}/(gRS)^{0.5}$ (4)	Froude number $\bar{U}/(gd)^{0.5}$ (5)	Reynolds number $\bar{U}D_{50}/\nu$ ($\times 10^{-4}$) (6)	Function of effective roughness concentration b calculated with Equation (26) (7)	Resistance function $(8/f)^{0.5}$ calculated with Equation (37) (8)	Square root of ratio of calculated f to measured f (9)
BARNES								
12-3455	3.91	3.275	4.486	0.642	23.48	0.767	4.235	1.059
11-2645	55.22	8.799	4.901	0.552	43.72	1.138	4.577	1.071
12-3215	71.65	10.942	4.383	0.609	41.95	1.239	4.832	0.907
12-3450	42.48	8.400	3.862	0.750	48.22	1.212	4.794	0.806
EMMETT								
Bernard Creek	1.51	6.077	3.020	0.428	3.70	0.656	4.331	0.697
Tiekel River	3.67	12.199	3.652	0.288	3.37	0.990	4.714	0.775

TABLE F4.--Parameters of Flow and Flow Resistance at Sites of Judd and Peterson (1969)

Site (1)	Discharge in cubic metres per second (2)	Relative submergence R/S_{50} (3)	Resistance function $(8/f)^{0.5} = \overline{U}/(gRS)^{0.5}$ (4)	Froude number $\overline{U}/(gd)^{0.5}$ (5)	Reynolds number $\overline{U}D_{50}/\nu$ (x 10^{-4}) (6)	Function of effective roughness concentration b calculated with Equation (26) (7)	Resistance function $(8/f)^{0.5}$ calculated with Equation (37) (8)	Square root of ratio of calculated f to measured f (9)
23A	1.36	4.466	4.801	0.545	7.85	0.812	4.579	1.048
	1.53	4.891	4.685	0.535	8.02	0.865	4.580	1.023
	1.81	5.369	4.453	0.515	8.11	0.906	4.637	0.960
	4.67	8.666	4.440	0.556	11.34	1.258	4.920	0.902
	7.08	10.420	4.583	0.594	13.31	1.410	4.961	0.924
30	4.79	2.306	2.822	0.521	32.55	0.684	4.091	0.690
	7.25	2.840	3.002	0.533	37.86	0.800	4.833	0.621
	9.83	3.124	3.425	0.633	46.65	0.853	4.890	0.700
	9.71	3.693	3.106	0.605	45.17	0.972	4.504	0.690
	21.55	4.027	4.905	0.889	75.30	1.023	5.421	0.905
	25.15	4.144	5.430	0.980	84.47	1.044	5.509	0.986
	23.90	4.227	5.008	0.906	78.68	1.058	5.523	0.907
	28.89	5.280	3.751	0.639	63.93	1.195	6.318	0.594
32	1.13	4.251	1.950	0.255	5.35	0.671	2.813	0.693
	1.16	4.352	1.969	0.260	5.46	0.683	2.812	0.700
	1.22	4.386	1.992	0.258	5.51	0.686	2.875	0.693
	1.33	4.453	2.009	0.253	5.60	0.692	2.996	0.670
	1.39	4.588	2.040	0.260	5.77	0.707	3.008	0.678
	2.41	6.444	2.416	0.337	8.10	0.898	2.531	0.955
	4.42	8.839	2.875	0.395	11.02	1.144	2.074	1.387
	4.70	9.143	2.880	0.410	11.50	1.168	1.975	1.459

Cont'd...

TABLE F4.--continued

(1)	(2)	(3)	(4)	(5)	(6)	(7)	(8)	(9)
32	4.36	9.548	3.012	0.451	12.00	1.214	1.588	1.897
	8.07	12.348	3.432	0.491	15.43	1.459	1.402	2.449
	9.15	13.158	3.581	0.510	16.47	1.529	1.300	2.753
	10.71	14.474	3.704	0.548	18.16	1.640	1.102	3.361
61	1.95	2.418	2.404	0.275	10.10	0.509	3.104	0.774
	2.10	2.418	2.588	0.296	10.88	0.509	3.144	0.823
	1.87	2.537	2.025	0.239	9.12	0.535	3.240	0.625
	2.92	2.916	2.607	0.303	12.23	0.590	3.677	0.709
	3.20	3.035	2.662	0.312	12.79	0.606	3.777	0.705
	5.44	3.367	3.818	0.445	19.25	0.657	4.214	0.906
	5.18	3.651	3.353	0.448	19.52	0.729	4.372	0.767
	9.49	4.220	4.697	0.539	25.90	0.776	4.778	0.983
	36.82	7.278	5.914	0.734	47.03	1.126	5.060	1.169
62	0.74	1.858	4.564	0.583	13.41	0.590	3.284	1.390
	0.43	1.887	2.405	0.329	7.63	0.597	3.129	0.769
	1.13	1.979	4.213	0.652	16.01	0.587	3.505	1.202
	1.47	2.088	5.103	0.785	19.35	0.595	3.549	1.438
	0.77	2.123	3.411	0.447	11.27	0.646	3.595	0.949
	0.74	2.125	3.298	0.451	11.22	0.650	3.554	0.928
	0.65	2.128	2.948	0.405	10.04	0.651	3.506	0.841
	0.74	2.146	3.404	0.457	11.31	0.653	3.522	0.967
	0.77	2.272	3.359	0.461	11.51	0.683	3.583	0.937
	0.94	2.330	3.650	0.494	12.84	0.693	3.790	0.963
	1.10	2.545	3.860	0.505	13.70	0.738	4.032	0.958
	4.33	3.883	5.176	0.773	26.33	0.918	4.542	1.140

TABLE F5.--Parameters of Flow and Flow Resistance at Sites of Virmani (1973)

Site	Discharge in cubic metres per second	Relative submergence R/S_{50}	Resistance function $(8/f)^{0.5}$ = $\bar{U}/(gRS)^{0.5}$	Froude number $\bar{U}/(gd)^{0.5}$	Reynolds number $\bar{U}D_{50}/\nu$ (x 10^{-4})	Function of effective roughness concentration b calculated with Equation (26)	Resistance function $(8/f)^{0.5}$ calculated with Equation (37)	Square root of ratio of calculated f to measured f
(1)	(2)	(3)	(4)	(5)	(6)	(7)	(8)	(9)
10-0115	0.91	2.162	2.895	0.313	4.74	0.343	2.154	1.344
	1.02	2.252	2.963	0.321	4.95	0.353	2.221	1.334
	1.10	2.342	2.938	0.318	5.01	0.363	2.262	1.299
	1.19	2.432	3.005	0.325	5.22	0.372	2.324	1.293
	1.36	2.567	3.140	0.340	5.60	0.385	2.420	1.297
	1.64	2.792	3.245	0.351	6.04	0.410	2.558	1.268
	2.49	3.378	3.600	0.389	7.37	0.467	2.889	1.246
	5.95	4.954	4.532	0.490	11.23	0.603	3.568	1.270
	17.56	7.791	6.146	0.665	19.10	0.823	4.045	1.520
	20.96	8.467	6.468	0.700	20.95	0.872	3.991	1.621
	24.36	9.007	6.652	0.719	22.22	0.908	3.946	1.686
	29.74	9.908	7.122	0.770	24.96	0.966	3.869	1.841
	37.52	10.899	7.627	0.825	28.03	1.032	3.769	2.024
	41.06	11.484	7.789	0.842	29.39	1.073	3.704	2.103
10-0190	0.17	2.965	3.804	0.125	0.75	0.336	1.670	2.278
	0.65	6.856	4.494	0.147	1.35	0.617	3.520	1.277
	1.19	7.689	5.511	0.181	1.75	0.654	3.823	1.442
	1.64	8.801	5.928	0.194	2.01	0.717	4.195	1.413
	2.27	10.284	6.284	0.206	2.30	0.800	4.332	1.451
	2.78	11.210	6.476	0.212	2.48	0.852	4.241	1.527
	4.25	13.897	6.935	0.227	2.96	0.990	3.944	1.759

Cont'd...

TABLE F5.--continued

(1)	(2)	(3)	(4)	(5)	(6)	(7)	(8)	(9)
10-0205	0.20	4.716	1.343	0.103	0.54	0.424	2.195	0.612
	0.43	6.131	1.776	0.136	0.82	0.492	2.842	0.625
	1.10	8.725	2.322	0.178	1.27	0.608	3.754	0.619
	1.53	9.787	2.578	0.197	1.50	0.649	4.049	0.637
	1.95	10.612	2.794	0.214	1.69	0.685	4.269	0.655
	2.49	11.791	2.898	0.222	1.85	0.728	4.510	0.642
	3.63	13.324	3.265	0.250	2.21	0.781	4.610	0.708
10-0320	1.76	5.369	3.804	0.290	3.59	0.561	3.359	1.132
	1.81	5.509	3.788	0.288	3.62	0.569	3.401	1.114
	2.04	5.788	3.977	0.303	3.89	0.587	3.514	1.132
	2.21	5.927	4.080	0.311	4.04	0.598	3.574	1.142
	2.55	6.276	4.223	0.322	4.30	0.625	3.706	1.140
	3.11	6.973	4.467	0.340	4.80	0.670	3.926	1.138
	4.53	8.019	5.005	0.381	5.77	0.742	4.228	1.184
	7.93	10.111	5.981	0.455	7.74	0.873	4.111	1.455
	15.29	13.249	7.255	0.552	10.74	1.059	3.752	1.934
	16.99	13.946	7.440	0.567	11.30	1.095	3.676	2.024
	19.26	14.644	7.759	0.591	12.08	1.131	3.601	2.155
10-0410	0.31	4.632	2.076	0.167	1.65	0.653	3.459	0.600
	0.37	4.864	2.216	0.178	1.80	0.677	3.608	0.614
	0.43	5.095	2.340	0.188	1.95	0.698	3.735	0.626
	0.48	5.404	2.434	0.196	2.09	0.730	3.916	0.622
	0.51	5.559	2.435	0.196	2.11	0.747	4.003	0.608
	0.62	5.867	2.635	0.212	2.35	0.772	4.042	0.652
	0.91	6.871	2.975	0.239	2.88	0.867	3.939	0.755
	1.59	8.492	3.569	0.287	3.83	1.009	3.731	0.957
	3.40	11.349	4.617	0.371	5.73	1.241	3.322	1.390
	4.39	12.353	4.975	0.400	6.45	1.326	3.170	1.570
	5.66	13.742	5.477	0.440	7.49	1.418	3.000	1.826

APPENDIX G

LIST OF SYMBOLS

Each symbol is defined where it first occurs in the text. Some symbols have been used for more than one purpose but their meanings in the text should be clear.

Symbol	Description
A	= constant in Equation (4);
A	= cross-sectional area of flow;
A_B	= basal plan area of a roughness element;
A_F	= wetted frontal cross-sectional area of a roughness element;
A_w	= total wetted roughness cross-sectional area at a section, Figure 17;
A_{bed}	= area of channel bed;
a	= constant in Equation (23);
B	= constant in Equation (4);
b	= function of effective roughness concentration, Equation (26);
C	= Chezy coefficient of resistance to flow;
C_D	= drag coefficient of a roughness element;
C_{DF}	= component of drag coefficient accounting for free surface drag;
c	= constant in Equation (23);
D	= drag force on a roughness element;
D_n	= size of median axis of a roughness element which by count is greater than or equal to n percent of the median axes of a sample of elements;
d	= mean depth of flow;
d'	= depth of flow from free surface to bed datum level;
Dd	= drainage density;
e	= constant in Equation (28);

Symbol	Description
Fr	= Froude number, $\overline{U}/(gd)^{0.5}$;
f	= Darcy-Weisbach coefficient of resistance to flow;
fn( )	= a function;
g	= acceleration due to gravity;
I	= total number of size class intervals in a size distribution;
i	= constant in Equation (33) and a subscript in Appendix A denoting size class interval in a size distribution;
j	= constant in Equation (33) and the lowest size class interval, in a size distribution, which contains protruding roughness elements (Appendix A);
k	= roughness element height;
L_n	= size of long axis of a roughness element which by count is greater than or equal to n percent of the long axes of a sample of elements;
log	= logarithm to the base of ten;
m	= constant in Equation (28);
N	= characteristic number of roughness elements at a section, Equation (17);
n	= number of roughness elements on an area of bed;
p	= constant in Equation (39);
Q	= water discharge;
Q_c	= critical water discharge at which bed material movement begins;
Q_s	= sediment discharge;
q	= water discharge per unit width of channel;
q_c	= critical water discharge per unit width of channel at which bed material movement begins;
q_s	= sediment discharge per unit width of channel;
R	= hydraulic radius;
S	= longitudinal channel slope and, for uniform flow, longitudinal energy gradient;

Symbol	Description
S_c	= critical Shields parameter;
S_n	= size of short axis of a roughness element which by count is greater than or equal to n percent of the short axes of a sample of elements;
S_g	= average valleyside slope;
sin	= sine of an angle;
t	= time of sampling during measurement of sediment discharge;
U	= velocity of flow;
$\overline{U}$	= mean velocity of flow;
u_*	= mean shear velocity at a point;
$\overline{u}_*$	= mean shear velocity at a section;
w	= surface width at a section;
X	= size of longstream axis of a roughness element;
X_n	= size of longstream axis of a roughness element which by count is greater than or equal to n percent of the longstream axes of a sample of elements;
x_i	= percentage by count of a sample of roughness elements in size class interval i in a size distribution (Appendix A);
Y	= size of cross-stream axis of a roughness element;
Y_n	= size of cross-stream axis of a roughness element which by count is greater than or equal to n percent of the cross-stream axes of a sample of elements;
α	= constant in Equation (38);
β	= constant in Equation (38);
γ	= specific weight of a fluid;
γ_s	= specific weight of a roughness element;
Δ	= constant in Equations (10) and (43);
Δ_x	= a length of channel;
λ_1	= frontal roughness concentration, Equation (14);

Symbol	Description
λ_2	= basal roughness concentration, Equation (15);
ν	= kinematic viscosity of a fluid;
ρ	= density of a fluid;
Σ	= symbol indicating summation;
σ	= standard deviation of a size distribution, Equation (18);
τ_c	= critical boundary shear stress at which bed material movement begins;
τ_o	= boundary shear stress at a point;
ϕ	= characteristic roughness size determined by fabric analysis, Equation (6); and
ψ	= Krumbein intercept sphericity, Equation (19).